Identification of a context-dependent Mpt5-mediated, post-transcriptional buffering system triggered by chromatin deregulation in *S. cerevisiae*

Inaugural-Dissertation

zur Erlangung des Doktorgrades

der Mathematisch-Naturwissenschaftlichen Fakultät

der Universität zu Köln

vorgelegt

David Zygmunt Kochan

aus Lublin, Polen

Köln, 2020

Diese Dissertation wurde von der Mathematisch-Naturwissenschaftlichen Fakultät der Universität zu Köln angenommen.

Berichterstatter: **Dr. Peter Tessarz**

                                      Prof. Dr. Jan Riemer

Tag der mündlichen Prüfung: 14.08.2020

Table of contents

I. List of figures

II. List of tables

III. List of abbreviations

(K) - lysine

(R) - arginine

4TU - 4-thiouracil

5-FOA - 5-Fluoroorotic Acid

Asf1 - anti-Silencing Function 1

CAF-1 - chromatin assembly factor 1 complex

Ccr4 - carbon catabolite repressor protein 4

Ccr4-Not - carbon catabolite repression 4 negative on TATA-less

Cenp-A - histone H3-like centromeric protein A

ChIP - chromatin immunoprecipitation

Co-REST - REST corepressor 1

CUT - cryptic unstable transcript

CWI - cell wall integrity pathway

Dhh1 - DEAD box Helicase Homolog 1

DNA - deoxyribonucleic acid

DNMT3a - DNA methyltransferase 3a

Dot1 - disruptor Of Telomeric silencing 1

dsDNA - double stranded DNA

ECL - enhanced chemiluminescence

EDTA - ethylenediaminetetraacetic acid

EtOH - ethanol

FACS - fluorescence-activated cell sorting

G1-phase - gap 1 phase

G2-phase - gap 2 phase

GFP - green fluorescent protein

GO - gene ontology

GW182 - glycine-Tryptophan Protein Of 182 kDa

H2A -histone H2A

H2B - histone H2B

H3 - histone 3

H3ac - histone 3 acetylation

H3K27ac - histone 3 lysine 27 acetylation

H3K27me3 - histone 3 lysine 23 tri-methylation

H3K36me3 - histone 3 lysine 36 tri-methylation

H3K36R- histone 3 lysine 36 arginine

H3K4 - histone 3 lysine 4

H3K4me2 - histone 3 lysine 4 di-methylation

H3K4me3 - histone 3 lysine 4 tri-methylation

H3K4R - histone 3 lysine 4 arginine

H3K56 - histone 3 lysine 56

H3K56A - histone 3 lysine 56 alanine

H3K56ac - histone 3 lysine 56 acetylation

H3K56Q - histone 3 lysine 56 glutamine

H3K56R - histone 3 lysine 56 arginine

H3K79A - histone 3 lysine 79 alanine

H3K9me3 - histone 3 lysine 9 tri-methylation

H3R2me2 - histone 3 arginine 2 di-methylation

H4 - histone 4

H4K12A - histone 4 lysine 12 alanine

H4K12ac - histone 4 lysine 12 acetylation

H4K16A - histone 4 lysine 16 alanine

H4K16ac - histone 4 lysine 16 acetylation

H4K16Q - histone 4 lysine 16 glutamine

H4K5A - histone 4 lysine 5 alanine

H4K5ac - histone 4 lysine 5 acetylation

HAT - histone acetyltransferase

HDAC - histone deacetylase

HKMT - histone lysine methyltransferase

HP1 - heterochromatin protein 1

iAID - improved Auxin-Inducible Degron

Ing1-5 - inhibitor Of Growth Protein 1-5

Jmjd6 - JmjC domain-containing protein 6

LB - lysogeny broth

Lsd1 - lysine-specific histone demethylase 1A

me1 - mono-methylation

me2 - di-methylation

me3 - tri-methylation

Mpt5 - multicopy suppressor of pop two

mRNA - messenger ribonucleic acid

Mst1 - mitochondrial aminoacyl-tRNA Synthetase, Threonine 1

Nanog - Homeobox Transcription Factor Nanog-Delta 48

ncRNA - noncoding RNA

NES - nuclear export signal

NLS - nuclear localization signal

Oct4 - octamer-binding transcription factor 4

Pab1 - poly(A) Binding protein 1

Pad4 - peptidyl arginine deiminase 4

Pan 2 - poly(A)-nuclease deadenylation complex subunit 2

Pan 3 - poly(A)-nuclease deadenylation complex subunit 3

P-body - processing body

PBS - phosphate-buffered saline

PCR - polymerase chain reaction

PEG - polyethylene glycol

PHD - plant homeodomain

poly(A) - polyadenylation

Pop2 - PGK promoter directed over production

PRC2 - polycomb Repressive Complex 2

PRMT - protein arginine N-methyltransferases

PTM - post-translational modification

Puf - pumilio homology domain

Pum1 - Pumilio RNA Binding Family Member 1

Pum2 - Pumilio RNA Binding Family Member 2

Rat1 - ribonucleic Acid Trafficking 1

RBD - recognition binding domain

RBDmut - RNA-binding domain mutant

RBP - rna binding protein

RNA - ribonucleic acid

RNAP I - rna polymerase I

RNAP II - rna polymerase II

RNA-seq - RNA sequencing

RNP - ribonucleoprotein

Rpl17b - ribosomal protein of the large subunit 2

r-protein - ribosomal protein

Rps16a - ribosomal protein of the small subunit 16a

Rps2 - ribosomal protein of the small subunit 2

Rps24b - ribosomal protein of the small subunit 24b

rRNA - ribosomal ribonucleic acid

Rtt106 - regulator of Ty1 Transposition 106

Rtt109 - regulator of Ty1 Transposition 109

S. cerevisiae - Saccharomyces cerevisiae

SD - synthetic defined (minimal media)

SDM - site-directed mutagenesis

SDS - sodium dodecyl sulfate

SDS-PAGE - sodium dodecyl sulfate–polyacrylamide gel electrophoresis

SET - su(var)3-9, Enhancer-of-zeste, Trithorax domain

SGA - synthetic genetic array

Snf5 - sucrose NonFermenting 5

Sox2 - SRY-Box Transcription Factor 2

S-phase - synthesis phase

Spt10 - suPpressor of Ty 10

SUnSET - surface sensing translation assay

t0 - time point zero

t240 - time point 240 minutes after treatment

t90 - time point 90 minutes after treatment

TBE buffer - Tris/Borate/EDTA buffer

TBST - tris-buffered saline, 0.1% Tween 20

TES - 2-[Tris-(hydroxymethyl)methylamino]-1-ethane sulfonic acid

TetOFF - tetracycline off

TOR - target of rapamycin

Ubc6 - UBiquitin-Conjugating 6

UMI - unique molecular identifiers

UTR - untranslated region

Wdr5 - WD repeat-containing protein 5

Xrn1 - exoribonuclease 1

YPD - yeast extract peptone dextrose

Commonly used abbreviations and SI units are not separately listed.

IV. Abstract

The flow of genetic information from DNA to mRNA, and subsequent translation of the mRNA into protein, is essential for cell survival. Both transcriptional regulation at the chromatin level and post-transcriptional regulation of mRNA turnover work in a dynamic and coordinated manner to maintain this flow and proper cell function. Although these two levels of regulation clearly control gene expression together, there is very little information about a specific connection between the two levels of control. Therefore, the aim of this study was to establish if such a connection exists. We used an H3K56A histone mutant as a screening candidate. This mutant prevents a well-researched lysine acetylation that is as an important contributor to the maintenance of chromatin architecture and transcriptional regulation in *Saccharomyces cerevisiae,* yet it does not cause significant changes in steady state mRNA levels. To identify potential links between chromatin-templated processes and post-transcriptional control, H3K56A was crossed against a genomic deletion library using the synthetic genetic array approach. This led to the identification of a synthetic lethal genetic interaction between the Pumilio-family protein Mpt5 and H3K56A. Mpt5 is a diverse RNA binding protein that can target around 16% of the yeast transcriptome and has been shown to promote both degradation and buffering of transcripts. Further investigation into the *MPT5*-H3K56A interaction shows that loss of H3K56 acetylation triggers changes to nascent transcription, and Mpt5 buffers against these changes by stabilizing transcripts in a context-dependent manner, thus ensuring balanced steady-state mRNA levels. Depletion of Mpt5 in an H3K56A background results in a loss of this buffering system, causing a significant decrease in Mpt5 targets. Strikingly, these targets are strongly enriched for ribosomal protein transcripts. The observed down-regulation of ribosomal protein genes leads to a strong decrease in translation efficiency and ultimately, cell cycle arrest. We also provide further evidence that the Mpt5-mediated buffering system extends to other disturbances to chromatin architecture. We show that loss of H3K4 methylation can also trigger Mpt5 buffering, but most likely through a different mechanism. Therefore, in this study, we identify a mechanism linking chromatin dependent transcriptional control and post-transcriptional regulation of mRNA through a context-dependent, mRNA buffering system that is crucial to proper cell function.

1 Introduction

A cornerstone of molecular biology is that cellular function revolves around the flow of information from DNA into functional forms of noncoding RNA and coding mRNA. This process of generating RNA from a DNA template is referred to as transcription, and it is essential for proper cell function and needs to be tightly regulated and controlled. Since transcription involves the production of a diverse range of transcripts, such as mRNAs and varying non-coding RNAs, this results in DNA templates with different features that not only need to be recognized, but transcribed at different rates based on cellular needs. Furthermore, once transcription has occurred, regulation of these transcripts does not stop, and post-transcriptional regulation is also essential for proper cell function. Therefore, the cell has numerous mechanisms to ensure proper and tight control of RNA abundance at both the transcriptional and post-transcriptional level.

1.1 Transcriptional regulation through histone modifications

An essential level of transcriptional control revolves around the underlying architecture and dynamics of chromatin and histone modifications. Chromatin is a dynamic structure consisting of DNA and associated histone and non-histone proteins. In order to fit the DNA within the confines of the nucleus in an individual cell, DNA is wrapped around proteins called histones, and the basic structural unit of DNA packaging in this manner can be defined as a nucleosome. Each nucleosome consists of DNA wrapped around eight core histone proteins, two copies each of H2A, H2B, H3, and H4 (Tessarz and Kouzarides, 2014). These nucleosomes, and more specifically, the tails and globular domains of the histones, are subject to a vast array of post-translation modifications (PTMs). By altering histone proteins with PTMs, chromatin structure can be altered to promote either closed or open chromatin, resulting in changes to DNA template access and regulation of transcription (Figure 1).

The specific effect on chromatin structure is dependent on the type and location of histone PTM. One of the most well-studied and important histone modifications in transcriptional regulation is histone methylation. Found on all the core histone proteins, the most common targets for histone
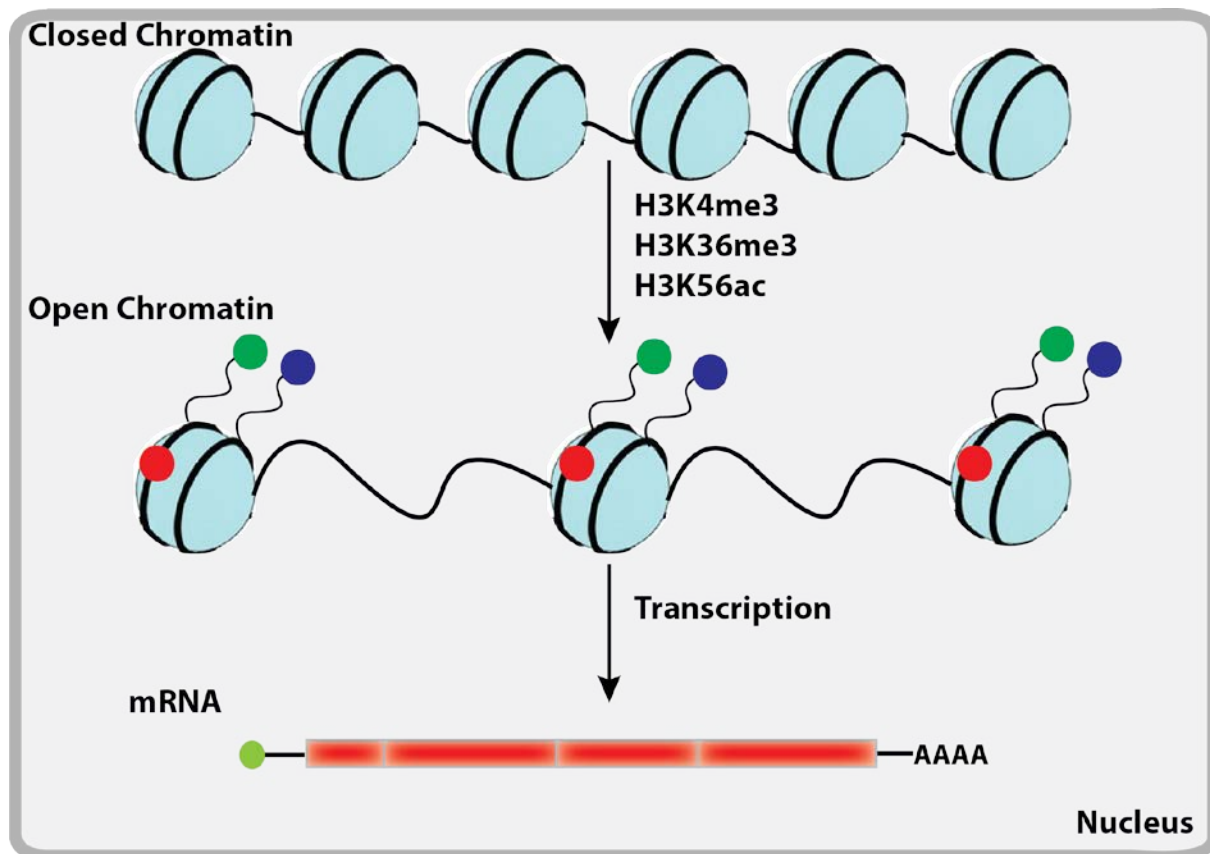
Figure 1: Regulation of chromatin structure and effect on transcription.
Schematic representation on the influence of post-translational histone modifications on chromatin structure and transcription. Specific histone modifications such as H3K4me3, H3K36me3, or H3K56ac influence chromatin structure by promoting a more open state, resulting in more access to the DNA template and transcription. The coloured dots correlate with the location of the histone modification on the histone protein, with the green and blue dots representing H3K4me3 and H3K36me3 on the histone tail, and the red dot representing H3K56ac on the globular part of the histone.

methylation are lysine (K) and arginine (R) residues (Jambhekar et al., 2019). Levels of histone methylation are precisely regulated by methyltransferases ("writers") and demethylases ("erasers") (Hyun et al., 2017; Jambhekar et al., 2019), and can exist in one of three states: mono- (me1), di- (me2), or tri-methylation (me3) (Bannister and Kouzarides, 2011). Arginine methylation can occur in me1 and me2 states, with me2 occurring in either a symmetrical or asymmetrical state (Bannister and Kouzarides, 2011). The writers responsible for arginine methylation are protein arginine N-methyltransferases (PRMTs) and these writers can be separated into two main classes, type 1 and 2. Both type-1 and type-2 PRMTs generate mono-methylated arginine, but type-1 and type-2 enzymes generate asymmetric and symmetric me2, respectively (Bannister and Kouzarides, 2011). The demethylation of arginine residues also occurs, and to date, two arginine erasers have been identified, Jmjd6 and Pad4 (Zhang et al., 2019). Jmjd6 directly converts a methylated arginine into arginine by directly removing the methyl group and is considered a traditional eraser (Zhang et al., 2019). On the other hand, there is debate whether Pad4 is a strict histone demethylase because it performs

2

demethylimination, which removes, but does not reverse the methylation state of arginine, resulting in the conversion of mono-methylated arginine to citrulline (Zhang et al., 2019). In terms of histone lysine methylation, it can occur in all three methylation states and is performed by histone lysine methyltransferases (HKMTs) (Bannister and Kouzarides, 2011). The vast majority of HKMTs, with the exception of Dot1 which methylates the globular domain of the histone, methylate the lysine residue on the N-terminal tail of the histone through the SET domain (Bannister and Kouzarides, 2011). Active removal of histone lysine methylation also occurs by erasers, with some lysine demethylases removing only specific states of lysine methylation, while others are capable of removing all three states. For example, LSD1 can either remove me1 or me2 lysine methylation if it is complexed with the Co-REST complex, or it can remove me3 in an androgen receptor manner (Bannister and Kouzarides, 2011). Taken together, the addition and removal of a methyl group on histone arginine or lysine residues is a very dynamic process that can encompass different methylation states and locations, and is highly regulated by a vast-array of writers and erasers.

In terms of a direct effect on chromatin structure, the addition of a methyl group to histones does not alter the electronic charge of the histone protein, resulting in no significant biochemical changes between the DNA and histone, and no direct changes to chromatin structure (Bannister and Kouzarides, 2011; Hyun et al., 2017). Therefore, histone methylation exerts its effect on chromatin and transcriptional regulation through the recruitment of downstream effector proteins. Although there is limited knowledge on effector proteins and arginine methylation, there is evidence of specific interplay between these proteins and this histone PTM. Tdrd3 has been shown to bind asymmetric me2 and promote transcriptional activation (Di Lorenzo and Bedford, 2011). There is also speculation that through its PHD domain, the de novo DNA methyltransferase DNMT3a can bind symmetrical arginine me2 and promote transcriptional repression (Di Lorenzo and Bedford, 2011). In terms of lysine methylation, many effector proteins have been identified and these proteins target different histone marks based on the methyl-lysine-binding motifs they contain. For example, tri-methylation of lysine 9 on histone 3 (H3K9me3) is performed by the methyltransferase Suv39 (Rea et al., 2000). This methylation mark results in the recruitment of heterochromatin protein 1 (HP1), a highly conserved effector protein that recognizes the methylation mark through its chromodomain binding motif (Nielsen et al., 2002). The recruitment of HP1 to H3K9me3 promotes the formation of closed chromatin and the repression of transcription. Another effector protein, Ing1-5 recognizes H3K4me3 through a PHD domain, which results in subsequent transcriptional activation (Champagne and Kutateladze, 2009). The methylation

state of H3K4 can also influence the effect it has on transcriptional regulation and the recruitment of proteins, with H3K4me2 resulting in a decrease in transcription through recruitment of the Set3 complex (Kim and Buratowski, 2009). Interestingly, H3K4me3 is often associated with promoting transcription in eukaryotes, but there appears to be a lack of a conserved mechanism to support this view (Howe et al., 2017). In alignment with this, one study argues that H3K4me3 mainly has a repressive role in transcription, and that this repressive role may be reversed with aging (Cruz et al., 2018). These types of findings align with the dynamic role of histone methylation, and show that a specific histone methylation mark can have a diverse role in transcriptional regulation. Furthermore, other histone marks can also indirectly effect H3K4me3 levels and influence transcription. H3R2me2 can impede the binding of the effector protein Wdr5 to H3K4me3 through interaction with its WD40 motif, and as a downstream effect, block the recruitment of transcriptional activators (Di Lorenzo and Bedford, 2011; Iberg et al., 2008). Therefore, a specific histone methylation site can promote and inhibit transcription through multiple mechanisms. Taken together, through the combination of methylation state and recruitment of effector proteins, histone methylation is a very fine-tuned PTM that can exert dynamic transcriptional regulation and influence numerous cellular processes.

Another prominent post-translational histone modification is histone acetylation. Found at only lysine amino acid residues, histone acetylation typically increases transcription because the addition of the acetyl group masks the positive charge of the lysine residue, resulting in a decreased affinity between the histone protein and DNA template (Barnes et al., 2019). Thus, in contrast to histone methylation, acetylation can change the biophysical properties of chromatin without the help of effector proteins. Acetylation at lysine residues is deposited by writers called histone acetyltransferases (HATs) and removed by erasers called histone deacetylases (HDACs), and the activity of HATs and HDACs can occur through both targeted and global mechanisms (Kurdistani and Grunstein, 2003). For example, as previously mentioned, lysine residues can undergo methylation, which can result in a competition between different chemical modifications. Therefore, target-specific H3K27ac results in an increase in transcription not only because of the acetyl mark, but also because it blocks the repressive H3K27me3 mark from being deposited (Tie et al., 2009). Other prominent histone acetylation marks include H4K5ac, H4K12ac, and H4K16ac. H4K5ac has been identified as a chromatin-based epigenetic bookmark, with its presence during interphase being maintained through mitosis, resulting in increased transcriptional kinetics in post-mitotic cells (Zhao et al., 2011). Loss of H4K12ac through depletion of the HAT Mst1, results in loss of chromatin

decompaction during meiosis, suggesting that H4K12ac plays a role in chromatin loosening during meiotic DNA replication (Ruan et al., 2015). In addition, both H4K5ac and H4K12ac are required for proper deposition of CENP-A, an H3 histone variant that is essential for proper centromere formation (Shang et al., 2016). Finally, H4K16ac is linked to cellular life span, with H4K16ac levels increasing with age and compromising transcriptional silencing at subtelomeric regions (Dang et al., 2009). Therefore, although histone acetylation typically promotes open chromatin and does not require the dynamic role of effector proteins, this histone PTM can still have a very diverse effect on cellular processes.

1.2 H3K56ac, a prominent histone mark that influences numerous cellular processes, including transcriptional regulation

Although most histone post-translational modifications occur on the histone tail, histone PTMs can also occur on the globular domain of a histone. One of the most studied globular histone marks is H3K56ac. This PTM has a profound effect on chromatin architecture. Located near the entry/exit site of DNA within the nucleosome, the presence of H3K56ac leads to enhanced "breathing" of the final 10 base-pairs of DNA within a nucleosome (Neumann et al., 2009). "Breathing" refers to unspooling of the DNA wrapped around the histone (Fierz and Poirier, 2019). In addition, H3K56ac has also been shown to regulate higher-order chromatin structure. Specifically, H3K56ac can strongly influence interactions between nucleosomal arrays, with its presence maintaining access to nucleosome-free regions for DNA replication and repair machinery (Watanabe et al., 2010). In alignment with this link to DNA replication and repair, levels of H3K56ac are regulated in a cell-cycle dependent manner, with peak acetylation occurring during S-phase and trough de-acetylation occurring during the G2-phase (Masumoto et al., 2005). One of the main defined roles for H3K56ac correlates with these high S-phase levels and involves a role in chromatin assembly following DNA replication (Li et al., 2008). The binding of newly synthesized H3/H4 dimers by the histone chaperone protein Asf1, results in the recruitment of the histone acetyltransferase Rtt109 and the acetylation of H3K56 (Recht et al., 2006). The presence of H3K56ac increases the affinity of CAF-1 and Rtt106 for the H3/H4 dimers, resulting in the rapid formation of H3/H4 tetramers and nucleosome formation on newly synthesized DNA (Li et al., 2008). This nucleosome assembly role for H3K56ac also extends to DNA damage. H3K56ac levels act as a signal that DNA repair is complete by triggering the formation of nucleosomes following the DNA damage response

(Costelloe and Lowndes, 2010). Loss of H3K56ac also results in sensitivity to genotoxic agents that cause DNA strand breaks (Masumoto et al., 2005), with this likely correlating to the decreased nucleosome assembly and increased exposure of the DNA. Therefore, these findings indicate that it is not just the presence or loss of H3K56ac that is important, but the fine-tuned switching between an acetylated and non-acetylated form based on specific cellular needs. Interestingly, although H3K56ac levels are globally abundant in yeast, this histone PTM appears to be very sparse in mammals and its impact in mammalian cells has been questioned (Xie et al., 2009). However, H3K56ac has been implicated in embryonic stem cell pluripotency, with its presence being a key regulator of pluripotency in both human and mouse embryonic stem cells. In humans, H3K56ac is involved in the core network of pluripotency revolving around Nanog, Sox2, and Oct4 (Xie et al., 2009), while in mice it promotes pluripotency by directly interacting with Oct4 (Tan et al., 2013). Taken together, it is clear that H3K56ac is a very dynamic histone modification that influences numerous cellular processes across different classes of eukaryotes.

The role of H3K56ac in transcriptional regulation has also been extensively investigated. As previously discussed, H3K56ac can promote nucleosome assembly following DNA replication. However, H3K56ac has also been shown to have the opposite effect by inducing promoter chromatin disassembly through Rtt109 and Asf1-dependent acetylation, with the presence of H3K56ac resulting in increased transcription (Williams et al., 2008). In alignment with these findings, another study found that H3K56ac is enriched in a target-specific manner at active genes and promotes transcription (Xu et al., 2005). Furthermore, another HAT, Spt10, is responsible for cell cycle-specific acetylation of H3K56 at histone genes, resulting in the recruitment of the nucleosome remodeling protein Snf5 and subsequent transcription (Xu et al., 2005). In addition, H3K56ac has been linked to regulation of transcription through the target of rapamycin (TOR) signaling pathway. Specifically, TORC1, a signaling branch of TOR that regulates transcriptional and translational processes necessary for growth and proliferation (Wullschleger et al., 2006), regulates acetylation of H3K56, and H3K56ac promotes RNAP I activity and increased transcription of rDNA (Chen et al., 2012). However, in contrast to these studies, which all show that H3K56ac promotes transcription, another study found that H3K56ac reduces transcriptional efficiency in a specific context. In eukaryotes, there is an mRNA synthesis lag that occurs on newly replicated genes, and this process has been termed expression homeostasis (Voichek et al., 2016). The deposition of H3K56ac on newly synthesized histones reduces transcription and promotes expression homeostasis (Voichek et al., 2016), with the suggested mechanism revolving around acetylation of H3K56 interfering

with post-replication recovery of H3K4me3 (Voichek et al., 2018). This role for H3K56ac in expression homeostasis also aligns with the previously discussed role in the promotion of nucleosome assembly following DNA replication, with formation of nucleosomes correlating with less access to the DNA template. Therefore, it seems that these divergent roles for H3K56ac in transcriptional regulation are influenced by specific dynamics, such as cell cycle progression. Nonetheless, it is clear that H3K56ac influences transcriptional regulation through many different avenues.

Surprisingly, although H3K56ac clearly plays a role in transcriptional regulation, its absence does not appear to have a significant effect on genome-wide steady state RNA levels (Topal et al., 2019). However, evidence is emerging that steady-state RNA levels are not the only important measure in gene expression, and that nascent transcription rate is crucial in investigating cellular function (Kirkconnell et al., 2016; Perez-Ortin et al., 2013; Wang et al., 2018b). A measure of *in situ* RNA production by RNA polymerase (Perez-Ortin et al., 2013), nascent transcription rate has been shown to strongly influence cellular processes. For example, nascent RNA can block repression of nearby transcripts by competing with chromatin for binding of repressive chromatin modifiers such as PRC2 (Skalska et al., 2017). Nascent RNA can also promote the expression of other genes by facilitating the transfer of transcription factors to nearby chromatin and inducing transcription (Skalska et al., 2017). The transcription rate of specific genes is highly regulated during the cell cycle, and fine-tuned regulation of nascent transcription is important in cell cycle progression (Liu et al., 2017). Interestingly, H3K56ac does influence nascent transcription, with its presence enhancing promoter nucleosome turnover and increasing genome-wide nascent transcription levels (Topal et al., 2019). Furthermore, the loss of H3K56ac may also promote more stable nucleosomes near the transcription termination site, thus promoting RNAP II stalling and/or blocking its release, and resulting in a lower transcription rate (Topal et al., 2019). Therefore, although loss of H3K56ac does not influence global steady state RNA levels, it does influence global nascent transcription, and these changes can have a significant effect on cellular function. Furthermore, in alignment with the previously discussed roles for H3K56ac in nucleosome assembly and transcription, it represses promiscuous transcription that occurs immediately following replication fork passage by promoting efficient nucleosome assembly (Topal et al., 2019). Therefore, the regulation of nascent transcription by H3K56ac echoes the previously discussed roles for this histone modification and the dynamic effects it can have on cellular processes.

1.3 Post-transcriptional control through RNA turnover

Another level of control in gene expression is the regulation of RNA abundance at the post-transcriptional level. Studies have shown a very low correlation between the level of transcription and the level of translation, and transcript levels are often not sufficient to predict protein levels (Liu et al., 2016). A major reason for this discrepancy between transcript and protein levels is due to post-transcriptional regulation of gene expression. Encompassing all avenues of regulation after RNA transcription, post-transcriptional regulation encompasses many dynamic processes and significantly influences cellular function (Figure 2).
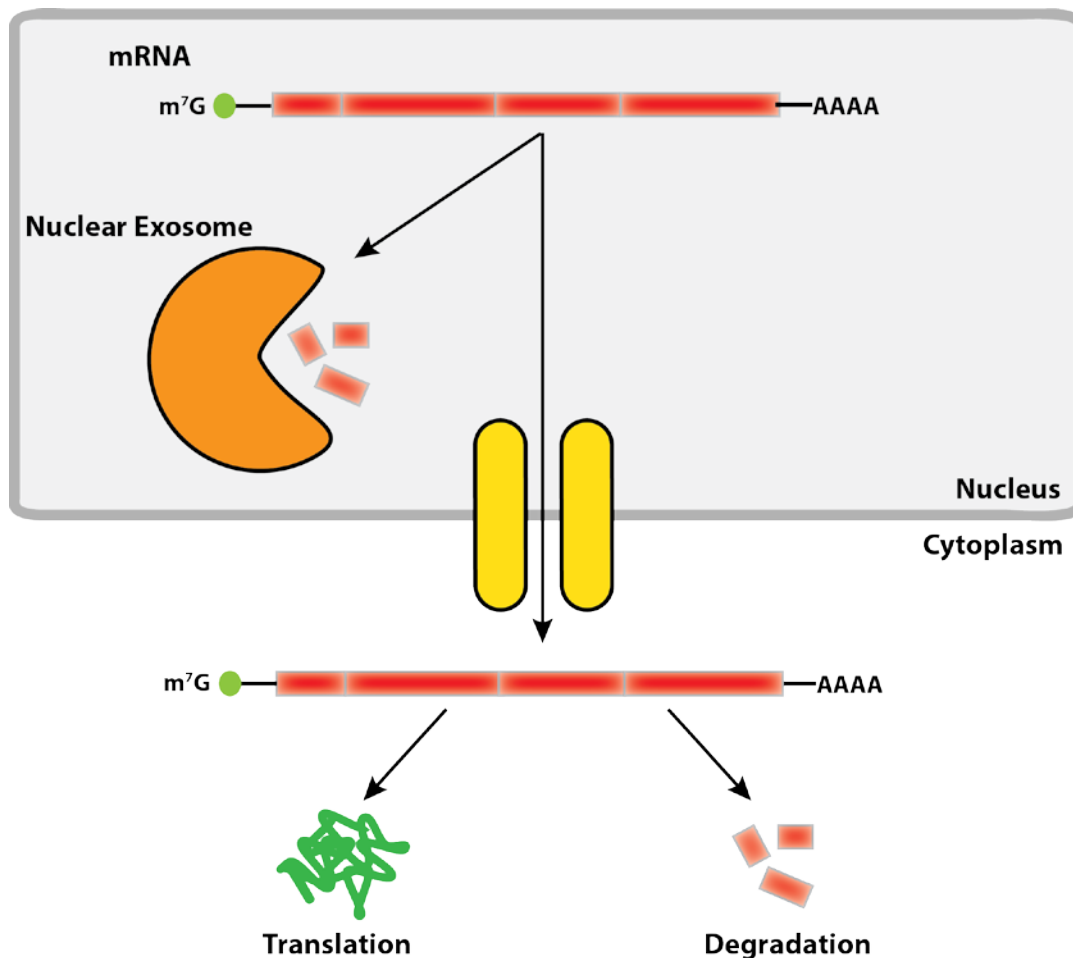
Figure 2: Basic overview of mRNA fate following transcription.
Schematic representation of the main post-transcriptional fates of mRNA. Transcribed mRNA can be degraded in the nucleus by the nuclear RNA-exosome, or it can be transported to the cytoplasm. Once in the cytoplasm, various post-transcriptional mechanisms create a balance between mRNA translation and degradation.

A major aspect of post-transcriptional regulation is the degradation of RNA. In eukaryotes there are two main degradation pathways: 3` to 5` decay through the RNA exosome, and 5` to 3` mRNA decay (Decker and Parker, 2002; Parker, 2012). The RNA exosome is a multisubunit molecular machine that acts on transcripts produced by RNA polymerases I, II, and III, and it can degrade RNA in both the nucleus and cytoplasm (Kilchert et al., 2016). On

the other hand, 5` to 3` decay occurs on mRNA transcripts and is triggered by the shortening (deadenylation) of 3` poly(A) tails (Mugridge et al., 2018; Parker, 2012). Following deadenylation, removal of the 5` 7-methylguanosine cap (decapping) occurs, which results in the subsequent decay of the mRNA in the 5` to 3` direction by exonucleases (Mugridge et al., 2018; Parker, 2012). In the nucleus, the major nuclease responsible for 5` to 3` RNA decay is Rat1 (Xiang et al., 2009), while the major cytoplasmic 5` to 3` exonuclease is Xrn1 (Parker, 2012). Interestingly, not only is mRNA decay linked to translation because it controls the abundance of transcripts, but there is also evidence of co-translational decay, with translation initiation and elongation kinetics strongly influencing mRNA decay (Mugridge et al., 2018). Therefore, 5` to 3` mRNA degradation serves as an important mechanism in controlling RNA quality and regulating gene expression in a post-transcriptional manner (Figure 3).
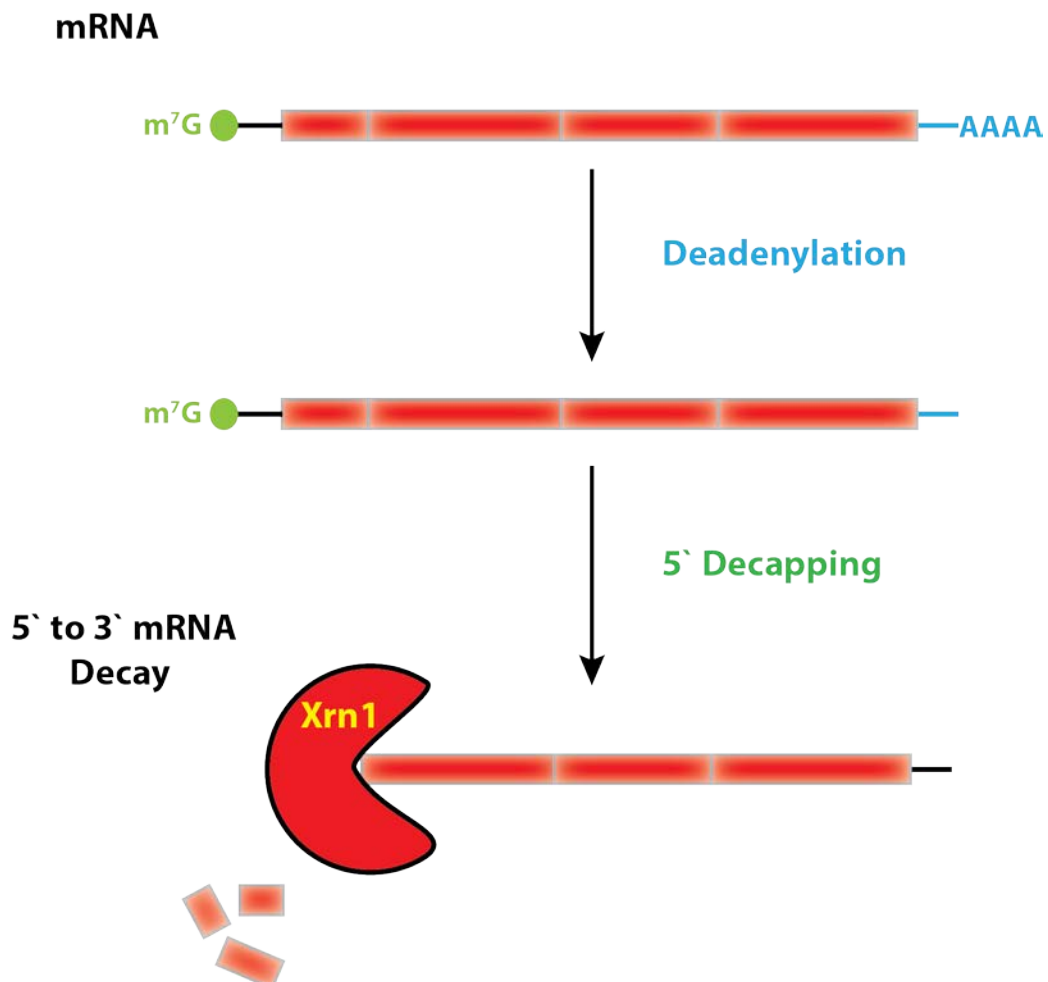
Figure 3: Overview of 5' to 3' mRNA decay.
Schematic representation of the main steps in 5` to 3` mRNA decay. Initiation of 5` to 3` decay begins with deadenylation of the 3` poly(A) tail of the mRNA (blue), which triggers the subsequent removal of the 5` 7-methylguanosine cap (green) through decapping. The mRNA is then degraded by 5` to 3` exonuclease activity by the exonuclease Xrn1.

1.4   The Ccr4-Not complex, a major regulator of mRNA turnover

As discussed, removal of the 3` poly(A) tail through deadenylation is the initial step in 5` to 3` mRNA decay, and therefore, it is crucial in the regulation of mRNA turnover. A multisubunit complex found in both the nucleus and cytoplasm, the Ccr4-Not complex is at the core of eukaryotic gene expression circuitry. Through its various protein subunits, this complex has been found to influence histone PTMs, regulate transcription initiation by interacting with transcription factors at promoters, regulate transcription elongation by rescuing backtracked RNAP II, and helping to preserve stalled translation (Collart, 2016; Collart and Panasenko, 2012; Villanyi and Collart, 2015). In addition to all these roles, Ccr4-Not is also a major deadenylation complex in all eukaryotes, and therefore, the trigger for downstream degradation of mRNA through 5` to 3` mRNA decay (Decker and Parker, 2002; Parker, 2012). Furthermore, the other major deadenylation complex in eukaryotes, Pan2/Pan3, has been found to selectively trim excessively long poly(A) tails and has little impact on mRNA stability and the transcriptome (Yi et al., 2018). Therefore, Ccr4-Not plays a major role in regulating mRNA turnover by being the predominant deadenylation complex in eukaryotes.

The two subunits of the Ccr4-Not complex responsible for deadenylation of mRNA are Ccr4 and Pop2. Both of these proteins have exonuclease activity, but Ccr4 removes Pab1 bound poly(A) tails, while Pop2 acts on transcripts that are Pab1-free and have low codon optimality (Webster et al., 2018). This distinct difference between the two exonucleases plays an important role in the balance between mRNA decay and the rate of translation. Pab1 binding to poly(A) tails promotes translation of mRNAs, and since only Ccr4 exonuclease activity can act on Pab1bound poly(A) tails, increased Pab1 binding causes a shift towards less deadenylation, and by extension less mRNA decay (Webster et al., 2018). On the other hand, low Pab1 binding results in more exposed poly(A) tails that can be removed by both Ccr4 and Pop2 activity, resulting in a shift towards less translation and more deadenylation and subsequent mRNA decay (Webster et al., 2018). Furthermore, the mRNAs with a low frequency of optimal codons are decoded more slowly by the ribosome during translation when compared to transcripts with a high frequency of optimal codons (Mugridge et al., 2018). The lower codon optimality correlates with increased binding by the 5` decapping protein Dhh1 and faster mRNA decay (Mugridge et al., 2018). Therefore, Pop2 activity helps to maintain this low translation rate by promoting mRNA decapping through removal of the poly(A) tail in transcripts with low codon optimality. Through these various nuances, the deadenylation of mRNAs is not only important in maintaining mRNA quality, but also crucial in maintaining a balance between mRNA decay

and translation rate. However, although Ccr4-Not plays a crucial role in mRNA decay and the regulation of gene expression, there is a lack of evidence that Ccr4-Not promotes generic decay. Instead, evidence points towards targeted mRNA decay and the recruitment of Ccr4-Not to the 3` untranslated regions (UTRs) of mRNAs (Collart and Panasenko, 2012), thus indicating another layer in the post-transcriptional regulation of mRNA turnover.

1.5 RNA binding proteins, an added layer to post-transcriptional regulation

RNA binding proteins (RBPs) play a crucial role in the post-transcriptional regulation of gene expression by influencing mRNA transport, decay, and translation. The association of RBPs with mRNAs is very important in proper cell function and can be strongly influenced by the cells response to stress or environmental cues (Alves and Goldenberg, 2016). One of the most diverse classes of RNA binding proteins are the evolutionarily conserved Pumilio (Puf) proteins. The Puf family of proteins are sequence-specific, RNA-binding proteins that can target a diverse range of RNA transcripts and influence multiple cellular processes. In *S. cerevisiae*, there are six different Puf proteins, and these proteins mainly target the 3` UTR of mRNAs by recognizing a 5`-UGUA tetranucleotide sequence and a 3`UA nucleotide sequence (Wilinski et al., 2015). However, the binding domain of the Puf proteins also includes a variable length spacer region in between these 5` and 3` nucleotide sequences, with the length of this recognition sequence ranging between 8 to 11 nucleotides and varying between mRNAs (Wilinski et al., 2015). Furthermore, different Puf proteins can target varying RBD lengths based on the curvature of the specific protein, resulting in both mRNA target overlap and target separation between the different Puf proteins (Gerber et al., 2004; Lapointe et al., 2017; Wilinski et al., 2015). Interestingly, this variability in the spacer sequence of the RBD also correlates with different biological functions of the target RNA (Figure 4). For example, RNA targets with a recognition sequence of 9, 10, and 11 nucleotides are linked to ribosome biogenesis, gene expression, and translation, respectively (Wilinski et al., 2015). This correlation then extends to the different Puf proteins and the type of cellular processes they influence. For example, Puf1 and Puf2 have a high-affinity for mRNAs linked to the plasma membrane, Puf3 shows a very high-affinity for mRNAs linked to mitochondria, and Puf4 targets are linked to the nucleolus and ribosome biogenesis (Gerber et al., 2004; Lapointe et al., 2017). Through this type of RNA targeting, the Puf proteins share target overlap, but at the same time target a distinct class of RNAs that influence specific cellular functions.
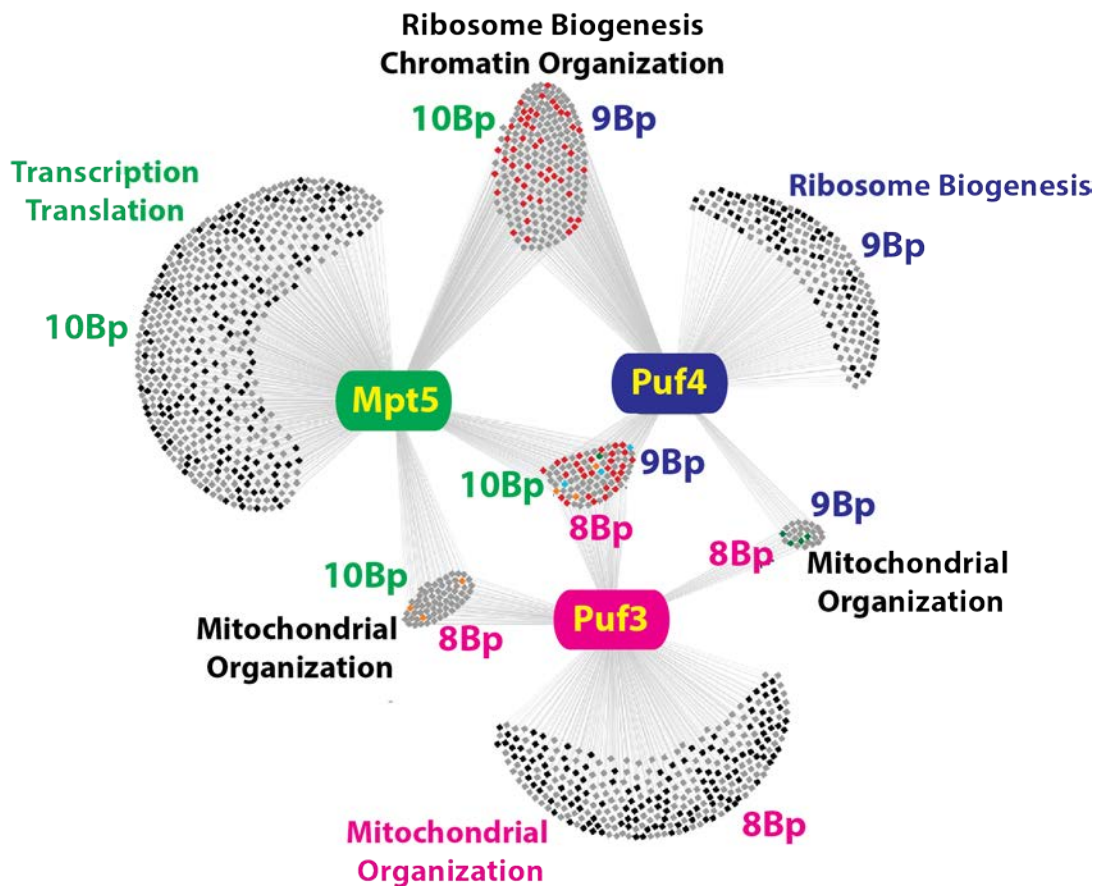
Figure 4: Overview of Puf proteins and the link between the length of their recognition sequence and target transcript function.
Overview showing the link between the length of the recognition sequence and function of the target transcript for Puf3 (pink), Puf4 (purple), and Mpt5 (green). All recognition sequences are given based on base pair (Bp) length and colour coordinated to the specific Puf protein. Target transcript function is based on Gene Ontology enrichment, and font colour is also coordinated to the specific Puf protein. Gene Ontology terms given in black font indicate transcript targets that are not exclusive to a single Puf protein. Each box represents a single target transcript. Image retrieved and modified from (Lapointe et al., 2017).

1.6 Mpt5, a robust RNA binding protein with a diverse role in mRNA turnover

Of all the Puf proteins found in *S. cerevisiae*, the most diverse in terms of RNA targets and potential function is Puf5/Mpt5. Crystal structures of Mpt5-RNA complexes have revealed that Mpt5 presents an exceptionally flat and extended interaction surface compared to the other Puf proteins, allowing it to recognize a longer spacer sequence and resulting in the ability to target 16% of the entire yeast transcriptome (Wilinski et al., 2015). More specifically, Mpt5 has a very high affinity for RNA targets coding for proteins linked to transcription and chromatin organization, the cytoskeleton, ribosome biogenesis, and translation (Gerber et al., 2004; Lapointe et al., 2017). As mentioned previously, evidence points towards a target-specific mechanism for Ccr4-Not deadenylation. For example, microRNA machinery has been shown

to promote recruitment of Ccr4-Not, with the binding of Argonaute to target mRNA triggering recruitment of the GW182 protein and subsequent target-specific Ccr4-Not deadenylation (Collart, 2016). Interestingly, Mpt5 has also been identified as a targeting protein for the Ccr4-Not complex. Specifically, Mpt5 promotes Ccr4 deadenylation and subsequent mRNA decay, but the interaction between Mpt5 and the Ccr4-Not complex is also dependent on Pop2, which acts as a bridging protein between Mpt5 and Ccr4-Not (Goldstrohm et al., 2006; Goldstrohm et al., 2007). Therefore, given the lack of evidence for a generic deadenylation mechanism in Ccr4-Not activity, these findings point towards Ccr4-Not deadenylation being dependent on targeting by RNA binding proteins. Furthermore, Ccr4-Not is a very robust deadenylation complex, which strongly correlates with the diverse mRNA targeting of Mpt5.

Although Mpt5 has been linked to Ccr4-Not and the promotion of deadenylation, it has also been implicated in promoting buffering against mRNA decay. A recent study has shown that upon glucose deprivation, Mpt5 shuttles mRNA to processing bodies (p-bodies) in a target specific manner (Wang et al., 2018a). P-bodies are cytoplasmic ribonucleoprotein (RNP) granules mainly composed of translationally repressed mRNAs and mRNA decay related proteins (Luo et al., 2018). Formed through liquid-liquid phase separation, p-bodies are very dynamic structures that can form and disassemble within seconds (Moon et al., 2019), and represent another layer of post-transcriptional control of RNA abundance (Figure 5) (Decker and Parker, 2012; Luo et al., 2018). Although the exact role of p-bodies has not yet been determined, evidence suggests that p-bodies act as a "buffer zone," in which mRNAs can be transported and stored. P-bodies can also give rise to another form of cytoplasmic RNPs that store nontranslating mRNAs called stress granules (Figure 5). However, unlike p-bodies, which contain mRNA decay proteins, stress granules contain many translation initiation components, indicating a "buffer zone" geared towards subsequent translation of mRNAs (Decker and Parker, 2012). Therefore, Mpt5-mediated transport of mRNAs to P-bodies highlights the diverse role Mpt5 can play in post-transcriptional regulation of mRNA. Furthermore, Mpt5 has been shown to be an upstream activator of the cell wall integrity pathway (CWI), which is the main source for maintaining cell wall homeostasis under stress conditions (Stewart et al., 2007). Interestingly, p-body assembly is linked to the activation of the CWI pathway, and mRNAs whose expression is regulated by this pathway also localize to p-bodies after the cell is exposed to stress (Garcia et al., 2019). Therefore, this identifies another link between Mpt5 and p-body assembly, and supports the notion that under cell stress conditions, Mpt5 activity can switch in a context-dependent manner and promote the buffering of mRNA abundance instead of mRNA decay.
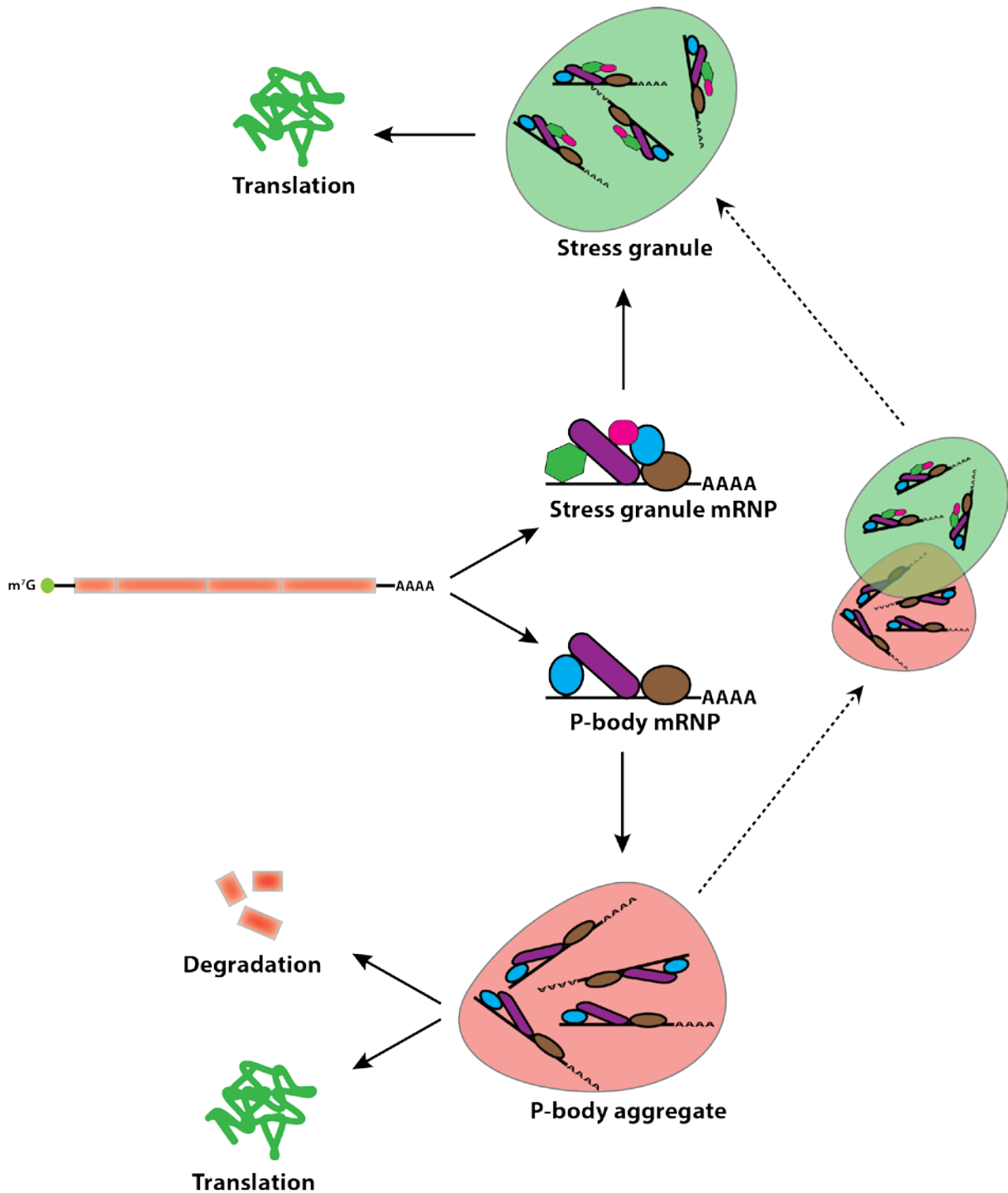
Figure 5: Role of p-bodies and stress granules in post-transcriptional regulation of mRNA.
Schematic representation of p-body and stress granule dynamics in post-transcriptional regulation of mRNA. Following transcription, mRNA can form p-body or stress granule mRNA-ribonucleoprotein (mRNP) complexes, resulting in the subsequent formation of p-bodies and stress granules through liquid-liquid phase separation, respectively. P-bodies can then trigger either subsequent degradation or translation of the mRNA, while stress granules can trigger subsequent mRNA translation. In addition, stress granule formation can occur directly from p-bodies (dashed lines).

2 Aims of the study

As discussed thus far, the control of gene expression relies heavily on both transcriptional and post-transcriptional mechanisms (Figure 6). Transcriptional control of gene expression is heavily influenced by the dynamic regulation of chromatin, with histone modifications playing a crucial role in regulating transcription and influencing numerous cellular processes. Post-transcriptional control of gene expression involves multiple avenues, and revolves around controlling mRNA abundance through deadenylation-induced decay, which can be influenced by other post-transcriptional mechanisms. Interestingly, a potentially significant overlap between chromatin and post-transcriptional regulation of gene expression may exist. Surprisingly however, there is very little literature that links chromatin based processes and post-transcriptional control pathways.

Although H3K56ac is an abundant, genome-wide histone modification that can significantly influence access to the DNA template, a disconnect exists in how such a robust and dynamic histone modification can clearly influence transcriptional processes, yet not cause any significant changes to steady state RNA levels (Rege et al., 2015; Topal et al., 2019). Rege et al. shed some light on this discrepancy by identifying a link between H3K56ac and the RNA exosome, indicating that global transcriptional roles for H3K56ac are masked by the nuclear RNA exosome (Rege et al., 2015). However, the interaction between H3K56ac and the nuclear RNA exosome was limited to the removal of cryptic unstable transcripts (CUTs), a class of divergently transcribed ncRNAs that are rapidly degraded upon their transcription (Rege et al., 2015). Furthermore, there was no proposed mechanistic link between H3K56ac and CUTs, or any identified phenotypic consequences in the cell due to changes in this H3K56ac-CUT relationship. To our knowledge, this is the only study that tries to establish a link between chromatin deregulation and post-transcriptional regulation of gene expression. Therefore, there is a clear gap in the literature in terms of linking transcriptional control at the chromatin level with post-transcriptional turnover of mRNA, especially in a biologically significant context.
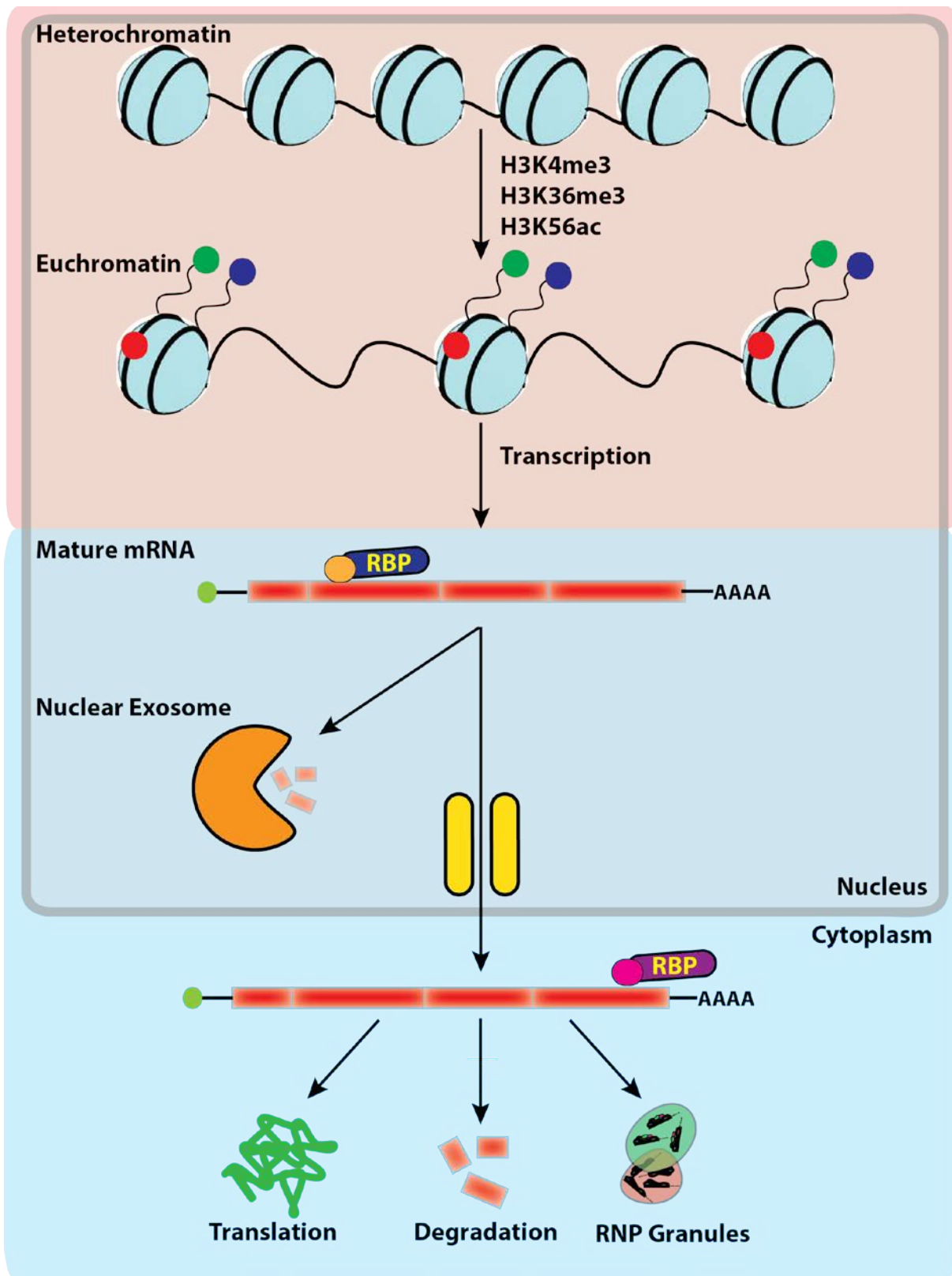
Figure 6: Overview of transcriptional and post-transcriptional regulation of mRNA levels.
Schematic representation of the discussed transcriptional (red box) and post-transcriptional (blue box) mechanisms responsible for regulation of mRNA levels.

In order to fill this gap, the first aim of this study was to identify a connection between transcriptional control at the chromatin level with post-transcriptional regulation of mRNA in *S. cerevisiae*. The focus was placed on the H3K56ac histone modification because of its diverse role in transcriptional regulation and because changes to H3K56ac do not correlate with changes to steady state RNA levels. Loss of H3K56ac was used as a probe to identify potential links to post-transcriptional regulators of gene expression. After significant genetic interactions to post-transcriptional regulators were identified, the second aim of this study was to unravel the mechanistic underpinnings involved in the identified genetic interactions. Through this approach, the goal of the study was to identify and elucidate a specific mechanistic link between H3K56ac and post-transcriptional regulation of mRNA, and thus provide a framework that connects chromatin based processes and post-transcriptional control pathways.

3 Results

3.1 Identification of a synthetic lethal *MPT5*-H3K56 genetic interaction

There is a vast array of evidence in previous literature showing that histone modifications and post-transcriptional mechanisms play a critical role in the control of gene regulation (Bannister and Kouzarides, 2011; Lawrence et al., 2016; Parker, 2012). However, there is very little evidence bridging these two-levels of control in a specific and direct context, with only one report suggesting specific crosstalk between histone modifications and the nuclear RNA exosome (Rege et al., 2015). Therefore, the goal of this study was to bridge transcriptional and post-transcriptional regulation of gene expression in a specific and direct context. Due to a lack of evidence, an initial high-throughput approach was required and a synthetic genetic array (SGA) was utilized. An SGA is an unbiased, systematic method that involves crossing a haploid yeast strain containing a specific mutation of interest, with an array of haploid single deletion mutants, resulting in heterozygous diploid double deletion mutants that are then separated through selective growth to identify haploid double mutant strains (Costanzo et al., 2013). The growth of the haploid double mutant strains is then compared to the growth of the array of haploid single deletion mutants to identify if cell fitness has changed in the presence of both mutations, thus allowing for the identification of specific genetic interactions and correlation to biological functions and processes (Costanzo et al., 2013). In this study, an SGA was conducted by combining an *S. cerevisiae* strain lacking H3K56ac due to an H3K56A mutation, with a single, gene knockout library, thus investigating potential genetic interactions between deregulation of transcription at the histone level with specific gene knockouts (Figure 7A) (SGA conducted by Dr. Julia Mawer). Based on the analysis of the SGA results, 174 synthetic sick growth phenotypes were identified when the H3K56A mutation was combined with single gene knockouts. In order to find patterns or links between all the identified genetic interactions and their influence on cell function, Gene Ontology (GO) enrichment analysis was performed through Metascape (Ashburner et al., 2000; Zhou et al., 2019). Based on the 174 growth phenotypes, maintenance of DNA trinucleotide repeats, cell
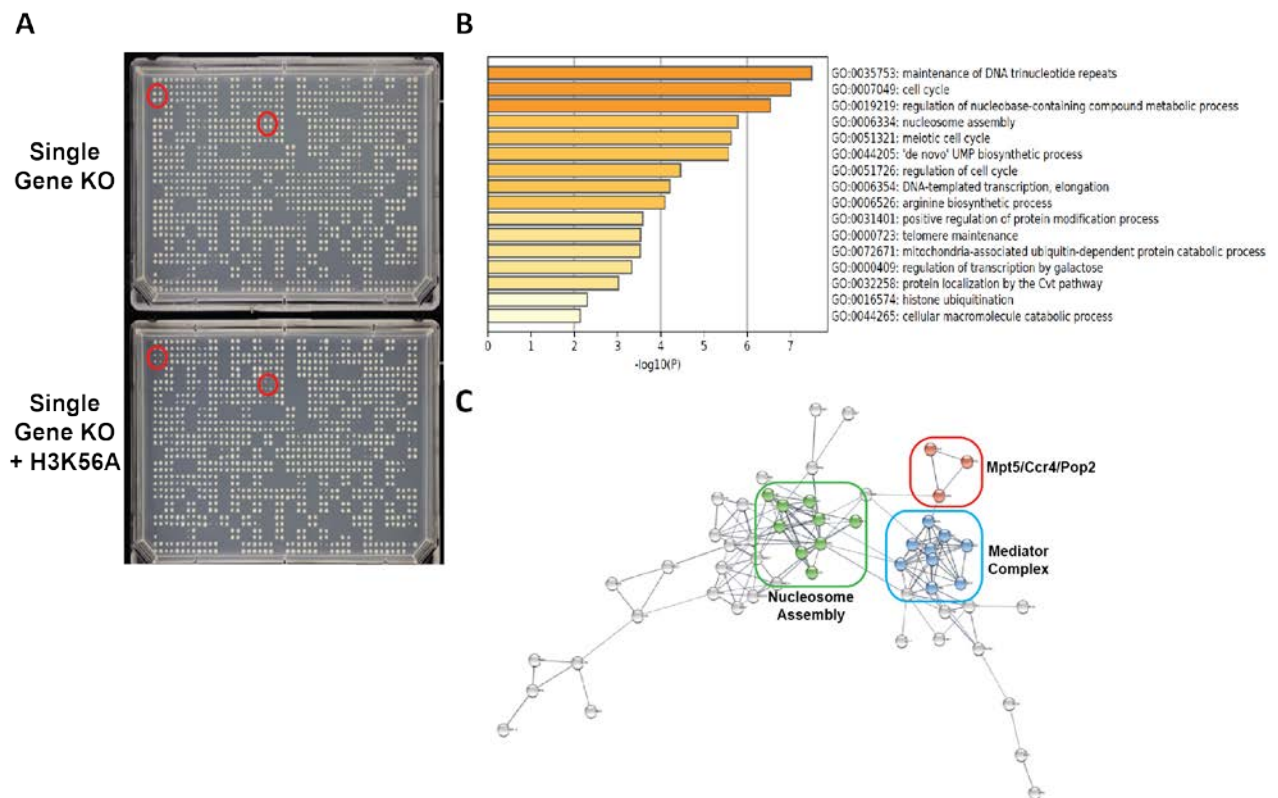
Figure 7: Synthetic Genetic Array (SGA) identifies genes that are synthetically sick in combination with an H3K56A mutation in *S. cerevisae*.
(A) Sample plate-combination from SGA. Top plate represents *S. cerevisiae* single gene knockout library, bottom plate represents single gene knockout library combined with an H3K56A mutant strain. The red circles represent corresponding strains between plates, spotted in quadruplicate. **(B)** Gene Ontology terms generated using Metascape for all 174 synthetic sick growth phenotypes identified from the SGA analysis. **(C)** Protein association network generated using STRING based on all 174 synthetic sick growth phenotypes identified from the SGA analysis. Each node represents an individual protein. The green and blue nodes represent proteins associated with nucleosome assembly and mediator complex GO-terms, respectively. The red nodes represent Ccr4, Pop2, and Mpt5 proteins. String analysis was conducted at the high interaction confidence interval (0.7).

cycle, and nucleosome assembly were identified as the top GO-terms (Figure 7B), while some of the top GO-terms based on STRING analysis were nucleosome assembly and mediator complex (Figure 7C) (Szklarczyk et al., 2019). Furthermore, outside of the GO-term analyses, an observation was made that proteins associated with the Ccr4-Not complex, specifically Mpt5, Ccr4, and Pop2, resulted in synthetic sick growth phenotypes and were present in the STRING analysis (Figure 7C). Since the goal of the SGA was to identify a potential link between transcriptional and post-transcriptional control of gene expression, the most interesting candidates from the SGA analysis were determined to be the genes associated with the Ccr4-Not complex.

Both Ccr4 and Pop2 are integral parts of the Ccr4-Not complex (Webster et al., 2018; Yi et al., 2018), and although not part of the Ccr4-Not complex, Mpt5 acts as a crucial targeting protein for Ccr4-Not (Goldstrohm et al., 2006; Goldstrohm et al., 2007). To verify and investigate the synthetic sick growth phenotypes associated with these genes at a higher

19

resolution, serial dilution spot tests were conducted in independently constructed strains (Figure 8). Based on analysis of the serial dilution spot tests, *mpt5Δ* and H3K56A individual mutant strains showed a very slight growth phenotype relative to the Wt strain (Figure 8A). However, when the two mutations were combined in an *mpt5Δ*/H3K56A double mutant strain, the genetic interaction resulted in a synthetic lethal phenotype (Figure 8A). Since it is not just the loss of H3K56ac that can influence cellular function, but the ability to switch between an acetylated and non-acetylated form, an *MPT5* knockout was combined with a constitutively acetylated form of H3K56ac (H3K56Q) (Masumoto et al., 2005), and the *mpt5Δ*/H3K56Q double mutant strain also produced a synthetic lethal phenotype (Figure 8A). Furthermore, since the *MPT5*-H3K56 genetic interaction produced a synthetic lethal phenotype, it was important to independently verify that the genetic interaction was not being caused by unforeseen effects that went beyond acetylation of H3K56, such as drastic structural changes due to the substitution of the lysine amino acid for an alanine or glutamine. Therefore, an *MPT5* knockout was combined with an H3K56R mutation, which also represents loss of H3K56ac but through a more biochemically similar amino acid to lysine (Masumoto et al., 2005). Serial dilution spot tests of the *mpt5Δ*/H3K56R double mutant strain independently verified the lethal phenotype (Figure 8A). Taken together, these results indicate a synthetic lethal *MPT5*-H3K56 genetic interaction that not only revolves around the loss of H3K56ac, but also around the dynamic nature of being able to switch between an acetylated and non-acetylated form of H3K56.

In terms of the *CCR4* gene, a *ccr4Δ* strain produced a slight growth phenotype, while a *ccr4Δ*/H3K56A double mutant strain produced a synthetic sick growth phenotype (Figure 8B). The *ccr4Δ*/H3K56Q double mutant strain also produced a synthetic sick growth phenotype, but it is significantly healthier when compared to the *ccr4Δ*/H3K56A double mutant strain (Figure 8B), thus indicating that in the *CCR4*-H3K56 genetic interaction, loss of H3K56ac may play a more prominent role. In terms of the *POP2* gene, neither the *pop2Δ* strain, the *pop2Δ*/H3K56A double mutant strain, nor the *pop2Δ*/H3K56Q double mutant strain produced a growth phenotype when compared to the individual mutations (Figure 8C). Based on the results of these serial dilution spot tests, it would appear that the *MPT5*-H3K56 genetic interaction does not revolve around promoting Ccr4-Not complex activity. First, if the *MPT5*-H3K56 genetic interaction was dependent on promoting Ccr4 activity, then the observed growth phenotypes generated in the *mpt5Δ*/H3K56A and *ccr4Δ*/H3K56A double mutant strains should be reversed, or the same, because Mpt5 acts upstream of the Ccr4-Not complex. Second, Pop2 not only has catalytic activity as part of the Ccr4-Not complex (Webster et al., 2018; Yi et al., 2018), but it
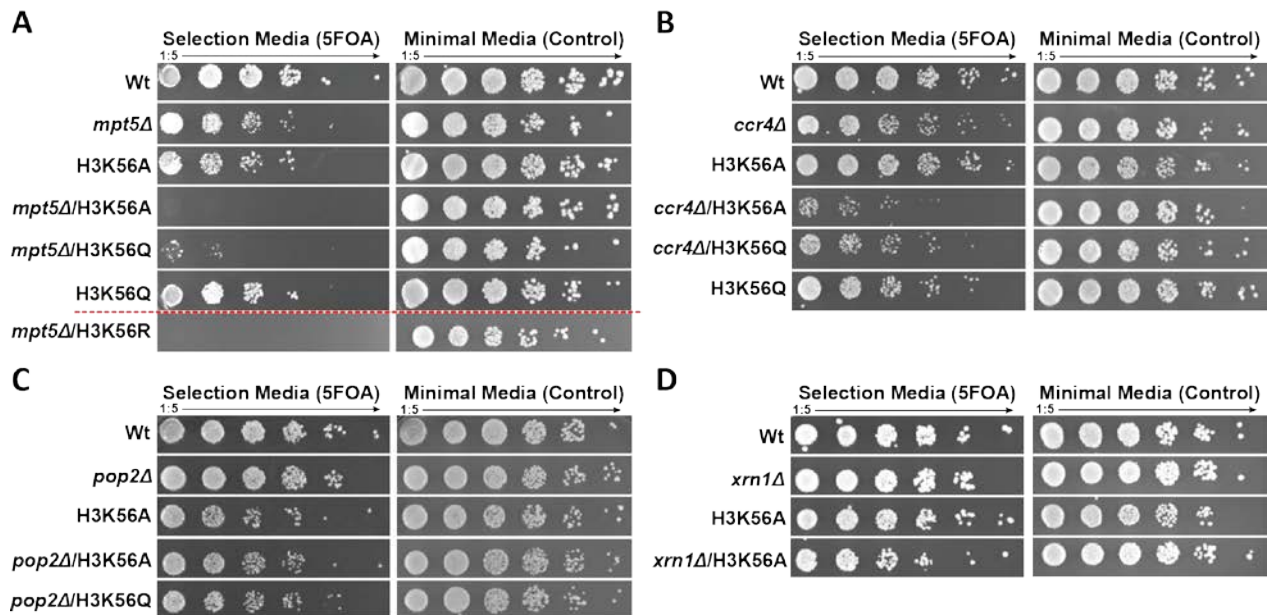
Figure 8: Serial dilution spot tests confirm a synthetic lethal phenotype between *MPT5* and H3K56 that appears to be Ccr4-Not independent.
(A) Serial dilution spot test showing a synthetic lethal phenotype between *mpt5Δ* and H3K56A, H3K56Q, and H3K56R mutations. The dashed red line indicates a spot test from a separate plate. **(B)** Serial dilution spot test showing a synthetic sick phenotype and a mild growth phenotype between *ccr4Δ* and H3K56A and H3K56Q mutations, respectively. **(C)** Serial dilution spot test showing no genetic interaction between *pop2Δ* and H3K56A and H3K56Q mutations. **(D)** Serial dilution spot test showing a slight growth phenotype between *xrn1Δ* and an H3K56A mutation. For all individual spot tests shown, the left image represents growth on 5FOA selection media and the right image represents growth on minimal control media. All spot tests were performed following a 1:5 serial dilution from left to right.

has also been identified as the only bridging protein between Mpt5 and Ccr4-Not (Goldstrohm et al., 2006; Goldstrohm et al., 2007). However, the *pop2Δ*/H3K56A and *pop2Δ*/H3K56Q mutant strains produce no growth phenotypes (Figure 8C), thus further indicating that the observed *MPT5*-H3K56 genetic interaction likely does not revolve around promoting Ccr4-Not activity.

Since the Ccr4-Not complex is linked to downstream mRNA degradation through its deadenylation of poly-A tails (Parker, 2012; Yi et al., 2018), investigation into the genetic interaction between degradation machinery and H3K56 was also warranted. Following deadenylation by the Ccr4-Not complex, and subsequent 5` end decapping, one of the major catalysts of mRNA degradation is the evolutionarily conserved 5`-3` exonuclease, Xrn1 (Boehm et al., 2016). Therefore, serial dilution spot tests were conducted to investigate the genetic interaction between *XRN1* and H3K56A, and the results show that the *xrn1Δ* single mutant strain produced no growth phenotype, while the *xrn1Δ*/H3K56A double mutant strain produced a very slight growth phenotype (Figure 8D). Since Xrn1 has been linked to Ccr4-Not activity and it produced only a mild genetic interaction with H3K56A, this even further

indicates that the *MPT5*-H3K56 genetic interaction does not revolve around promoting Ccr4-Not activity.

Unfortunately, in this instance, the combination of an SGA and serial dilution spot tests cannot distinguish whether the *MPT5*-H3K56 and *CCR4*-H3K56 genetic interactions involve separate or overlapping pathways because of the overlap between Mpt5 and Ccr4-Not activity. However, if it is the same pathway, then the different growth phenotypes highlight specific nuances and mechanisms within the pathway in relation to Mpt5 and Ccr4 activity. In either case though, it is clear that *MPT5* presence plays a more crucial role in the described genetic interactions with H3K56ac because it produces the most severe phenotype.

3.2 Mpt5 presence does not influence genome-wide histone acetylation levels

Based on existing literature, there is a proposed link between Mpt5 and chromatin related GO-terms based on Mpt5-RNA target studies (Lapointe et al., 2017; Wilinski et al., 2015). However, there is no direct evidence on the influence of Mpt5 presence on chromatin structure or histone modifications genome-wide. Therefore, to investigate whether Mpt5 directly influences chromatin structure, genome-wide H3ac levels, which correlate to overall open chromatin structure, and genome-wide H3K56ac levels were measured through ChIP-seq analysis in Wt and *mpt5Δ* strains (Figure 9). Since there was no significant difference in the total number of peak counts for H3ac and H3K56ac between the Wt and *mpt5Δ* strains (Figure 9A), this indicates no experimental bias when comparing the two datasets. Analysis of peak count frequency relative to the Transcription Start Site for either H3ac or H3K56ac levels resulted in no significant difference due to *mpt5Δ* (Figure 9B), indicating no difference in the distribution of H3ac and H3K56ac levels. Analyzing the Wt and *mpt5Δ* strain genome tracks, also further confirmed no significant difference in H3ac and H3K56ac levels, and identified no difference in H3 levels due to the presence of Mpt5 (Figure 9C).

Furthermore, a chromatin immunoprecipitation was also attempted for an Mpt5-Myc tagged strain (data not shown). However, the pulldown was unsuccessful, indicating that barring any technical limitations in the attempted immunoprecipitation, Mpt5 does not appear to have any direct interaction with chromatin. Taken together, this indicates that Mpt5 presence does not influence genome-wide histone acetylation or H3 levels, and therefore, it is unlikely that Mpt5 directly influences chromatin architecture on the level of H3 occupancy and H3 acetylation.
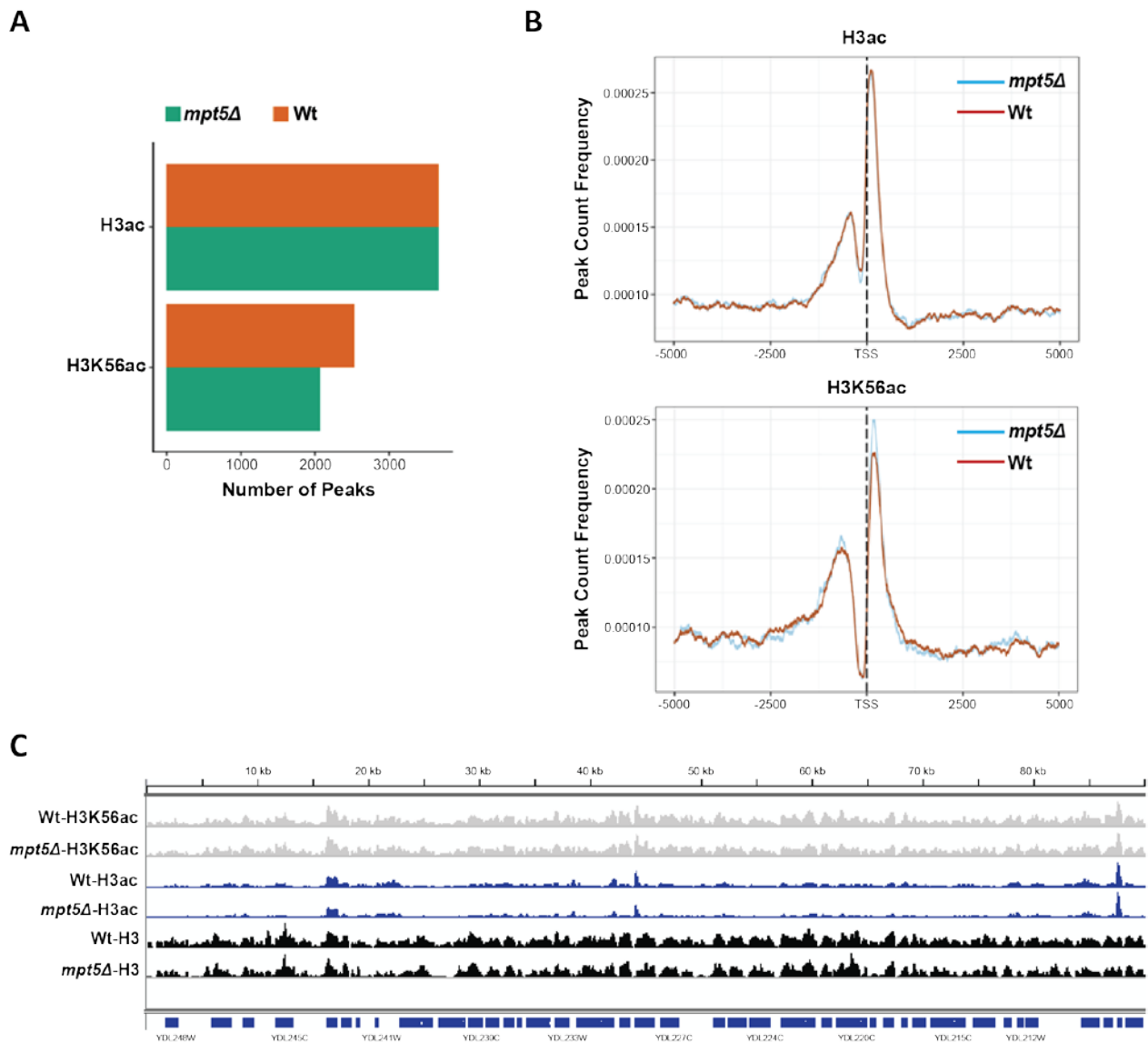
Figure 9: ChIP-seq analysis identifies no significant changes genome-wide in H3ac and H3K56ac levels due to *mpt5Δ*.
(**A**) Comparison of the total number of peaks between Wt and *mpt5Δ* strains for H3ac and H3K56ac (N=2). (**B**) Comparison of peak count frequency between Wt and *mpt5Δ* strains for H3ac (upper image) and H3K56ac (lower image) relative to the transcription start site (TSS) (N=2). (**C**) Snap shot of genome tracks (~90 kb) showing H3K56ac (light grey), H3ac (blue), and H3 (black) peaks between Wt and *mpt5Δ* strains. Genome tracks were generated using Integrative Genomics Viewer.

3.3 Mpt5 cytoplasmic localization and RNA-binding are crucial in the observed *MPT5*-H3K56 genetic interaction

Mpt5 has been found to be present in both the nucleus and the cytoplasm, and both nuclear and cytoplasmic functions for Mpt5 have been proposed (Gerber et al., 2004; Kennedy et al., 1997; Wang et al., 2018a). Therefore, investigation into whether nuclear or cytoplasmic activity of Mpt5 is important in the observed *MPT5*-H3K56 genetic interaction would provide valuable insight. To address this, strains expressing Mpt5 tagged with a nuclear localization

23

signal (NLS) or a nuclear export signal (NES) were generated following guidelines from previous literature (Kosugi et al., 2008). To verify if the localization tags were functioning properly, GFP-tags were also incorporated into the localization-tagged strains and microscopy images were taken to visualize Mpt5 localization (Figure 10A). The Mpt5-GFP/H3K56A strain did not produce any GFP signal in either the nucleus or the cytoplasm, while the Mpt5-NLS-GFP/H3K56A strain generated a GFP signal in the nucleus (Figure 10A), indicating a functioning NLS-tag. The reason there was no visible GFP signal in the Mpt5-GFP/H3K56A strain could be due to the number of Mpt5 molecules per cell being significantly lower when compared to the average number of molecules per cell for other proteins in *S. cerevisiae* (http://www.yeastgenome.org; Ho et al., 2018). Furthermore, large-scale analysis across multiple datasets has also shown that a C-terminal GFP tag can lower the level of protein molecules per cell even further (Ho et al., 2018). Therefore, the signal in the Mpt5-GFP/H3K56A strain may not be strong enough to detect, while in the Mpt5-NLS-GFP/H3K56A strain, the Mpt5-GFP signal is concentrated into the nucleus and therefore a signal is visible.

Next, to investigate whether Mpt5 cellular localization plays a role in the *MPT5*-H3K56 genetic interaction, serial dilution spot tests were performed in the Mpt5 localization strains (Figure 10B). Based on analysis of the serial dilution spot tests, neither the Mpt5-NLS or Mpt5-NES strains showed a growth phenotype relative to the Wt strain (Figure 10B), indicating that Mpt5 localization by itself has no influence on cell growth. However, when the localization tagged strains were combined with an H3K56A mutation, the Mpt5-NES/H3K56A strain produced no growth phenotype, while the Mpt5-NLS/H3K56A strain produced a significantly sick growth phenotype (Figure 10B). This indicates that specific cellular localization is important in the observed *MPT5*-H3K56 genetic interaction and that cytoplasmic Mpt5 activity plays a crucial role.

Since Mpt5 is a robust RNA-binding protein (Wilinski et al., 2015), it was also important to determine if Mpt5 RNA binding ability played an important role in the *MPT5*-H3K56 genetic interaction. Therefore, an Mpt5 RNA-binding domain mutant (RBDmut) was generated by substituting two amino acids in the Mpt5 RNA binding domain (Goldstrohm et al., 2006). Serial dilution spot tests were then performed to investigate if Mpt5 RNA binding influenced the *mpt5Δ*/H3K56A lethal phenotype. As expected, when the *mpt5Δ*/H3K56A double mutant strain was transformed with a plasmid containing a wild-type Mpt5 ORF insert, the synthetic lethal phenotype was rescued (Figure 10C). However, when the *mpt5Δ*/H3K56A double mutant strain was transformed with a plasmid containing the Mpt5-RBDmut insert, there was no rescue of the synthetic lethal phenotype (Figure 10C).
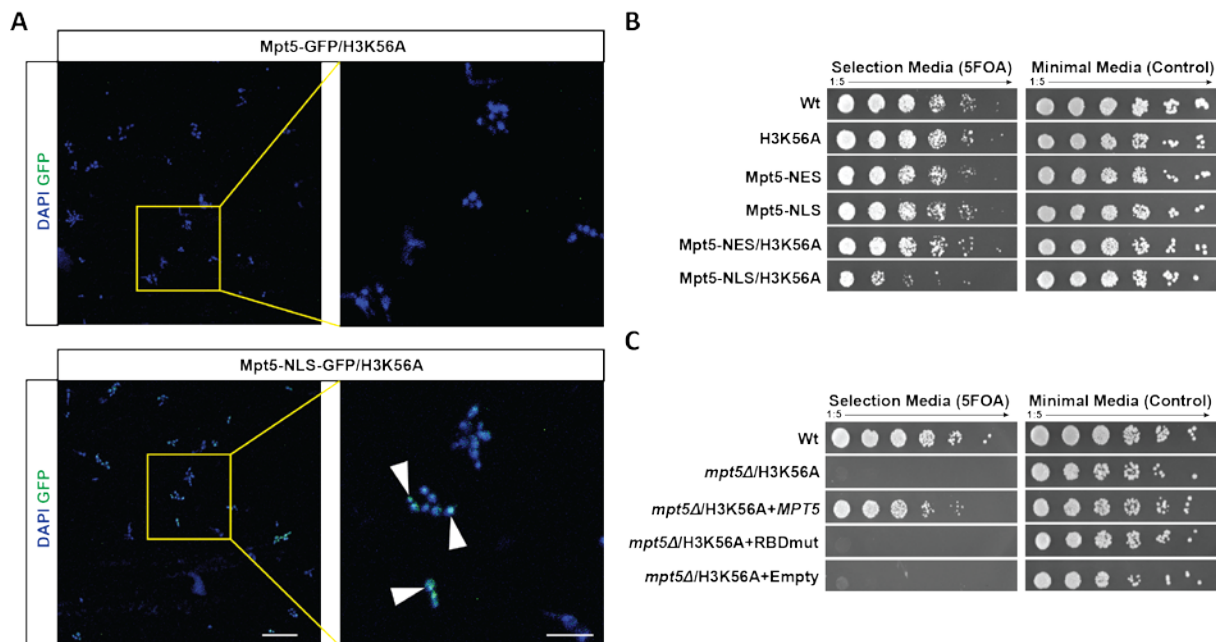
Figure 10: Mpt5 cellular localization and Mpt5 RNA-binding play an important role in the observed *MPT5*-H3K56 genetic interaction.
(A) Overview images (left) and detailed images (right) of Mpt5-GFP tagged strains. The upper images represent the Mpt5-GFP strain without a localization signal and the lower images represent the Mpt5 nuclear localization signal (NLS) tagged strain. Yellow insets in overview images indicate regions of detailed images. White arrow heads indicate nuclear localization of Mpt5-NLS-GFP protein. Scale bar 50 μm (overview image) and 20 μm (detailed image). **(B)** Serial dilution spot test showing the effect of Mpt5 cellular localization on the Mpt5-H3K56A growth phenotype. NLS denotes nuclear localization signal and NES denotes nuclear export signal. **(C)** Serial dilution spot test showing the effect of Mpt5 RNA binding on the *mpt5Δ*/H3K56A growth phenotype. The + denotes the transformation of a pRS413 expression plasmid into a *mpt5Δ*/H3K56A strain with either a Mpt5 ORF insert, a Mpt5-RNA binding domain mutant (RBDmut) insert, or no insert (empty). For all individual spot tests shown, the left image represents growth on 5FOA selection media and the right image represents growth on minimal control media. All spot tests were performed following a 1:5 serial dilution from left to right.

Taken together with the previous results, this indicates that Mpt5 cytoplasmic activity, in combination with Mpt5 RNA binding, are crucial in the observed *MPT5*-H3K56 genetic interaction.

3.4 Improved Auxin Inducible Degron (iAID) system as a tool to investigate the *MPT5*-H3K56 genetic interaction

So far, the results have pointed towards a cytoplasmic, post-transcriptional role for Mpt5 that revolves around Mpt5 RNA binding. To investigate the molecular underpinnings for the synthetic defect in an unbiased manner, we wanted to investigate gene expression changes upon Mpt5 depletion in an H3K56A background. Since an *mpt5Δ*/H3K56A strain is not viable, we needed an approach to induce depletion of Mpt5 while minimizing off-target effects. Therefore, an Improved Auxin Inducible Degron (iAID) system, which allows for gene-specific transcriptional shut-off in combination with target specific protein degradation, was applied

(Tanaka et al., 2015). Since there are no commercially available antibodies for Mpt5 in *S. cerevisiae*, the iAID-Mpt5 construct was created with an N-terminal AID-tag and a C-terminal Myc-tag (Figure 11A). Through this design, Mpt5 protein levels could be detected using different antibodies at both terminal ends, thus ensuring accurate detection of Mpt5 protein. Upon exposure of the iAID-Mpt5/H3K56A strain to 40 μg/mL doxycycline and 1 mM auxin, significant Mpt5 degradation was observed after 60 min (Figure 11B). However, despite this, no significant growth phenotype was present in the iAID-Mpt5/H3K56A strain relative to the single mutant strains (Figure 11C). This absence of an expected growth phenotype in the presence of significant protein degradation has also been identified in previous literature and can be explained because of a "tight phenotype," which refers to a phenotype that can only be observed following very stringent depletion of target protein levels (Tanaka et al., 2015). Since there was still a very small amount of Mpt5 protein remaining and it appeared to be preventing the induction of a growth phenotype (Figure 11B and C), a doxycycline pre-treatment was implemented to overcome the iAID-Mpt5/H3K56A tight phenotype and a framework was generated for investigation into Mpt5 depletion in an H3K56A background (Figure 11D). This approach not only resulted in increased degradation of Mpt5 protein levels (Figure 11E), but also generated an iAID-Mpt5/H3K56A growth phenotype relative to the single mutant strains (Figure 11F and G). Therefore, despite the lack of a lethal phenotype in the iAID-Mpt5/H3K56A strain, a significant iAID-Mpt5/H3K56A growth phenotype can be observed, providing a valid tool to investigate the effect of Mpt5 depletion in an H3K56A background, and by extension, a means to investigate the *MPT5*-H3K56 genetic interaction.
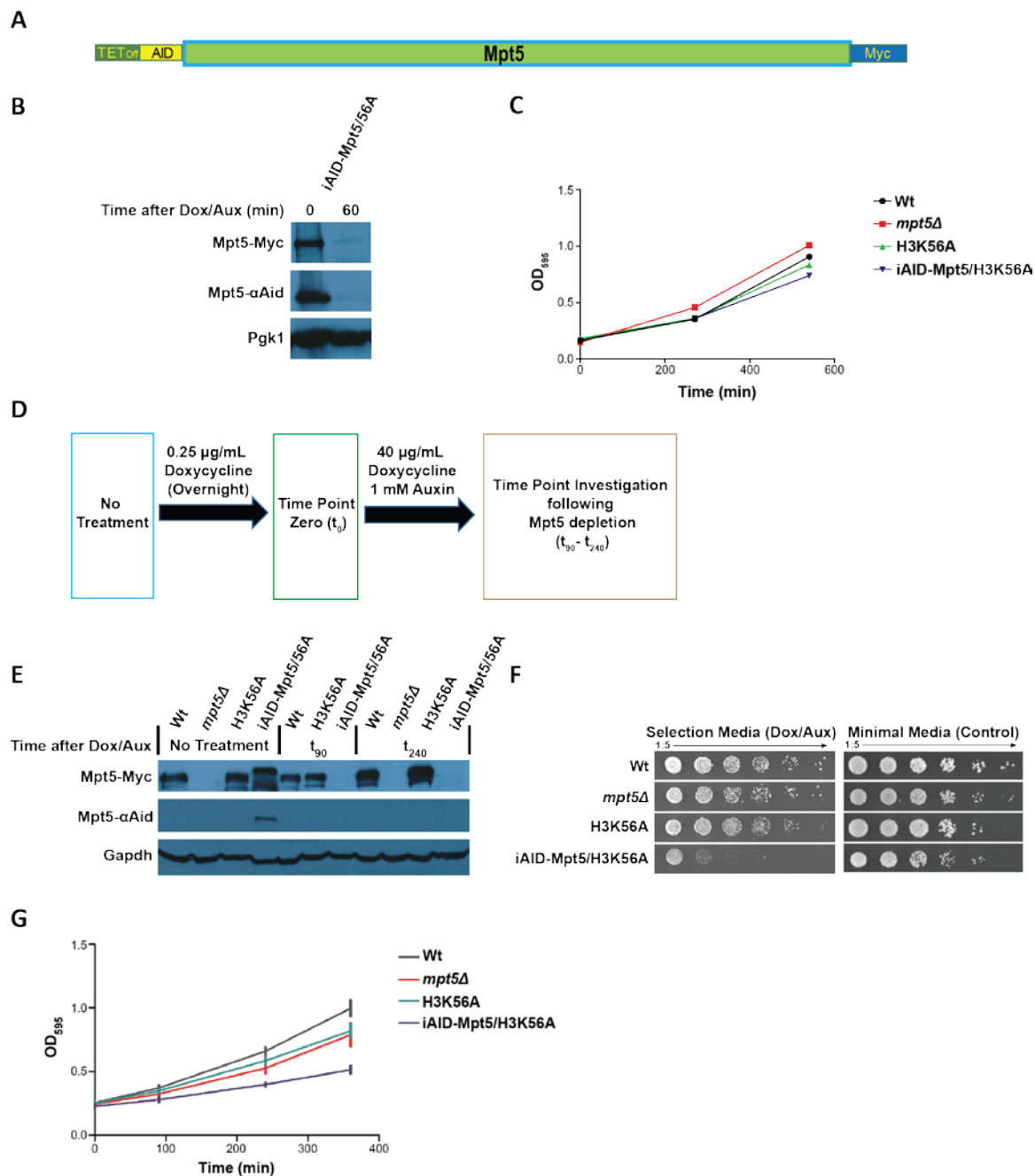
Figure 11: Improved Auxin Inducible Degron (iAID) system as a tool to investigate the synthetic lethal *mpt5Δ*-H3K56A phenotype.
(**A**) Schematic representation of the iAID design with regards to the Mpt5 ORF. (**B**) Western blot analysis of Mpt5 protein levels in the iAID-Mpt5/H3K56A strain following the addition of 40 μg/mL doxycycline and 1 mM Auxin. The first two panels represent Mpt5 protein levels detected through a Mpt5-Myc tag and AID tag, and the bottom panel represents the loading control via Pgk1 protein levels. (**C**) Growth curve of Wt, *mpt5Δ*, H3K56A, and iAID-Mpt5/H3K56A strains following addition of 40 μg/mL doxycycline and 1 mM auxin. The y-axis represents OD_{595} measurements and the x-axis represents time in minutes (min). (**D**) Schematic of the treatment parameters to induce an iAID-Mpt5/H3K56A growth phenotype. Colored boxes represent sample extraction time points for further analysis. (**E**) Western blot analysis of Mpt5 protein levels following the treatment parameters in (D). The first two panels represent Mpt5 protein levels detected through a Mpt5-Myc tag and AID tag, and the bottom panel represents the loading control via Gapdh protein levels. (**F**) Serial dilution spot test showing the iAID-Mpt5/H3K56A growth phenotype after plating from t_0 in (D). The left image represents growth on 40 μg/mL doxycycline and 1 mM auxin selection media and the right image represents growth on minimal control media. The spot test was performed following a 1:5 serial dilution from left to right. (**G**) Growth curve of Wt, *mpt5Δ*, H3K56A, and iAID-Mpt5/H3K56A strains following the treatment parameters depicted in (D). The y-axis represents OD_{595} measurements and the x-axis represents time in minutes (min); N = 6; Error bars = 95% CI.

27

3.5 Depletion of Mpt5 in an H3K56A background results in a decrease of Mpt5-target mRNAs linked to cytoplasmic translation

To investigate the effect of Mpt5 depletion in an H3K56A background, the iAID-Mpt5/H3K56A strain was utilized and 3`-end RNA-seq was performed. Since different mutant strains and treatment conditions were involved in this process (Figure 11D and G), an investigation into the experimental design parameters relative to the gene expression changes was warranted (Figure 12). First, all strains were compared in terms of gene expression changes before any addition of doxycycline or auxin (No Treatment group). As expected from previous bulk-RNA-seq results (data not shown), the *mpt5Δ* strain showed the most significant change in gene expression relative to the Wt strain, while the H3K56A strain showed no significant change in gene expression relative to the Wt strain (Figure 12A). Importantly, the gene expression profile of the iAID-Mpt5/H3K56A strain showed no significant difference relative to the Wt and H3K56A strains (Figure 12A). Moreover, both the iAID-Mpt5/H3K56A and H3K56A strain showed similar changes in gene expression when compared to the *mpt5Δ* strain (Figure 12A). Therefore, these results indicated that the iAID construct had no effect on Mpt5 function because there was no significant difference in gene expression between the iAID-Mpt5/H3K56A and H3K56A strain before depletion of Mpt5. Since multiple treatment conditions were used and all the strains were exposed to doxycycline and auxin, it was also important to investigate what effect this had on the different strains. Based on the analysis, only the iAID-Mpt5/H3K56A strain showed a significant change in gene expression after exposure to doxycycline and auxin (Figure 12B). This indicates that the presence of doxycycline and auxin only influenced gene expression in the strain with an active iAID-Mpt5 construct, and that any changes in gene expression were not due to any negative effect from the treatment conditions. In terms of the gene expression changes within the iAID-Mpt5/H3K56A strain due to the treatment conditions, No treatment vs. exposure to doxycycline and auxin for 240 min (t240) resulted in the most significant changes in gene expression (Figure 12C). Furthermore, these gene expression changes correlated with the depletion of Mpt5 at both the transcriptional and post-transcriptional level in the iAID-Mpt5/H3K56A strain. Specifically, *MPT5* transcript levels significantly decreased following pre-treatment with doxycycline, but this change did not result in significant changes in gene expression, and further exposure to a higher concentration of doxycycline did not result in a more significant decrease in *MPT5* transcript levels (Figure 12C and D). However, the decrease in *MPT5* transcript levels (Figure 12D), in combination
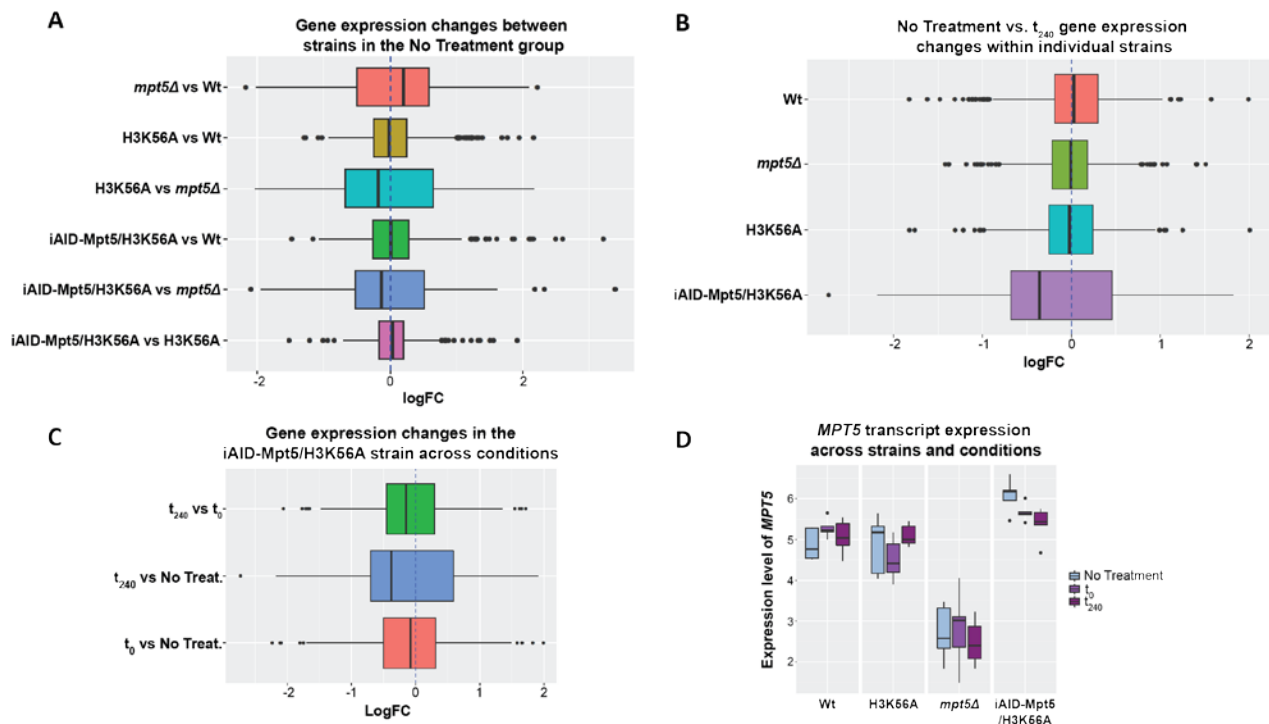
Figure 12: RNA-seq analysis reveals that the observed gene expression changes in the iAID-Mpt5/H3K56A strain are due to a decrease in *MPT5* expression.
(A) Comparison of log fold changes of all genes between all strains, Wt, *mpt5Δ*, H3K56A, and iAID-Mpt5/H3K56A before any treatment (No Treatment). **(B)** Comparison of gene expression log fold changes within individual strains across the treatment parameters (No Treatment vs t_{240}). **(C)** Comparison of log fold changes of all genes within the iAID-Mpt5/H3K56A strain across the treatment conditions. **(D)** Comparison of *MPT5* transcript levels between the different strains and treatment parameters. Treatment parameters define the steps used to induce the iAID-Mpt5/H3K56A growth phenotype: No Treatment (no doxycycline or auxin), t_0 (overnight 0.25 µg/mL doxycycline), t_{240} (240 min after 40 µg/mL doxycycline and 1 mM auxin).

with the observed decrease in Mpt5 protein levels (Figure 11E), resulted in the most significant changes in gene expression in the iAID-Mpt5/H3K56A strain (Figure 12C). Taken together with the previously discussed results (Figure 12), this indicates that the observed gene expression changes in the iAID-Mpt5/H3K56A strain are not due to any experimental design parameters, but due to the depletion of Mpt5 in an H3K56A background.

Since the identified gene expression changes were due to depletion of Mpt5 in an H3K56A background, we then wanted to investigate these changes in the context of cellular function. Since the H3K56A strain showed no significant changes in overall gene expression relative to the Wt strain, but the *mpt5Δ* strain did (Figure 12A), it was also important to investigate the effects of *MPT5* knockout in a normal H3K56ac background to identify any potential overlap compared to the iAID-Mpt5/H3K56A strain. Therefore, Metascape analysis was conducted on all differentially expressed genes in the *mpt5Δ* strain (Figure 13). Some of the top upregulated GO-terms identified were DNA integration, cytoplasmic translation, ribosome biogenesis, and chromatin organization (Figure 13A); while some of the top downregulated GO-terms were oxidation-reduction process, and carbohydrate metabolic and

A

B
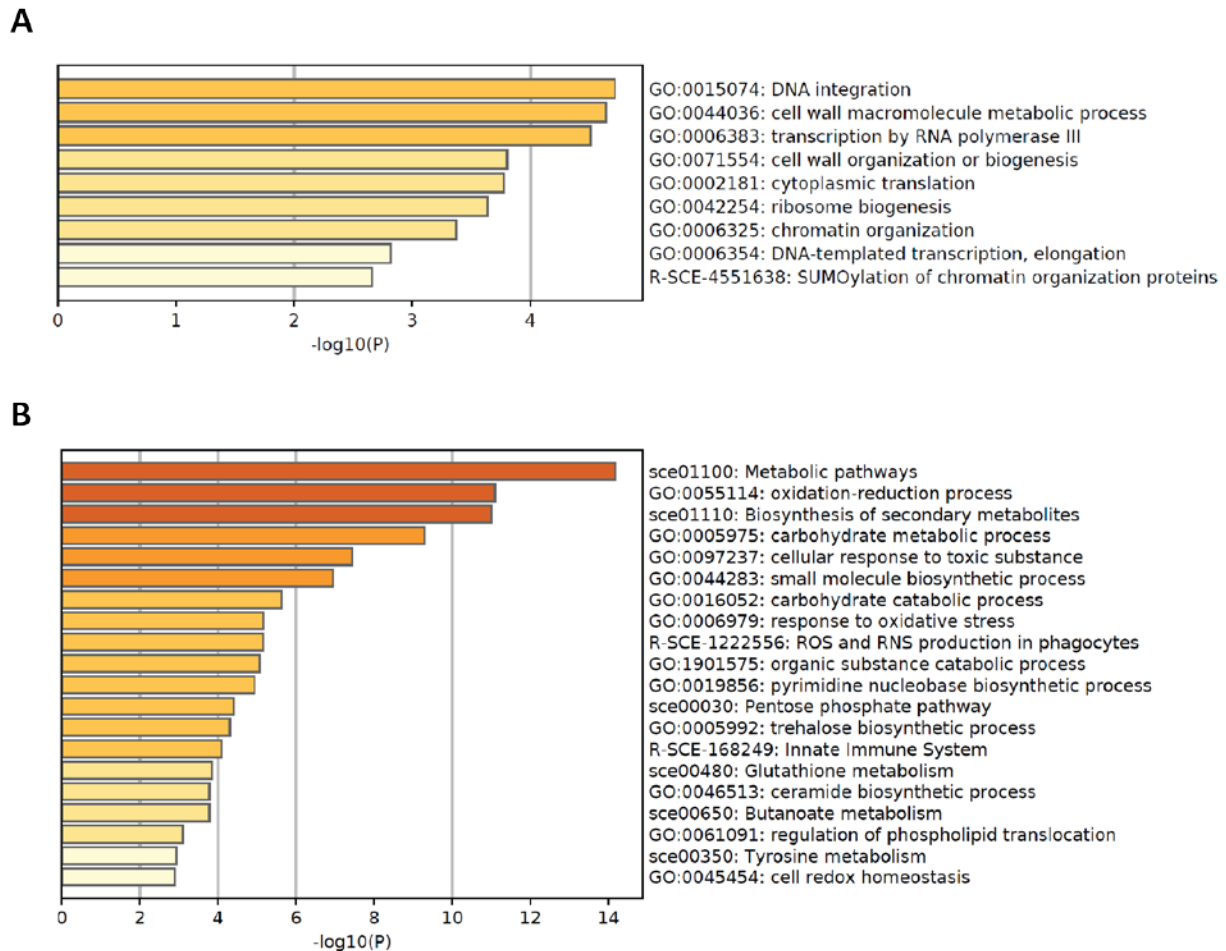
Figure 13: *mpt5Δ* results in significant gene expression changes in a wild-type H3K56ac background.
(A) Gene Ontology terms generated using Metascape for all upregulated genes in the *mpt5Δ* strain relative to the Wt strain at t_{240} of the treatment parameters. **(B)** Gene Ontology terms generated using Metascape for all downregulated genes in the *mpt5Δ* strain relative to the Wt strain at t_{240} of the treatment parameters. Treatment parameters define the steps used to induce the iAID-Mpt5/H3K56A growth phenotype: No Treatment (no doxycycline or auxin), t_0 (overnight 0.25 μg/mL doxycycline), t_{240} (240 min after 40 μg/mL doxycycline and 1 mM auxin).

catabolic process (Figure 13B). In terms of the iAID-Mpt5/H3K56A strain, in total, 238 genes were significantly upregulated, while 410 genes were significantly downregulated following depletion of Mpt5 (Figure 14A). GO-terms for upregulated genes based on Metascape analysis were DNA integration, nucleosome and chromatin organization, and budding cell bud growth (Figure 14B). However, since some of the these upregulated GO-terms overlapped with GO-terms in the *mpt5Δ* strain (Figure 13A and Figure 14B), this indicated that the upregulated GO-terms generated may not necessarily be due to depletion of Mpt5 in an H3K56A background, but due to overlap from the individual mutations. In terms of the downregulated genes in the iAID- Mpt5/H3K56A strain, some of the top GO-terms were formation of a pool of free 40S subunits, ribosome assembly, and rRNA export from the nucleus (Figure 14C). Unlike the upregulated gene analysis, the downregulated GO-terms in the iAID-Mpt5/H3K56A strain did not overlap with downregulated GO-terms in the *mpt5Δ* strain (Figure 13B and Figure 14C).
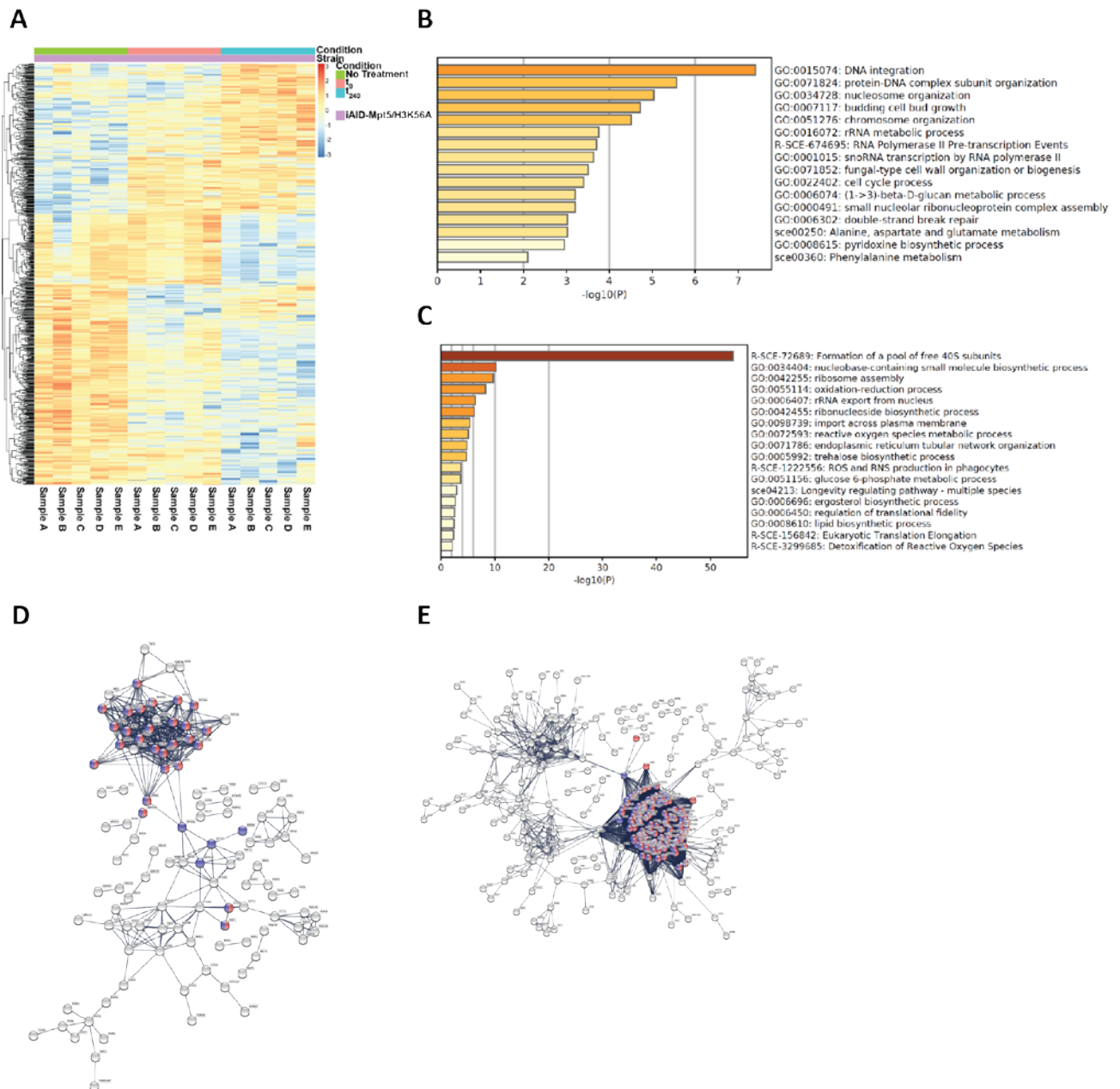
Figure 14: RNA-seq identifies a dramatic downregulation of genes linked to cytoplasmic translation upon Mpt5 depletion in an H3K56A background.

(A) Heat map depicting changes in genome-wide gene clusters within the iAID-Mpt5/H3K56A following Mpt5 depletion in an H3K56A background. The specific treatment condition is depicted by the upper multi-colored row. Each individual column represents an iAID-Mpt5/H3K56A replicate, with the same corresponding replicate being analyzed across the treatment conditions. Treatment conditions define the parameters used to induce the iAID-Mpt5/H3K56A growth phenotype: No Treatment (no doxycycline or auxin), t_0 (overnight 0.25 µg/mL doxycycline), t_{240} (240 min after 40 µg/mL doxycycline and 1 mM auxin). **(B)** Gene Ontology terms generated using Metascape for all upregulated genes depicted in (A). **(C)** Gene Ontology terms generated using Metascape for all downregulated genes depicted in (A). **(D)** Protein association network generated using STRING based on all upregulated genes depicted in (A). Each node represents an individual protein, and the red and blue nodes represent proteins associated with ncRNA processing and ncRNA metabolic process GO-terms, respectively. **(E)** Protein association network generated using STRING based on all downregulated genes depicted in (A). Each node represents an individual protein, and the red and blue nodes represent proteins associated with cytoplasmic translation and cytosolic ribosome GO-terms, respectively. Thickness of branches connecting the nodes correlates to the strength of interaction between proteins. Network analysis was conducted at the highest interaction confidence interval (0.9).

31

Furthermore, the *mpt5Δ* strain showed an upregulation of GO-terms linked to translation, while depletion of Mpt5 in an H3K56A background showed the opposite trend for translation-related GO-terms (Figure 13A and Figure 14B and C). This indicates that unlike the upregulated GO-terms, these changes are likely due to the depletion of Mpt5 in an H3K56A background and not because of overlap with single mutations. To get an even better understanding for potential complexes that may be up- or downregulated upon depletion of Mpt5 in an H3K56A background, STRING network analysis on the gene expression changes was performed. In terms of the upregulated genes, the most prominent node clusters revolved around ncRNA processing and ncRNA metabolic process (Figure 14D), indicating a slight overlap with the GO-enrichment analysis (Figure 14B). In terms of the downregulated genes, the analysis revealed a very clear and striking link to cytoplasmic translation (Figure 14E), which confirmed the previously mentioned GO-enrichment analysis (Figure 14C).

Since previous data indicated that Mpt5 RNA binding was playing a crucial role in the *MPT5*-H3K56 genetic interaction (Figure 10C), it was important to investigate this in the context of the gene expression data (Figure 15). Therefore, to identify Mpt5 mRNA targets that were deregulated due to the depletion of Mpt5 in an H3K56A background, deregulated genes in the iAID-Mpt5/H3K56A strain, Mpt5 RNA binding targets based on publically available data (Wilinski et al., 2015), and deregulated genes in the *mpt5Δ* strain relative to the H3K56A strain were analyzed for gene overlap. Applying this approach to all the upregulated genes from the RNA-seq data, resulted in only 50 potential genes of interest (Figure 15A), and the corresponding STRING analysis did not produce any striking or definitive protein clusters (Figure 15B). On the other hand, overlap analysis for all the downregulated genes resulted in 159 potential genes of interest (Figure 15C), and the STRING network analysis indicated a clear link to cytoplasmic translation (Figure 15D). Strikingly, the vast majority of the proteins identified in the downregulated network were ribosomal protein genes. Therefore, r-protein gene expression changes in the Wt, *mpt5Δ*, H3K56A, and iAID-Mpt5/H3K56A strains were investigated and the results clearly indicate that the vast majority of ribosomal protein genes are significantly downregulated due to depletion of Mpt5 in an H3K56A background (Figure 15E), which also strongly correlates with the ribosomal protein genes being Mpt5 RNA targets.

Taken together, these results indicate that depletion of Mpt5 in an H3K56A background results in a significant decrease in Mpt5-target mRNAs linked to cytoplasmic translation, and more specifically, that loss of ribosomal protein transcripts may be at the heart of the *MPT5*-H3K56 genetic interaction.
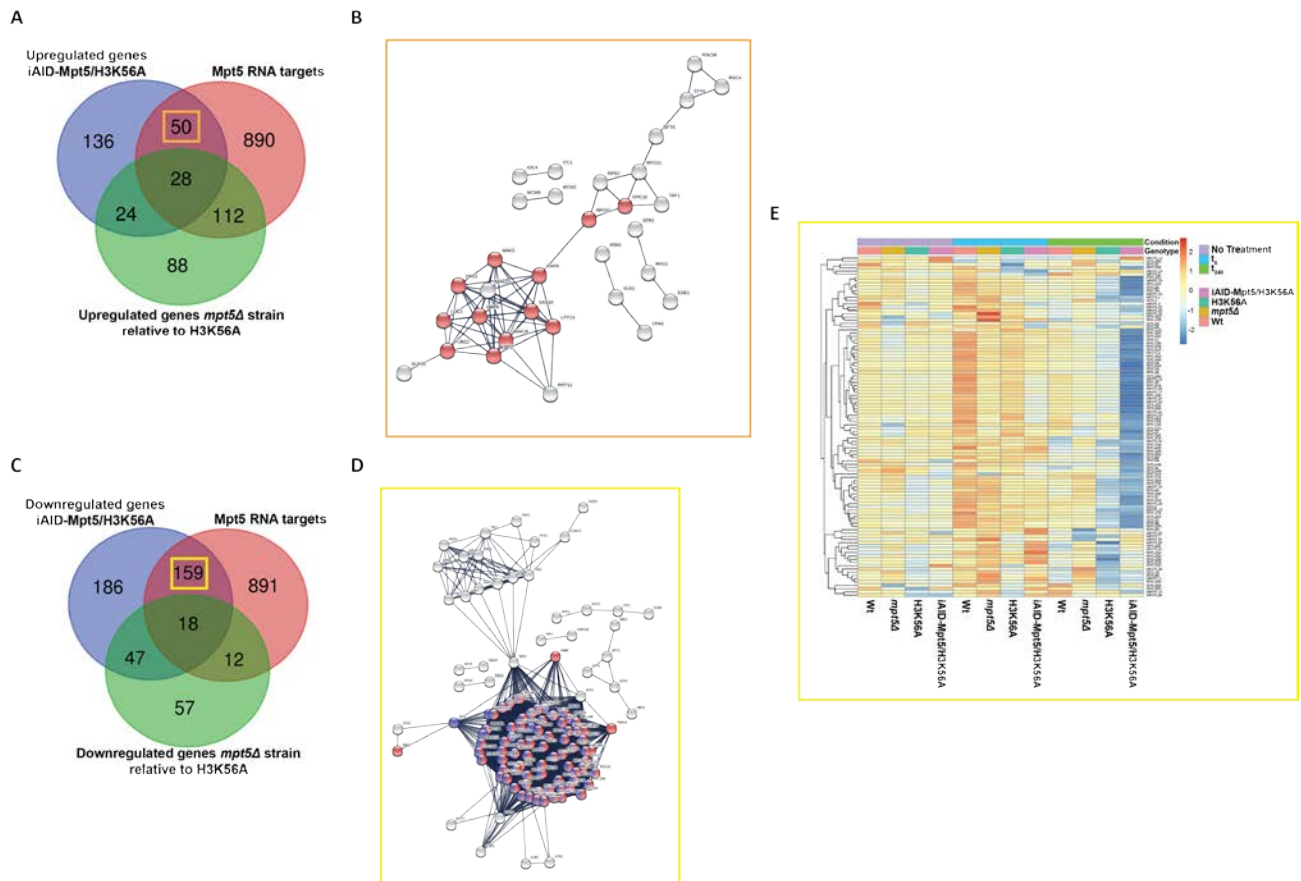
Figure 15: Mpt5 target RNAs, specifically ribosomal protein genes are crucial in the *MPT5*-H3K56A genetic interaction.
(A) Venn diagram depicting the number of genes that overlap between the upregulated genes in the iAID-Mpt5/H3K56A strain (No Treatment vs t240), the upregulated genes in the *mpt5Δ* strain relative to the H3K56A strain, and Mpt5 RNA targets*. **(B)** Protein association network generated using STRING based on all overlapping genes depicted in the orange box in (A). Red nodes represent proteins linked to ncRNA metabolic process. **(C)** Venn diagram depicting the number of genes that overlap between the downregulated genes in the iAID-Mpt5/H3K56A strain (No Treatment vs t240), the downregulated genes in the *mpt5Δ* strain relative to the H3K56A strain, and Mpt5 RNA targets*. **(D)** Protein association network generated using STRING based on all overlapping genes depicted in the yellow box in (C). The red and blue nodes represent proteins associated with cytoplasmic translation and cytosolic ribosome, respectively. **(E)** Heat map depicting changes in expression of all ribosomal protein genes within Wt, *mpt5Δ*, H3K56A, and iAID-Mpt5/H3K56A across the treatment conditions. The specific treatment condition is depicted by the upper multi-colored row. Each individual column represents a specific strain (N=5), with the same corresponding strain being analyzed across the treatment conditions. Treatment conditions define the steps used to induce the iAID-Mpt5/H3K56A growth phenotype: No Treatment (no doxycycline or auxin), t_0 (overnight 0.25 µg/mL doxycycline), t_{240} (240 min after 40 µg/mL doxycycline and 1 mM auxin). *Mpt5 RNA targets based on public eCLIP data (Wilinksi et al. 2015). In terms of STRING analysis: String analysis was conducted at the highest interaction confidence interval (0.9). Each node represents an individual protein, and the thickness of branches connecting the nodes correlates to the strength of interaction between proteins.

3.6 The downregulation of ribosomal protein genes is not due to a general stress response or cell death

In order to respond to various stressors, a common stress response in cells is to decrease global protein synthesis (Liu and Qian, 2014). Since the gene expression data pointed towards a significant decrease in genes associated with cytoplasmic translation, it was important to

investigate whether the observed downregulation of ribosomal protein genes was due to a general stress response. Therefore, qPCR analysis was performed to investigate relative gene and rRNA expression in the iAID-Mpt5/H3K56A strain following depletion of Mpt5. Both ribosomal protein genes tested, *RPS2* and *RPS24b*, showed a significant decrease in expression in the iAID-Mpt5/H3K56A strain following depletion of Mpt5 (Figure 16A). This correlated with the RNA-seq results (No Treatment vs. t_{240}). However, the timing in the decrease of gene expression was different between the two genes following depletion of Mpt5. *RPS2* showed a significant decrease in gene expression already 90 minutes after Mpt5 depletion, while *RPS24b* did not show a significant drop in gene expression until 240 minutes after Mpt5 depletion (Figure 16A). This suggests that the decrease in ribosomal protein genes observed in the RNA-seq data may not occur at the same rate for each transcript following depletion of Mpt5 (Figure 15D and Figure 16A). Since the ribosome is also composed of non-coding RNA, it was important to investigate the level of 18S, 25S, and 35S transcription, with 35S levels representing an indirect measure of nascent transcription rate of rDNA (Pérez-Ortín et al., 2019). Based on qPCR analysis, neither 18S, 25S, nor 35S rRNA levels significantly changed following Mpt5 depletion in an H3K56A background (Figure 16A). Since a general stress response induces translational shutdown that includes a decrease in rRNA transcription (Warmerdam and Wolthuis, 2019), this indicates that the significant decrease in ribosomal protein gene expression upon Mpt5 depletion does not extend to rRNA expression, suggesting a specific response to Mpt5 depletion in an H3K56A background and not a general stress response.

Since the *mpt5Δ*/H3K56A double mutant strain produced a synthetic lethal phenotype, it was important to investigate whether the decrease in translation-related gene expression in the iAID-Mpt5/H3K56A strain was due to the cells dying. Therefore, we depleted Mpt5 in an H3K56A background as previously described (Figure 11D) and took OD_{595} measurements over a longer timeframe (Figure 16B). Although the iAID-Mpt5/H3K56A strain grew at a slower rate, the OD_{595} measurements continued to increase even in the presence of auxin and doxycycline, suggesting a continued proliferation of the strain. To further investigate if the cells were dying, serial dilution spot tests were performed upon depletion of Mpt5 after four hours. When low Mpt5 levels were maintained by spotting cells on media containing doxycycline, a very sick growth phenotype was observed (Figure 16C). On the other hand, when Mpt5 levels were allowed to recover by omitting doxycycline from the media, the yeast significantly recovered growth (Figure 16C). These data suggest that depletion of Mpt5 in an H3K56A background rather leads to a reversible arrest in cell growth rather than cell death.
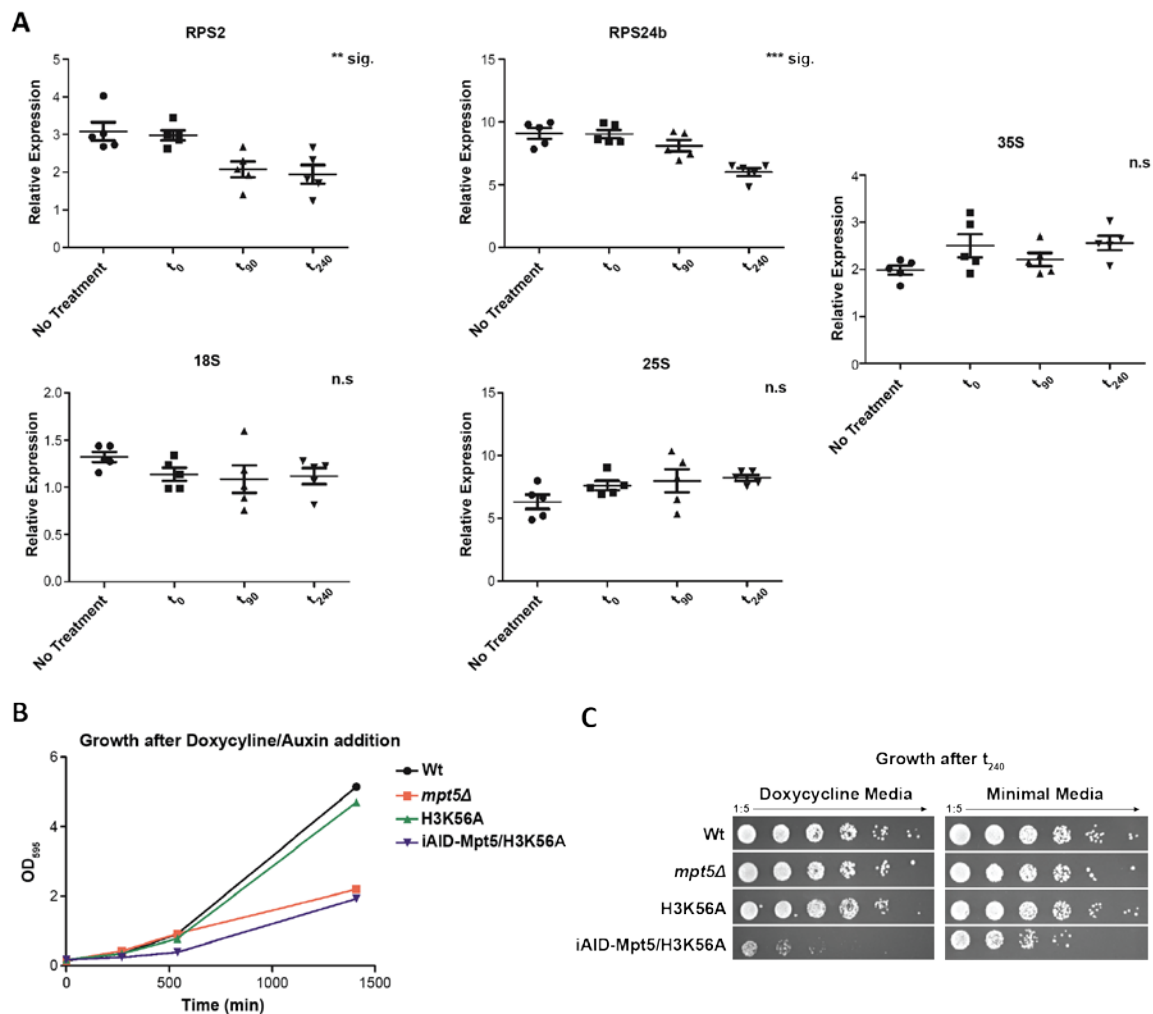
Figure 16: The downregulation of ribosomal protein genes in an H3K56A background is not due to a general stress response or cell death.

(A) qPCR analysis of relative gene and rRNA expression in the iAID-Mpt5/H3K56A strain across treatment conditions. The y-axis represents relative expression normalized to Act1 expression (Act1 was identified as the most stable gene based on the UMI-seq data). The x-axis represents the treatment conditions: No Treatment, t_0, t_{90}, and t_{240}. N = 5; Error bars = SEM; Significance (sig.) based on ANOVA test (** $p \leq 0.01$; *** $p \leq 0.001$; n.s – not significant). **(B)** Growth curve of Wt, *mpt5Δ*, H3K56A, and iAID-Mpt5/H3K56A strains following the t_0 treatment condition. The y-axis represents OD_{595} measurements and the x-axis represents time after 40 μg/mL doxycycline and 1 mM auxin addition. **(C)** Serial dilution spot test of Wt, *mpt5Δ*, H3K56A, and iAID-Mpt5/H3K56A following all the treatment conditions (No Treatment to t_{240}) to investigate the degree of cell death. The left image represents growth on 40 μg/mL doxycycline media and the right image represents growth on minimal media. The spot test was performed following a 1:5 serial dilution from left to right. Treatment conditions define the steps used to induce the iAID-Mpt5/H3K56A growth phenotype: No Treatment (no doxycycline or auxin), t_0 (overnight 0.25 μg/mL doxycycline), t_{240} (240 min after 40 μg/mL doxycycline and 1 mM auxin).

Taken together with previously mentioned results, this indicates that the downregulation in ribosomal protein genes is not due to a general stress response or cell death, but due to depletion of Mpt5 in an H3K56A background.

3.7 The depletion of Mpt5 in an H3K56A background results in lower translational efficiency and cell cycle arrest

Although the results thus far have pointed at a molecular underpinning between Mpt5 and H3K56A that revolves around a significant decrease in multiple ribosomal protein transcripts, it was also important to identify the physiological consequence as to why the cells stop proliferating upon Mpt5 depletion in an H3K56A background. Since ribosomal proteins are an essential component of the ribosome, it was a logical extension to investigate how translation rate may change upon depletion of Mpt5. Therefore, a Surface Sensing of Translation (SUnSET) assay, which measures nascent protein synthesis through incorporation of puromycin into the polypeptide chain, was applied (Schmidt et al., 2009). In line with the downregulation of ribosomal protein genes, the t_{240} group had a significantly lower puromycin incorporation rate (Figure 17A), thus indicating that depletion of Mpt5 in an H3K56A background led to a slower translation rate (Figure 17A). To ensure that the observed results from the SUnSET assay were a measure of translational efficiency due to nascent translation, puromycin incorporation was also measured following inhibition of translation through cycloheximide (Schneider-Poetsch et al., 2010). As can be clearly seen, no signal was generated in both the No Treatment and t_{240} groups following treatment with cycloheximide (Figure 17A), thus indicating no presence of nascent translation in these samples and that any signal generated from the assay was due to nascent translation.

Since repression of ribosomal protein genes can cause specific cell cycle phenotypes based on the r-protein gene being repressed (Thapa et al., 2013), it was also important to investigate whether the decrease in ribosomal protein genes influenced cell cycle progression in the iAID-Mpt5/H3K56A strain. Therefore, Wt, *mpt5Δ*, H3K56A, and iAID-Mpt5/H3K56A strains were arrested in G1, incubated in doxycycline and auxin for one hour, and then released to investigate cell cycle progression through FACs analysis (Figure 17B). Based on the results, the *mpt5Δ* and H3K56A strains showed slightly slower and significantly slower cell cycle progression when compared to the Wt strain, respectively (Figure 17B). Strikingly, yeast depleted of Mpt5 in an H3K56A background never exited the G1 phase (Figure 17B). These results indicate that in the presence of H3K56A, there is already a significant loss of cell cycle progression, and depletion of Mpt5 further exacerbates this phenotype and results in G1 cell cycle arrest.
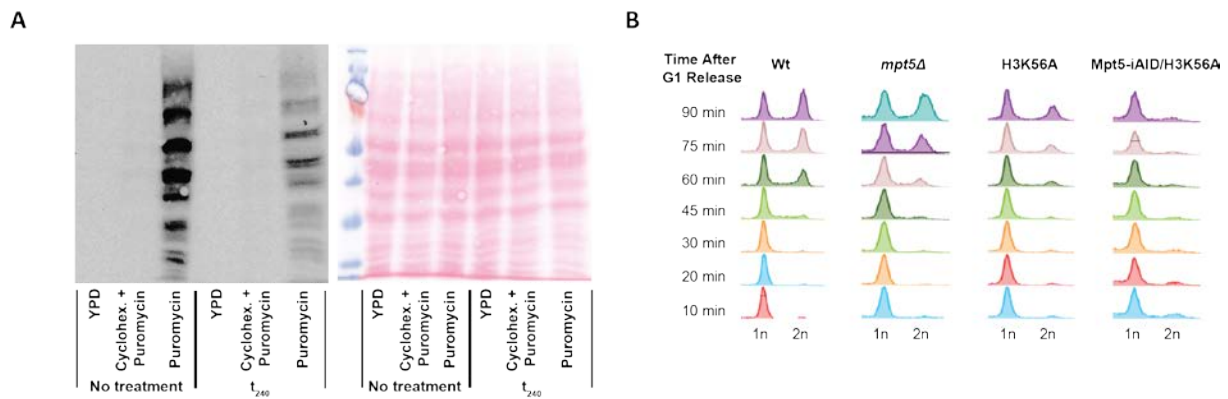
Figure 17: The downregulation of ribosomal protein genes in an H3K56A background results in decreased translation rate and G1 cell cycle arrest.

(**A**) Surface Sensing of Translation (SUnSET) assay in the iAID-Mpt5/H3K56A strain based on treatment conditions (No treatment vs t_{240}). The left image represents detection of nascent translation rate through incorporation of puromycin, the right image represents the loading control through a Ponceau stain. Vertical lines on the x-axis for each image represent the treatment time course groups (No Treatment and t_{240}), and the vertical labels refer to additional growth conditions for 15 min before sample collection; YPD media, YPD media supplemented with 100 µg/mL cycloheximide (cyclohex.) + 10 µg/mL puromycin, and YPD media supplemented with 10 µg/mL puromycin. Treatment conditions define the steps used to induce the iAID-Mpt5/H3K56A growth phenotype: No Treatment (no doxycycline or auxin), t_0 (overnight 0.25 µg/mL doxycycline), t_{240} (240 min after 40 µg/mL doxycycline and 1 mM auxin).(**B**) Cell cycle analysis of Wt, *mpt5Δ*, H3K56A, and iAID-Mpt5/H3K56A strains. Cells were arrested in G1, media was supplemented with 40 µg/mL doxycycline and 1 mM auxin for 60 min, and then cells were released from G1 and samples were collected for FACs analysis. The y-axis represents time after G1 release, the top labels refer to the specific strain, and the bottom x-axis labels refer to the DNA content based on FACs analysis.

Taken together, these results indicate that loss of Mpt5 in an H3K56A background results in a significant decrease in both translational efficiency and cell cycle progression through an Mpt5-dependent mechanism.

3.8 Ribosomal protein transcripts have a slower degradation rate in an H3K56A background

Although our data showed no significant changes in genome-wide steady state mRNA levels in an H3K56A mutant strain (Figure 12A), this does not exclude potential changes in nascent transcription. A measure of *in situ* mRNA production by RNA polymerase, nascent transcription rate has been shown to strongly influence cellular processes (Perez-Ortin et al., 2013). Furthermore, recent evidence has emerged that H3K56ac is a genome-wide activator of nascent transcription by inducing transcriptional initiation and promoting elongation (Topal et al., 2019), indicating that loss of H3K56ac does influence global transcription rate. Given this fact, it is likely that nascent transcription of many ribosomal protein genes is lower in the presence of H3K56A. Since many ribosomal protein genes are also Mpt5 RNA targets, it was important to investigate the degradation rate of these transcripts in an H3K56A background. Therefore, 4-thiouracil (4TU) pulse-chase labelling, which detects transcript degradation by

exposing the cells to a labelled compound (4TU-pulse) and then to the same compound in an unlabeled form (Uracil-chase) (Zeiner et al., 2008), was applied over a specific timeframe to measure the degradation rate of ribosomal protein transcripts through qRT-PCR (Figure 18A). Based on the qPCR analysis, *RPL17b* and *RPS16a* appeared to have a slower degradation rate in the H3K56A strain relative to the Wt strain (Figure 18B). Although these results need to be taken with caution because they are preliminary and not statistically significant, it appears that the trend may be pointing towards a slower degradation rate in ribosomal protein genes in an H3K56A background. Furthermore, there also appears to be a difference in the degradation rate between the ribosomal protein genes across the different timeframes (Figure 18B), which echoes the previously identified difference in changes to steady state mRNA levels for r-protein genes due to depletion of Mpt5 in the iAID-Mpt5/H3K56A strain (Figure 16A). This hints at the possibility that Mpt5 activity may be playing a role in the slower degradation rate of ribosomal protein transcripts in the H3K56A strain.

As a comparison, the degradation rate of *UBC6*, an *S. cerevisiae* housekeeping gene (Teste et al., 2009), was also measured. Although there was no significant difference between the H3K56A and Wt strain, the degradation rate appeared to be much faster in both strains when compared to the ribosomal protein genes (Figure 18B). This difference in degradation rate between the ribosomal protein genes and *UBC6* could be explained by transcript characteristics influencing the degradation rate (Neymotin et al., 2016). Taken together, these results indicate that the ribosomal protein transcript degradation rate is slower in an H3K56A background.
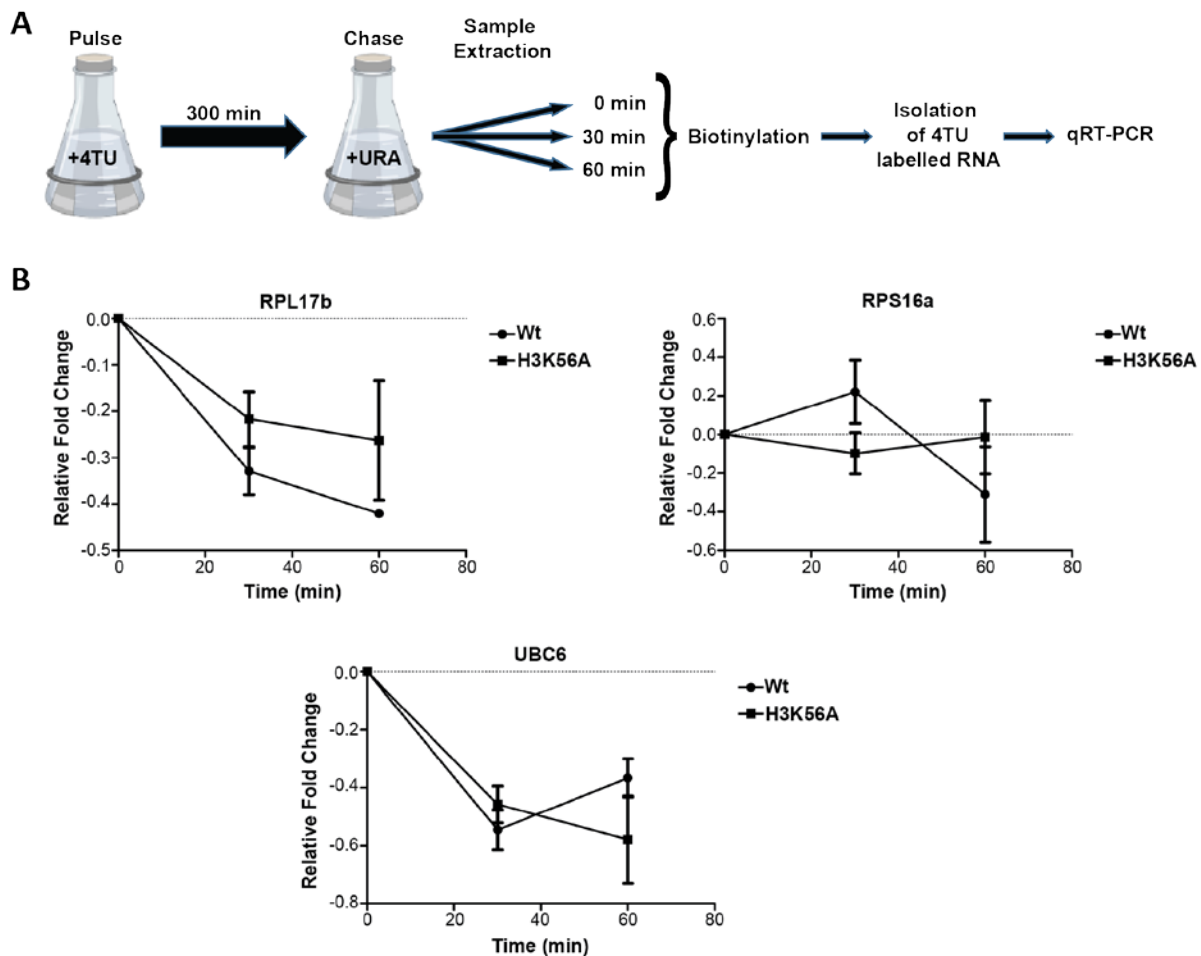
Figure 18: Ribosomal protein transcript degradation rate may be slower in an H3K56A background.
(A) Overview of the 4-Thiouracil (4TU) Pulse-Chase experiment parameters. The pulse consisted of growing *S. cerevisiae* cells in YPD media supplemented with 0.2 mM 4TU for 300 min. The chase consisted of switching the cells to YPD media supplemented with 20 mM uracil. Sample extractions were performed 0, 30, and 60 min following the chase. Following sample extraction, cells were biotinylated, 4TU RNA was isolated through streptavidin beads, and qRT-PCR analysis was performed. (B) qPCR analysis of RPL17b, RPS16a, and UBC6 transcript levels from the 4TU labelled cells prepared in (A). The Y-axis represents relative fold change normalized to Act1. Act1 was chosen because it was identified as the most stable gene based on the UMI-seq data and because it has been used in previous degradation rate studies (Wang et al., 2018). The X-axis represents time after chase in min. N=2; error bars = SEM.

3.9   No other *PUF* knockout produces a synthetic lethal genetic interaction with H3K56A, but there is some genetic interaction with Puf3 and Puf4

In *S. cerevisiae*, there are six different Puf family member proteins, and many of these proteins share significant RNA target overlap (Lapointe et al., 2017). Therefore, to investigate if the *MPT5*-H3K56 synthetic lethal genetic interaction extended to any other Puf proteins, serial dilution spot tests of *PUF* gene knockout and H3K56 mutations were performed (Figure 19). Both *puf1Δ* and *puf2Δ* did not produce any growth phenotype in combination with either

an H3K56A or H3K56Q mutation when compared to the single mutant strains (Figure 19A and B). Both the *puf3Δ*/H3K56A and *puf3Δ*/H3K56Q double mutant strains produced slight synthetic sick growth phenotypes when compared to the individual mutant strains (Figure 19C). In terms of *PUF4*, only the *puf4Δ*/H3K56A double mutant strain produced a mild growth phenotype (Figure 19D), while in terms of *PUF6*, no significant growth phenotype was identified in the *puf6Δ*/H3K56A and *puf6Δ*/H3K56Q double mutant strains (Figure 19E). Since *PUF3* and *PUF4* did produce genetic interactions with an H3K56A mutation, this warranted further investigation. Therefore, Puf3 and Puf4 RNA targets based on publically available data (Lapointe et al., 2017), where overlapped with all downregulated genes due to depletion of Mpt5 in an H3K56A background (Figure 14) and STRING network analysis was performed (Figure 20). Both the Puf3 and Puf4 networks produced r-protein genes as the most significant cluster (Figure 20A and B), but the number of r-protein genes was only a fraction of the total identified in the RNA-seq performed in this study upon depletion of Mpt5 (Figure 15D). An r-protein gene target overlap between Mpt5, Puf3, and Puf4 revealed that Puf3 and Puf4 had no separate target overlap and Mpt5 encompassed all but two r-protein gene targets (Figure 20C). Taken together, this indicates that the growth phenotypes identified in the *PUF3*-H3K56A and *PUF4*-H3K56A genetic interactions may have partial overlap with the *MPT5*-H3K56A genetic interaction. However, although *PUF3* and *PUF4* knockouts did produce a growth phenotype in combination with an H3K56 mutation, none of the growth phenotypes were comparably sick to the *MPT5*-H3K56 growth phenotypes, and Mpt5 is clearly the only *PUF* family member that produces a lethal genetic interaction with an H3K56 mutation (Figure 8 and Figure 19).
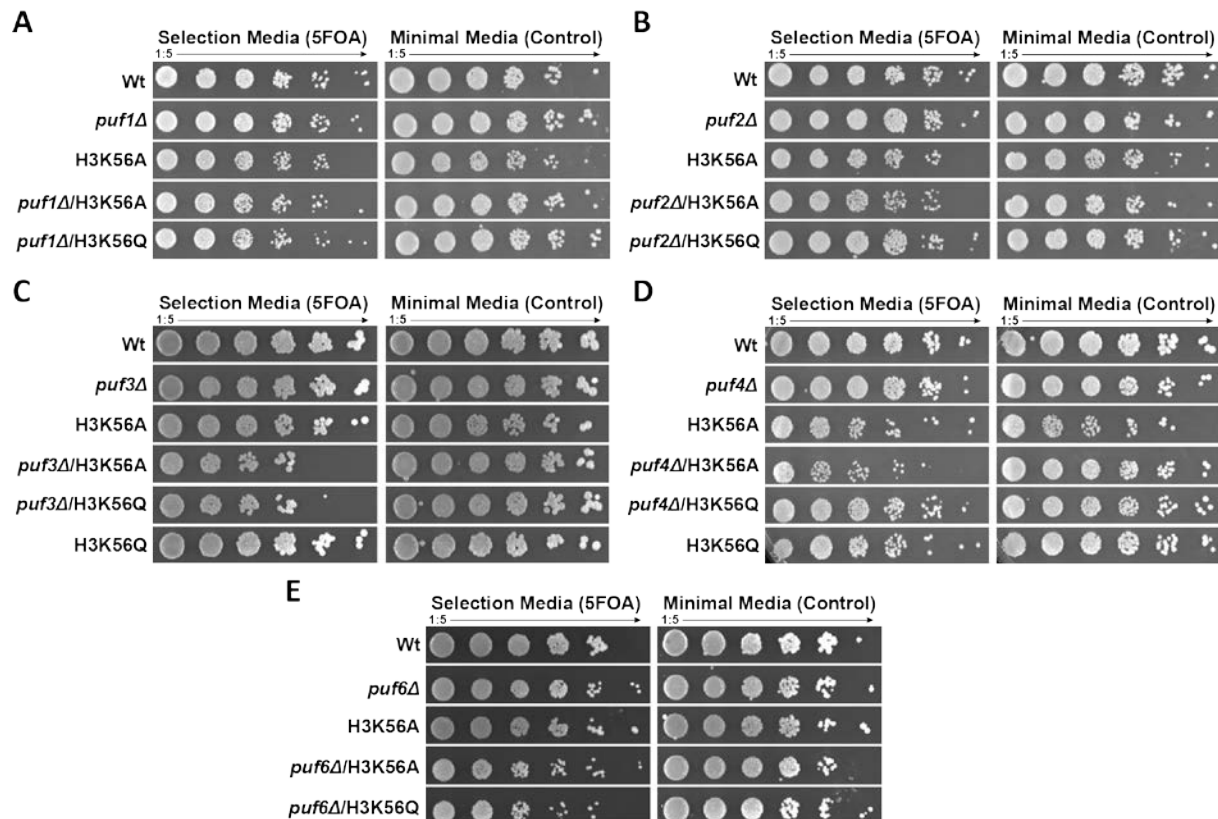
Figure 19: Mpt5 is the only Puf protein with a synthetic lethal genetic interaction with an H3K56 mutation in *S.cerevisae*.
(**A**) Serial dilution spot test showing no genetic interaction between *puf1Δ* and H3K56A and H3K56Q mutations. (**B**) Serial dilution spot test showing no genetic interaction between *puf2Δ* and H3K56A and H3K56Q mutations. (**C**) Serial dilution spot test showing a slight growth phenotype between *puf3Δ* and H3K56A and H3K56Q mutations. (**D**) Serial dilution spot test showing a mild growth phenotype between *puf4Δ* and an H3K56A mutation. (**E**) Serial dilution spot test showing no genetic interaction between *puf6Δ* and H3K56A and H3K56Q mutations. For all individual spot tests shown, the left image represents growth on 5FOA selection media and the right image represents growth on minimal control media. All spot tests were performed following a 1:5 serial dilution from left to right.
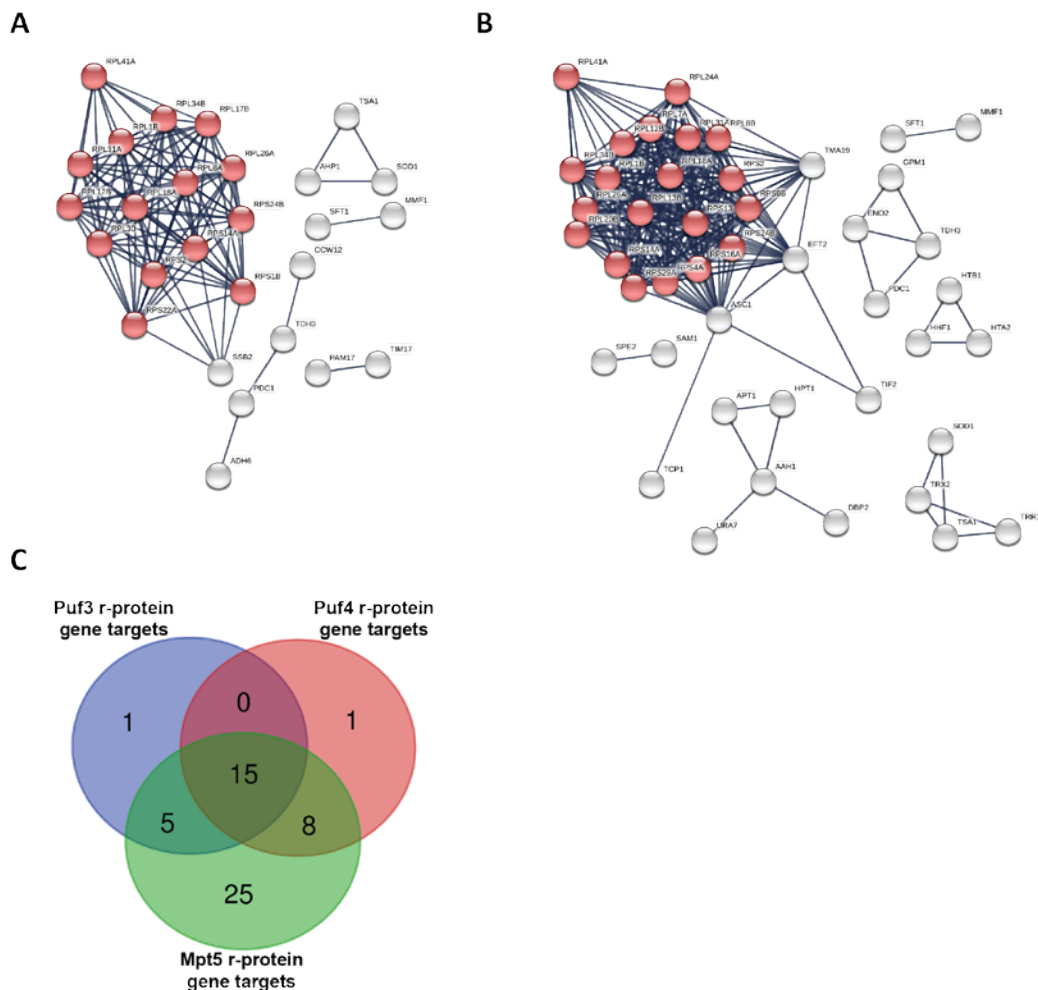
Figure 20: Puf3 and Puf4 target a fraction of the ribosomal protein genes that are downregulated upon depletion of Mpt5 in an H3K56A background.
(A) Protein association network generated using STRING based on all Puf3 RNA targets* overlapped with all downregulated genes after depletion of Mpt5 in an H3K56A background (Figure 14). Red nodes represent r-protein genes. **(B)** Protein association network generated using STRING based on all Puf4 RNA targets* overlapped with all downregulated genes after depletion of Mpt5 in an H3K56A background (Figure 14). Red nodes represent r-protein genes. **(C)** Venn diagram depicting the number of r-protein gene targets* that overlap between Puf3, Puf4, and Mpt5. In terms of STRING analysis: String analysis was conducted at the highest interaction confidence interval (0.9). Each node represents an individual protein, and the thickness of branches connecting the nodes correlates to the strength of interaction between proteins. *RNA targets based on public data (Lapointe et al. 2017).

3.10 Mpt5 post-transcriptional buffering extends beyond H3K56ac, and may involve different mechanisms

Finally, we were interested in understanding if H3K56A is a specific case or if other histone mutants involved in chromatin-templated processes would also produce synthetic lethal genetic interactions with *MPT5*. Therefore, an *MPT5* knockout was combined with various histone mutations and serial dilution spots tests were performed (Figure 21). While an *MPT5* knockout in combination with H3K36R, H4K16A, H4K16Q, H4K5A, H4K12A, and H3K79A produced no significant growth phenotype (Figure 21B - E), the *mpt5Δ*/H3K4R double mutant
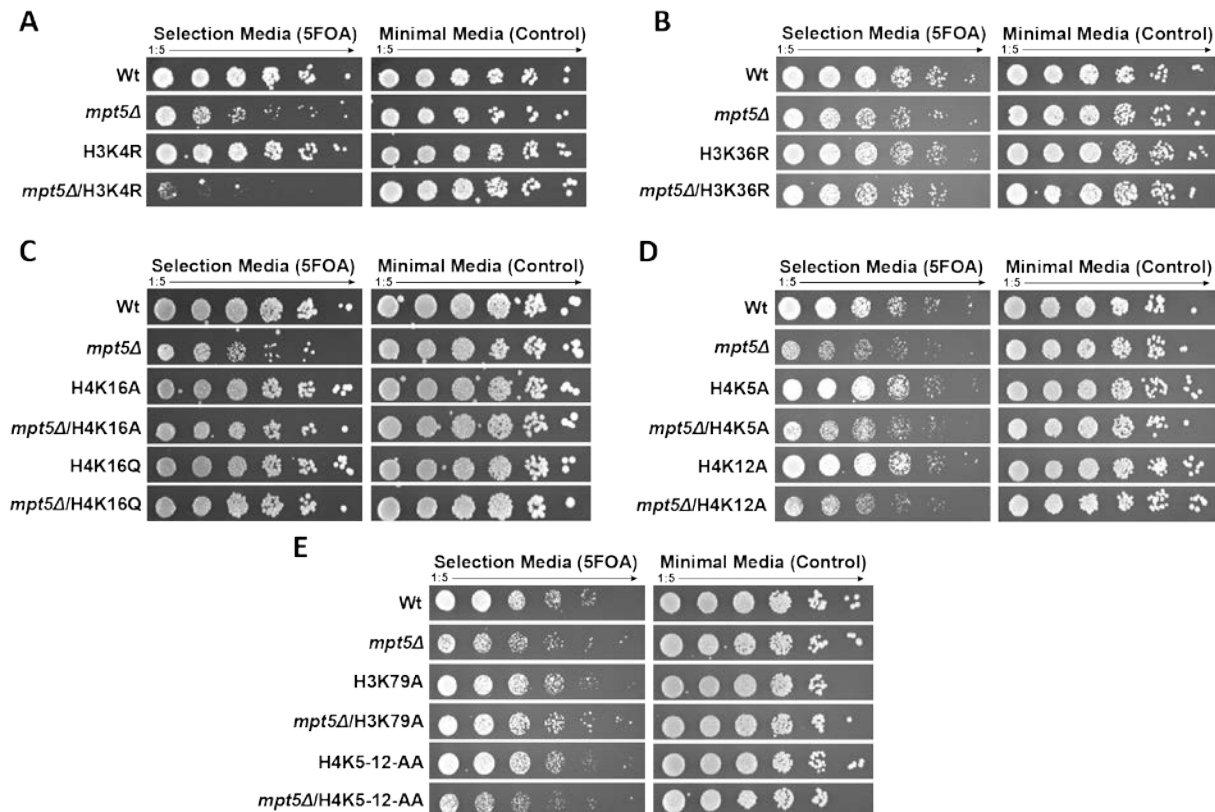
Figure 21: *mpt5Δ* **also produces a synthetic lethal genetic interaction with an H3K4R mutation, but not with other histone mutations.**
(A) Serial dilution spot test showing a synthetic lethal phenotype between *mpt5Δ* and an H3K4R mutation. **(B)** Serial dilution spot test showing no genetic interaction between *mpt5Δ* and an H3K36R mutation. **(C)** Serial dilution spot test showing no genetic interaction between *mpt5Δ* and H4K16A and H4K16Q mutations. **(D)** Serial dilution spot test showing no genetic interaction between *mpt5Δ* and H4K5A and H4K12A mutations. **(E)** Serial dilution spot test showing no genetic interaction between *mpt5Δ* and H3K79A and H4K5-12-AA mutations. For all individual spot tests shown, the left image represents growth on 5FOA selection media and the right image represents growth on minimal control media. All spot tests were performed following a 1:5 serial dilution from left to right.

strain was synthetic lethal (Figure 21A). Taken together, these results indicate that Mpt5 is essential in other histone mutants, indicating a more widespread role for Mpt5 in buffering de-regulated chromatin-templated processes.

As previously mentioned, based on the current literature, one of the main roles for Mpt5 is its link to the Ccr4-Not complex. Since the *CCR4*-H3K56 genetic interaction resulted in a synthetic sick phenotype (Figure 8B), it was also important to investigate if the observed *mpt5Δ*/H3K4R synthetic lethal phenotype extended to Ccr4-Not activity. Serial dilution spot tests for *ccr4Δ*/H3K4R and *pop2Δ*/H3K4R double mutant strains were performed, and neither of the double mutant strains produced a growth phenotype relative to the individual mutations (Figure 22A and B). These results indicate that the observed *MPT5*-H3K4R genetic interaction is independent of Ccr4-Not activity.
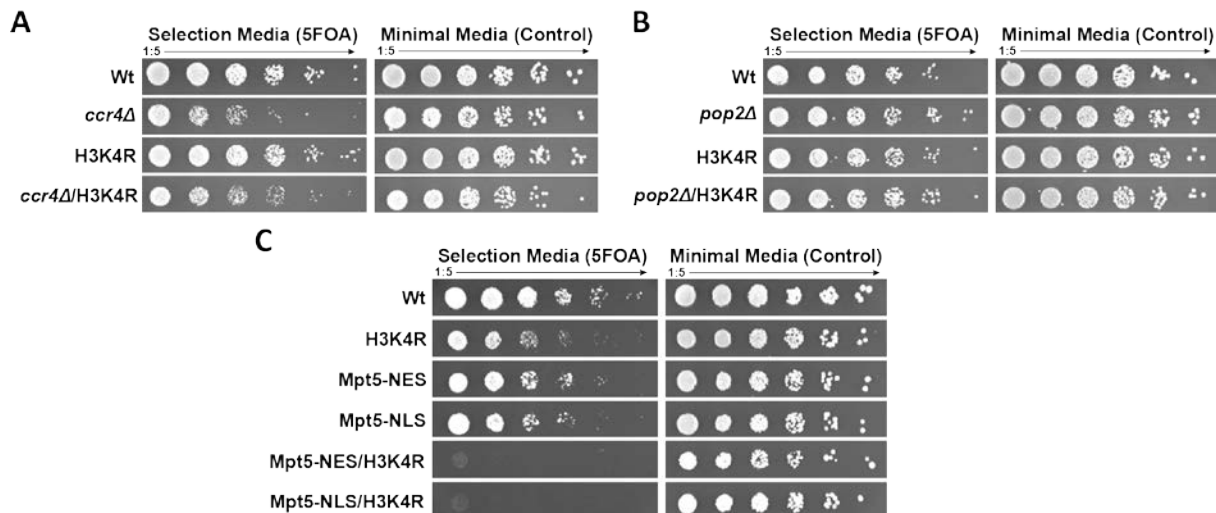
Figure 22: The *MPT5*-H3K4R genetic interaction appears to also be Ccr4-Not independent, but it may involve different dynamics than the *MPT5*-H3K56 genetic interaction.
(A) Serial dilution spot test showing no genetic interaction between *ccr4Δ* and an H3K4R mutation. (B) Serial dilution spot test showing no genetic interaction between *pop2Δ* and an H3K4R mutation. (C) Serial dilution spot test showing the effect of Mpt5 cellular localization on the Mpt5/H3K4R growth phenotype. NLS denotes nuclear localization signal and NES denotes nuclear export signal. For all individual spot tests shown, the left image represents growth on 5FOA selection media and the right image represents growth on minimal control media. All spot tests were performed following a 1:5 serial dilution from left to right.

Since both the *MPT5*-H3K56 and H3K4R genetic interactions produce synthetic lethal phenotypes, and both histone marks are found genome-wide and involved in transcriptional regulation, it was important to distinguish if the genetic interactions involved the same dynamics. Therefore, serial dilution spot tests combining Mpt5 cellular localization and an H3K4R mutation were performed. Surprisingly, both the Mpt5-NES/H3K56A and Mpt5-NLS/H3K56A strains produced synthetic lethal phenotypes (Figure 22C). This indicates that unlike the *MPT5*-H3K56 genetic interaction, specific cellular localization does not influence the growth phenotype, and that Mpt5 needs to be present in both the nucleus and the cytoplasm; thus hinting that the *MPT5*-H3K4R genetic interaction may involve a different mechanism in terms of Mpt5 activity.

Taken together, these results indicate a synthetic lethal genetic interaction between *MPT5*-H3K4R that is Ccr4-Not independent, and may revolve around a different Mpt5 mechanism when compared to the *MPT5*-H3K56 genetic interaction.

4 Discussion

4.1 Identification of a connection between transcriptional and post-transcriptional gene regulation through an *MPT5*-H3K56A genetic interaction

Although there is robust knowledge in the literature in terms of transcriptional and post-transcriptional control of gene expression (Bannister and Kouzarides, 2011; Lawrence et al., 2016; Parker, 2012), there is very little information about specific connections between the two levels of control. Therefore, the goal of this study was to investigate and elucidate if there is a link between transcriptional and post-transcriptional control of gene expression. Due to the lack of knowledge, an initial high-throughput approach was required to address this goal. Therefore, since H3K56ac is found genome-wide in *S. cerevisiae* and has been identified as a robust regulator of chromatin structure that can both promote and inhibit transcription (Voichek et al., 2016; Williams et al., 2008), an H3K56A mutation was used as a probe to identify potential links between deregulation of chromatin structure and post-transcriptional regulators of gene expression. Through an SGA analysis, numerous genetic interactions between an H3K56A mutation and single, gene knockouts in *S. cerevisiae* were identified (Figure 7). As expected, based on previous literature on the role of H3K56ac (Kaplan et al., 2008; Xu et al., 2005), many of the genetic interactions revolved around nucleosome assembly and cell cycle (Figure 7B and C). Interestingly, mediator complex was also identified (Figure 7C). Although previous literature has identified a link between histone acetylation and mediator complex activity (Zhu et al., 2011), to our knowledge, this is the first evidence of a potential link between H3K56ac and the mediator complex. This genetic interaction might be linked to H3K56ac promoting chromatin disassembly during transcriptional activation (Williams et al., 2008), which would align with Mediator complex interacting with upstream regulatory regions and core promoters, and its role in transcriptional initiation (Poss et al., 2013). However, the observation that genes linked to the Ccr4-Not complex produced genetic interactions with H3K56A, was deemed more interesting based on the goal of this study (Figure 7). Coined the "control freak" of gene expression, the Ccr4-Not complex is conserved in all eukaryotes and a major post-transcriptional regulator of gene expression (Miller and Reese, 2012). Therefore, the synthetic

sick phenotypes identified between Ccr4, Pop2, Mpt5 and H3K56A, hinted at the potential identification of a direct interaction between transcriptional and post-transcriptional regulation of gene expression.

Since the common link between Mpt5, Ccr4, and Pop2 is the Ccr4-Not complex, and since Ccr4-Not is a robust regulator of gene expression, the initial assumption was that the critical component in the identified genetic interactions revolved around Ccr4-Not activity. However, if Ccr4-Not was the crucial component in all the genetic interactions, then all the growth phenotypes should be the same, or at the very least, the *CCR4* knockout should produce the most severe growth phenotype because it is the major catalytic subunit in the Ccr4-Not complex. The *CCR4*-H3K56A genetic interaction did produce a sicker growth phenotype when compared to *POP2*-H3K56A, but the *MPT5*-H3K56A genetic interaction produced the only lethal phenotype (Figure 8). Additionally, Mpt5 is not a subunit, but has been identified as a targeting protein for Ccr4-Not (Goldstrohm et al., 2006), *i.e.* the functional role for Mpt5 would occur upstream of Ccr4-Not activity. Such an upstream role for Mpt5 cannot be reconciled with the strongest growth phenotype (Figure 8). Furthermore, Pop2 has been identified as the only bridging protein between Mpt5 and Ccr4-Not (Goldstrohm et al., 2006). Yet, there is no *POP2*-H3K56 genetic interaction (Figure 8C). Taken together, although some of the previous literature shows a significant link between Mpt5 and the promotion of target specific degradation through Ccr4-Not (Goldstrohm et al., 2006; Goldstrohm et al., 2007); here we identify an *MPT5*-H3K56 genetic interaction that appears to be – at least in parts - independent of Ccr4-Not activity. Therefore, although Ccr4-Not activity is important in an H3K56A background, the focal point in the identified H3K56ac genetic interactions is Mpt5. Furthermore, these results suggest an additional role for Mpt5, independent of Ccr4-Not, when compared to previous literature that links Mpt5 in the promotion of Ccr4-Not activity (Goldstrohm et al., 2006; Goldstrohm et al., 2007).

4.2 Mpt5 presence prevents degradation of ribosomal protein genes in an H3K56A background

Target prediction algorithms have linked Mpt5 to chromatin related GO-terms and Mpt5 activity has also been linked to the rDNA locus (Kennedy et al., 1997; Lapointe et al., 2017; Wilinski et al., 2015), thus indicating that Mpt5 might regulate chromatin structure. However, we found no changes in genome-wide H3ac, H3K56ac, or H3 levels (Figure 9). An attempted chromatin immunoprecipitation was also unsuccessful in an Mpt5-Myc tagged strain (data not

shown). Together with the absence of any other ChIP data, these results indicate no direct link between Mpt5 and chromatin architecture, suggesting that Mpt5 does not play a direct role in transcriptional regulation. However, this does not exclude the possibility for a downstream role via the stabilization or degradation of Mpt5 target mRNAs. In alignment with this possibility, we show that cytoplasmic localization and Mpt5-RNA binding activity are crucial to maintain proper cell function in an H3K56A background (Figure 10). Therefore, our findings align with previously published literature that Mpt5 is an RNA-binding protein and post-transcriptional regulator of gene expression (Goldstrohm et al., 2007; Wilinski et al., 2015). Furthermore, because Mpt5 cellular localization has no influence on cell growth without loss of H3K56ac (Figure 10B), this points towards a specific response by Mpt5 upon loss of H3K56ac. Taken together, this indicates that Mpt5 activity is crucial upon chromatin deregulation.

To investigate the molecular underpinnings of the *MPT5*-H3K56 genetic interaction, we utilized an Improved Auxin Inducible Degron (iAID) system and RNA-seq analysis (Tanaka et al., 2015) (Figure 11 and Figure 12). Investigation of the results identified that *MPT5* knockout in a Wt background has a significant effect on overall steady state transcript levels (Figure 12A). On the other hand, although H3K56ac is a genome-wide histone mark that is linked to transcriptional regulation (Kurat et al., 2014; Williams et al., 2008), the loss of H3K56ac did not result in a significant change in overall steady state gene expression (Figure 12A). A previous study found similar results, showing that inactivation of Rtt109, the H3K56 histone acetyltransferase, resulted in no significant change to steady state RNA levels (Rege et al., 2015). Interestingly, here we show that upon depletion of Mpt5 in an H3K56A background, overall transcript levels significantly decrease (Figure 12). Since as previously mentioned, H3K56ac has no significant influence on steady state transcript levels; this suggests the change in steady state transcript levels is due to loss of Mpt5 in an H3K56A background. Interestingly, since loss of Mpt5 in a Wt background results in a significant increase in most transcripts (Figure 12A), this decrease in transcript levels suggests a different role for Mpt5 in an H3K56A background. In alignment with these findings, many of the upregulated GO-terms in the *mpt5Δ* strain are downregulated due to Mpt5 depletion in an H3K56A background (Figure 13 and Figure 14). Recent literature has shown evidence to support this theory and that Mpt5 activity can either promote or inhibit mRNA degradation in a context-dependent manner (Wang et al., 2018a). To investigate this theory even further, we overlapped the gene expression changes upon Mpt5 depletion in an H3K56A background with identified Mpt5 RNA binding targets (Wilinski et al., 2015). The results generated highlight that the vast majority of downregulated genes are ribosomal protein (r-protein) genes (Figure 15). As discussed previously, Mpt5

activity has been linked to the Ccr4-Not complex by promoting target specific transcript degradation (Goldstrohm et al., 2006). However, here we show that loss of Mpt5 in an H3K56A background results in a dramatic decrease of Mpt5-target r-protein transcripts (Figure 15). These findings provide evidence for a context-dependent change in Mpt5 function that revolves around preventing mRNA decay, and that r-protein genes are the focal mRNA targets in an H3K56A background.

4.3 Loss of H3K56ac triggers a context-dependent Mpt5-mediated, post-transcriptional buffering system that is crucial for proper cellular function

As mentioned previously, loss of H3K56ac does not influence steady state RNA levels, but mutations abolishing H3K56ac decrease nascent transcription genome-wide (Topal et al., 2019). It is tempting to speculate that the context-dependent shift that triggers the proposed Mpt5-buffering system may be the decrease in nascent transcription rate (of r-protein genes) due to loss of H3K56ac. If loss of H3K56ac results in a decrease in nascent transcription, which triggers an Mpt5-mediated buffering system, then the degradation rate of Mpt5-target transcripts should be slower in an H3K56A background in order to offset the decrease in nascent transcription. In alignment with this theory, the degradation rate of r-protein transcripts shows a slower trend in an H3K56A background (Figure 18). Therefore, combined with the previously discussed results that identify ribosomal protein genes as the focal point in an Mpt5-mediated mechanism (Figure 14, Figure 15, and Figure 16), we propose that the slower degradation rate of the r-protein genes is due to Mpt5 activity. This conclusion aligns with a previous study showing that glucose starvation can trigger Mpt5 mediated, target-specific mRNA buffering through transport to p-bodies (Wang et al., 2018a). Here, we show that the degradation rate of r-protein transcripts is buffered in an H3K56A background (Figure 18), and based on previously discussed results, propose that this is due to an Mpt5-mediated effect. Furthermore, another study has shown that H3K56ac works antagonistically with the nuclear RNA exosome to control mRNA expression, and changes in steady state RNA levels due to loss of RTT109 are observed only in combination with loss of the nuclear RNA exosome (Rege et al., 2015). Here, we show no changes in steady state RNA levels upon loss of H3K56ac, and propose that this is due to an Mpt5-mediated, post-transcriptional buffering mechanism against nascent transcription changes due to loss of H3K56ac.

A common stress response in eukaryotes is to trigger a global decrease in translation, which involves a decrease in rRNA transcription levels (Liu and Qian, 2014; Warmerdam and Wolthuis, 2019). Our results show a significant decrease in ribosomal protein transcript levels due to depletion of Mpt5 in an H3K56A background (Figure 15). Given that the global stress response in cells is to decrease translation, the logical assumption would be that this decrease in r-protein transcripts is linked to a general stress response. However, the decrease in r-protein transcripts is not accompanied by a decrease in rRNA levels (Figure 16). Therefore, it is not a general stress response that is causing a decrease in r-protein transcripts, but loss of the Mpt5-mediated buffering system in an H3K56A background. Furthermore, the loss of Mpt5 in an H3K56A background results in a significant decrease in nascent translation rate (Figure 17A). Since there is no change in rRNA levels, this decrease in nascent translation is linked to the decrease in Mpt5-target ribosomal protein transcripts, which echoes the argument that it is not due to a general stress response but due to the loss of the Mpt5-mediated buffering system in an H3K56A background. Interestingly, a recent study has shown that imbalances in r-proteins and rRNAs can compromise essential cellular functions (Tye et al., 2019). Our results align with these findings by showing a clear loss of cellular function due to an imbalance between r-protein transcript levels and rRNA (Figure 8A and Figure 16A). In addition, we show that this imbalance can be triggered by the loss of Mpt5-mediated buffering due to chromatin deregulation. Furthermore, previous literature has linked ribosomal protein genes to the cell cycle, and that loss of individual r-protein genes can dramatically inhibit cell cycle progression (Thapa et al., 2013). Our results show that in an H3K56A background there is significantly slower cell cycle progression, but depletion of Mpt5 in an H3K56A background results in cell cycle arrest (Figure 17B). This suggests that in an H3K56A background, Mpt5 buffering of r-protein genes also serves to prevent cell cycle arrest. Taken together with the previous results, this points towards an Mpt5-buffering system that is context dependent and triggered in an H3K56A background, and loss of this buffering system results in a decrease of r-protein transcripts, translation rate, cell cycle arrest, and as a consequence, the observed physiological changes in the yeast cells.

4.4 The Mpt5-mediated buffering system extends to other chromatin modifications, and may potentially involve other RNA-binding proteins

The Puf proteins are a family of very dynamic RNA-binding proteins with significant target overlap (Lapointe et al., 2017; Wilinski et al., 2015). However, despite the vast target overlap, *MPT5* is the only *PUF* knockout that produces a synthetic lethal genetic interaction with an H3K56 mutation (Figure 19). Interestingly, Puf3 and Puf4 share the most common targets with Mpt5 (Lapointe et al., 2017), and knockouts of these genes in an H3K56A background produce modest growth phenotypes (Figure 19C and D). Given that all three proteins belong to the same protein family and Puf3 has been shown to buffer transcript degradation (Lee and Tu, 2015), it is possible that Puf3 and Puf4 also provide a buffering mechanism in an H3K56A background. However, even together, Puf3 and Puf4 only bind a fraction of the r-protein transcripts compared to Mpt5 (Figure 20). Therefore, the majority of r-protein transcripts are still being buffered by Mpt5 in an H3K56A background, resulting in less severe phenotypes in the *PUF3* and *PUF4* knockouts. Together, this suggests that the deregulation of a large fraction of r-protein transcripts in an H3K56A background is the molecular underpinning for the observed phenotype.

Interestingly, the finding that other RNA-binding proteins might buffer chromatin-mediated defects, hints at the possibility that we observe here only one example of such a post-transcriptional buffering mechanism, and that this concept might extend to other RNA-binding proteins and different chromatin-related triggers. In alignment with this theory, a synthetic lethal genetic interaction was identified between an *MPT5* knockout and an H3K4R mutation (Figure 21), with the Mpt5 buffering activity in an H3K4R background being independent of Ccr4-Not (Figure 22A and B). Since this lethal genetic interaction also revolves around Mpt5 activity, this finding suggests that either the *MPT5*-H3K4R genetic interaction is connected to the *MPT5*-H3K56A genetic interaction, or it is a separate Mpt5 buffering mechanism. Both H3K56ac and H3K4 methylation have been linked through expression homeostasis, with the theory being that deposition of H3K56ac on newly synthesized histones interferes with post-replication recovery of H3K4me3, thus resulting in a transcriptional lag on newly synthesized genes (Voichek et al., 2016; Voichek et al., 2018). However, although a subsequent publication did identify a stepwise increase in transcription as cells progressed through S phase, the response to increased gene dosage did not require H3K56ac (Topal et al., 2019). Furthermore, although H3K56ac does not influence steady state RNA levels (Figure 12A), loss of H3K4

methylation results in expression changes to almost 500 genes (Cruz et al., 2018). Therefore, these facts suggest a different context-dependent trigger due to loss of H3K4 methylation when compared to loss of H3K56ac. In alignment with this, the synthetic lethal *MPT5*-H3K4R genetic interaction is not rescued by nuclear or cytoplasmic presence of Mpt5 (Figure 22C), thus providing evidence for a different Mpt5 buffering mechanism. Taken together, this indicates that the described Mpt5-mediated, post-transcriptional buffering system not only extends beyond an H3K56ac interaction, but also likely involves different Mpt5-mediated buffering mechanisms based on context-dependent changes due to specific chromatin modifications.

4.5 Potential physiological consequences of post-transcriptional buffering

As previously discussed, our results point towards a context-dependent buffering system that extends to different chromatin modifications. The evolutionary conservation of Puf family member proteins indicates the potential for a conserved, post-transcriptional buffering system that may be crucial to maintaining proper cell function. For example, many post-translational modifications on histones, such as loss of H3K56ac levels, are strongly perturbed during the ageing process (Dang et al., 2009; Wang et al., 2018c). Therefore, a post-transcriptional buffering system may be important in negating the effects due to loss of histone acetylation in order to maintain proper cell function. In alignment with this, overexpression and loss of Mpt5 prolongs and decreases replicative life span, respectively (Kaeberlein et al., 2004; Kaeberlein and Guarente, 2002; Kaeberlein and Kennedy, 2005; Kennedy et al., 1995). Puf proteins are also not the only class of RNA-binding proteins, and many of these proteins regulate gene expression in a dynamic manner by binding target RNAs (Finn et al., 2010; Huang et al., 2018; Kamina and Williams, 2017; Oliveira et al., 2017). Together, these observations hint at the potential for a wider array of post-transcriptional buffering systems that function in a context dependent manner based on changes at the chromatin level. To investigate to what extent such post-transcriptional buffering mechanisms may exist, genetic screens incorporating different histone mutations and gene knockouts of known RNA-binding proteins would be a warranted first step. By understanding the scope of such buffering mechanisms, it would provide valuable insight into the dynamic and context-dependent function of cellular activity.

4.6 Outlook

In this study, we identify a novel, Mpt5-mediated, post-transcriptional mRNA buffering mechanism that revolves around r-protein transcript levels and is triggered by loss of H3K56ac. To our knowledge, this is the first identified, context-dependent, post-transcriptional buffering system induced by specific chromatin changes. Furthermore, we show that this buffering system is crucial to normal cell function and that loss of this mechanism results in dire physiological consequences in the cell. Although this study identifies a very specific buffering system in a context-dependent manner, we also provide evidence that this buffering mechanism extends beyond H3K56ac and may involve different molecular mechanisms. However, future experiments are needed to pinpoint the potential differences in Mpt5 activity relative to the different chromatin modifications. Therefore, Mpt5 depletion in an H3K4R background combined with RNA-seq analysis is a logical next step to investigate the context-dependent influence on Mpt5 buffering. Furthermore, although we propose that changes in nascent transcription trigger the post-transcriptional buffering mechanism, investigation into the molecular underpinnings of how Mpt5 switches from target-specific mRNA decay to buffering is still missing. Interestingly, a study found that post-translational modifications on a Puf protein can direct whether targeted transcripts undergo decay or translation (Lee and Tu, 2015). Therefore, identifying differences in Mpt5 post-translational modifications between a normal, H3K56A, and H3K4R background, and then investigating how these modifications influence the Mpt5-mediated buffering system could provide valuable insight into the proposed buffering mechanism.

As previously discussed, Puf family member proteins are evolutionarily conserved. In mammals, there are two Puf proteins, Pum1 and Pum2. A recent study identified that Pum1 and Pum2 target a vast array of mRNAs, and although they show significant target overlap, they do possess distinct mRNA targets (Sternburg et al., 2018). Furthermore, although Pum protein activity is typically repressive, there is evidence for context-dependent changes in Pum activity (Sternburg et al., 2018). These facts, in combination with the findings in this study, make it feasible that there may also be a Pum-mediated, post-transcriptional buffering system in mammals. Interestingly, the significance and role of H3K56ac in humans is debated, and there is little evidence for a significant role for H3K56ac in cellular processes. In light of the post-transcriptional buffering system identified in this study, perhaps Pum1 and Pum2 are buffering the changes due to loss of H3K56ac in human cells in a context-dependent manner. Therefore, identifying if there is a Pum1- and/or Pum2-mediated, post-transcriptional buffering system in

an H3K56A background is a very interesting future endeavor that would not only shed light on the role of H3K56ac and Pum proteins in mammals, but also provide valuable insight into the importance of the novel, post-transcriptional buffering system identified in this study.

5 Materials

5.1 Equipment

Agarose gel chambers and trays	Bio-Rad
Analytical balance	Mettler Toledo
Balances	VWR
Centrifuge (Megastar 1.6R)	VWR
PCR machine (T100 Thermal Cycler)	Bio-Rad
SDS gel chambers and tanks	Bio-Rad
Ultracentrifuges (Fresco 21)	Thermo Fisher Scientific
Western blot transfer system (Turbo)	Bio-Rad
Flasks and Bottles	VWR
Frogger	Lab
Spectrophotometer (UV-1600PC)	VWR
Confocal microscope	Leica
Tape station (2200)	Agilent
Ultrasonicator (M220)	Covaris
Shaker/Incubator (Innova 44)	New Brunswick Scientific
Incubator (Incu-line)	VWR
Water bath (VWB6)	VWR
Vortex (Vortex Genie 2)	Scientific Industries
Gel Viewer (BL Star 16)	Biometra
Thermomixer (Pro)	Cell Media
Heat Block (Analog)	VWR
Power Pac (Basic)	Bio-Rad
Nano-photometer (N60)	Implen
Hotplate (VMS C7)	VWR
Micropipettes	Gilson
qPCR machine (Light Cycler 96)	Roche

Qubit 3 Fluoromoeter   Thermo Fisher Scientific

Curix 60 developer   AGFA

5.2 Software

Office XP   Microsoft Corp.

EndNote X7   ISI ResearchSoft

Illustrator CS6   Adobe

GraphPad Prism   GraphPad Software Inc.

A plasmid Editor (ApE)   Wayne Davis

SnapGene 4.0.5   GSL Biotech

IrfranView   Irfan Skiljan

Acrobat Reader DC   Adobe

5.3 Expendable items

Cell culture plasticware   Sarstedt

Cuvettes   Sarstedt

Falcon and Eppendorf Tubes   Sarstedt

Sterile Filters   Milipore

Nitrocellulose membrane   Bio-Rad/GE Healthcare

5.4 Primers, plasmids, and strains

5.4.1 Primers

Table 1: Primers used in this study. Primer name and sequence in 5`-3` orientation.

Primer Name	Sequence (5`-3`)
18s (qPCR) F	AACCTTGAGTCCTTGTGGCT
18s (qPCR) R	CCCCGACCGTCCCTATTAAT
25s (qPCR) F	TCCGGAACCTGGATATGGAT
25s (qPCR) R	GTACGACCTGGCATGAAAACT
35s (qPCR) F	CAAGAGGGAATAGGTGGGAAAA

Primer Name	Sequence (5`-3`)
35s (qPCR) R	GACAAGCATATGACTACTGGCA
LEU2 Seq #1 F	ATCGATGCTACAGGTGTCCC
LEU2 Seq#2 F	TGATTGATTCTGCCGCCATG
HHT2 Seq F	CGGTGGTGTTAAGAAGCCTC
HHT2 Seq R	TCACCTCTTAGTCTTCTGGCC
HHT2 Upstream F	CTCGCGTTGCTTCTTGTGAC
HHF2 UpStream R	ATATTAGGATGAGGCGGTGAA
HHF2 Seq F	GCCAAGCGTCACAGAAAGAT
HHF2 Seq R	TCTCTTGGCGTGTTCAGTGT
Mpt5 UpStream (-380bps) F	TCAAAACCTTGGGTACTGTTGA
Mpt5 UpStream (-153bps) F	TGCTACTACAACCGCCACTT
Mpt5 iAID N1 F	AAAAAAAACCTCCTCAACTCCTCTCCAACACATAGTAAAGACAAGAACAATGCAATAGCGC
Mpt5 ATG Seq F	ATGGTATGTATTATCTCTTAATTCCC
Mpt5 iAID N2	TGGCGAAGAAAAATATTGGGAATTAAGAGATAATACATACCATGGAACCTCCTCTAGGTACAAGATC
Mpt5 iAID N3	TGGCGAAGAAAAATATTGGGAATTAAGAGATAATACATACCATCGAATTGATCCGGTAATTTAGTG
Mpt5 R2 R	TGGCGAAGAAAAATATTGGGAATTAAGAGATAATACATAC
Mpt5 Full/Mini F	AAAAACCCGGGTCTCTCTTGCCATTCTTAAACGT
Mpt5 Seq #1 F	CCATTTCCATCTGCCGACTC
Mpt5 Seq #2 F	GCGATTATTTAACTGCCGAGC
Mpt5 Seq #3 F	TCTGATGACGTGATTAATGCTTC
Mpt5 Seq #5 F	CAGCATATTGGTCAAGGCCC
Mpt5 Prom (Cloning) F	AAAAAGAGCTCTCTCTCTTGCCATTCTTAAACGT
Mpt5 Prom (Cloning) R	AAAAACCGCGGAAGAGAAACTGGAAAAATCGTAATTG
Mpt5 Start (Cloning) F	AAAAACCGCGGATGGTATGTATTATCTCTTAATTCCC

Primer Name	Sequence (5`-3`)
Mpt5 End-NLS (Cloning) R	AAAAACCCGGGTTACACTTTGCGTTTTTTTTTCGGTGGCAAAGTGAATTGAAGTTCATC
Mpt5 End-NES (Cloning) R	AAAAACCCGGGTTACAAGCCAATGCCGCTCAAATGCTCCCTCAATGGCAAAGTGAATTGAAGTTCATC
Mpt5 End (Cloning) R	AAAAACCCGGGTTATGGCAAAGTGAATTGAAGTTCATC
Mpt5 Term (Cloning) F	AAAAACCCGGGTACTTTTTTTTCTTTCTTTTTCTTT
Mpt5 Term (Cloning) R	AAAAACTCGAGACCAAGACAGGAACCAGTAGA
Mpt5 RBD-Muta F	TTGTTTGAAGTTCTCCGCCGCCGTTGTGGAAAAATTCA
Mpt5 RBD-Muta R	TGAATTTTTCCACAACGGCGGCGGAGAACTTCAAACAA
Mpt5 End-NoTAA (Cloning) R	AAAAACCCGGGTGGCAAAGTGAATTGAAGTTCATC
Mpt5 "Real" Prom (Cloning) F	AAAAAGAGCTCTCCTAGGCTTATACTCCAAAATCGGC
Mpt5 "Real" Prom (Cloning) R	AAAAACCGCGGTAAGGAGTTATTTGATGTAGACGTAG
Mpt5 "Real" Start (Cloning) F	AAAAACCGCGGATGTCTTACAATCATCAGCCTC
Mpt5 "Real" iAID N1 F	ATTCTTTTATTCAATCAGATCAATAACGAACCATTTCCATACAAGAACAATGCAATAGCGC
Mpt5 "Real" iAID N2 R	GGACGGAGTTAATAGATAGTTGAGGCTGATGATTGTAAGACATGGAACCTCCTCTAGGTACAAGATC
Mpt5 "Real" iAID N3 R	GGACGGAGTTAATAGATAGTTGAGGCTGATGATTGTAAGACATCGAATTGATCCGGTAATTTAGTG
Tet Op. UpStr. F	CGCTAGGGATAACAGGGTAATAT
Tet Op. DwnStr. R	TCGATCGAGACCACTGCATG
ADH1 Term F	ATTGACCACACCTCTACCGG
Mpt5 GFP (Cloning) F	AAAAACCCGGGAGTAAAGGAGAAGAACTTT
Mpt5 GFP (Cloning) R	AAAAACCCGGGCTATTTGTATAGTTCATCCA
Mpt5 GFP Check F	TTTTCAAGAGTGCCATGCCC
Mpt5 GFP Check R	CCATGTGTAATCCCAGCAGC
GFP-Spacer (Cloning) F	AAAAACCCGGGTCAGGATCAGGATCAGCAAGTAAAGGAGAAGAACTTT
Mpt5 Big (Cloning) F	AAAAACCCGGGCCTGGACACTGTACATGGTTG
Mpt5 Mini (Cloning) R	AAAAACTCGAGGCGAATGAGCCTTTTGATGG

Primer Name	Sequence (5`-3`)
Mpt5 Full/Big (Cloning) R	AAAAACTCGAGACCAAGACAGGAACCAGTAGA
Act1 F	TCCATCCAAGCCGTTTTGTC
Act1 R	ATCTCTACCGGCCAAATCGA
Pfa6aHis Seq #1 F	GCCCAGAATACCCTCCTTGA
Pfa6aHis Seq#2 F	GCATTCAAGCAGGCTATGGG
Pfa6a His Seq End R	GAATTCGAGCTCGTTTAAAC
AID*9Myc F Seq	CGTACGCTGCAGGTCGAC
AID*9Myc R Seq	ATCGATGAATTCGAGCTCG
Ccr4 S1 (Janke)	ACCAGCAAGGGAACTCCGACTGACGTTATCCCTGCAAACTACCGCTAATGCGTACGCTGCAGGTCGAC
Ccr4 S2 (Janke)	AGGTAGTGTACAGAGAGGAGGGAGGGAGTGGGATGAAAGTGTGCGGTTTAATCGATGAATTCGAGCTCG
Ccr4 S3 (Janke)	TGTTAGCAAGATTTGAATTTATGAAGACAAACACAGGCAGTAAGAAAGTACGTACGCTGCAGGTCGAC
Pop2 S1 (Janke)	AAACAGGCAACTCAATTTTATACATTTATAAAGGGTCAAAAAGGATTATGCGTACGCTGCAGGTCGAC
Pop2 S2 (Janke)	TTAAACTTTTTTTTTTAAAATTGTGTATACATATAGTACATAAATGATCAATCGATGAATTCGAGCTCG
Pop2 S3 (Janke)	CGGATTTCGCCAAGTACCAAGGTGTCATATACGGTATTGATGGGGACCAACGTACGCTGCAGGTCGAC
Mpt5 S1 (Janke)	ATTCTACGCAAATTTATAAATCAATTACGATTTTTCCAGTTTCTCTTATGCGTACGCTGCAGGTCGAC
Mpt5 S2 (Janke)	AAATATTTGTACAGTAAGAAGGAAAGAAAAAGAAAGAAAAAAAAGTATTAATCGATGAATTCGAGCTCG
Mpt5 S3 (Janke)	CTGCCATGAATACCGCTAGAACATCTGATGAACTTCAATTCACTTTGCCACGTACGCTGCAGGTCGAC
Pop2 F2 (LT)	CAAGTACCAAGGTGTCATATACGGTATTGATGGGGACCAACGGATCCCCGGGTTAATTAA
Pop2 R1 (LT)	TTTTTTTTTAAAATTGTGTATACATATAGTACATAAATGAGAATTCGAGCTCGTTTAAAC
Mpt5 F2 (LT)	TACCGCTAGAACATCTGATGAACTTCAATTCACTTTGCCACGGATCCCCGGGTTAATTAA
Mpt5 R1 (LT)	TGTACAGTAAGAAGGAAAGAAAAAGAAAGAAAAAAAAGTAGAATTCGAGCTCGTTTAAAC

Primer Name	Sequence (5`-3`)
Ccr4 F1 (LT)	AGGGAACTCCGACTGACGTTATCCCTGCAAACTACCGCTACGGATCCCCGGGTTAATTAA
Ccr4 F2 (LT)	ATTTGAATTTATGAAGACAAACACAGGCAGTAAGAAAGTACGGATCCCCGGGTTAATTAA
Ccr4 R1 (LT)	GTACAGAGAGGAGGGAGGGAGTGGGATGAAAGTGTGCGGTGAATTCGAGCTCGTTTAAAC
Ccr4 Internal F	ACTCCGCCGTATACGAATTG
Ccr4 UpStr. F	ACCACGTGGATCGTGCTCTA
Pop2 Internal F	CAACAGCAGCAGCAATATTCA
Pop2 UpStr. F	ACGGAATTCGGTCCTTACCC
Mpt5 AID* F	TACCGCTAGAACATCTGATGAACTTCAATTCACTTTGCCACGTACGCTGCAGGTCGAC
Mpt5 AID* R	TGTACAGTAAGAAGGAAAGAAAAAGAAAGAAAAAAAAGTAATCGATGAATTCGAGCTCG
H3K56R Site-Muta F	GAGAAATTAGAAGATTCCAAAGATCTACTGAACTGTTGATCAG
H3K56R Site-Muta R	CTGATCAACAGTTCAGTAGATCTTTGGAATCTTCTAATTTCTC
H3K36R Site-Muta F	CATCTACCGGTGGTGTTAGAAAGCCTCACAGATATAA
H3K36R Site-Muta R	TTATATCTGTGAGGCTTTCTAACACCACCGGTAGATG
H3K4R Site-Muta F	CCACAATGGCCAGAACTAGACAAACAGCTAGAAAATC
H3K4R Site-Muta R	GATTTTCTAGCTGTTTGTCTAGTTCTGGCCATTGTGG
H4K16A Site-Muta F	GGAAAAGGTGGTGCCGCACGTCACAGAAAGATT
H4K16A Site-Muta R	AATCTTTCTGTGACGTGCGGCACCACCTTTTCC
H4K16Q Site-Muta F	GGAAAAGGTGGTGCCCAACGTCACAGAAAGATT
H4K16Q Site-Muta R	AATCTTTCTGTGACGTTGGGCACCACCTTTTCC
Puf1 S1 (Janke)	GTGTATGTGTGAGAAAGAGCGTGAACGTCTATTTATTCCTTCTTAAGATGCGTACGCTGCAGGTCGAC
Puf1 S2 (Janke)	GGCGTGGTCTCCCAATGATGACGGAAATAAAAGAAACATGGGGACGTCAATCGATGAATTCGAGCTCG
Puf1 F1 (LT)	TGTGAGAAAGAGCGTGAACGTCTATTTATTCCTTCTTAAGCGGATCCCCGGGTTAATTAA
Puf1 R1 (LT)	TCTCCCAATGATGACGGAAATAAAAGAAACATGGGGACGGAATTCGAGCTCGTTTAAAC
Puf1 Upstr. F	CCCTTCTAAGTGTTTCCTTTGCA

Primer Name	Sequence (5`-3`)
Puf1 Internal F	GTTATCCTGGCGTCTTCCCT
Puf2 S1 (Janke)	AGATATATCTACTATCGCTGTCCCTTGCTACTGTTTTCTGAATTCTGATGCGTACGCTGCAGGTCGAC
Puf2 S2 (Janke)	TTGAAAAAAAAAAAAGTTTAATAGAACAGAATGATTAAAATCATTAGCTAATCGATGAATTCGAGCTCG
Puf2 F1 (LT)	TCTACTATCGCTGTCCCTTGCTACTGTTTTCTGAATTCTGCGGATCCCCGGGTTAATTAA
Puf2 R1 (LT)	AAAAAAAAGTTTAATAGAACAGAATGATTAAAATCATTAGGAATTCGAGCTCGTTTAAAC
Puf2 Upstr.F	TCGTGCGTTGCGTTAGAAAA
Puf2 Internal F	AACTTTAACCCAGCCCCGAT
Puf3 S1 (Janke)	ACTACGCATTTAAATTTCTTCTGAATAACGCAATATTGCGGGTATAAATGCGTACGCTGCAGGTCGAC
Puf3 S2 (Janke)	AAAAAAAAAAATAGTAAAAAGTGAAAGGAGAACGATGATAACACTAATCAATCGATGAATTCGAGCTCG
Puf3 F1 (LT)	ATTTAAATTTCTTCTGAATAACGCAATATTGCGGGTATAACGGATCCCCGGGTTAATTAA
Puf3 R1 (LT)	AAAATAGTAAAAAGTGAAAGGAGAACGATGATAACACTAAGAATTCGAGCTCGTTTAAAC
Puf3 UptStr.F	CGCACTCTGTTACCCTGAAC
Puf3 Internal F	CGGCTGTAGGGTCATTCAAAG
Puf4 S1 (Janke)	AGAAAGAGAGAACTAAGCGCTGTAACATTTTTAAGTGGACCTACGTTATGCGTACGCTGCAGGTCGAC
Puf4 S2 (Janke)	ATATGAGGCTAACGTAAAAAAAGCTAAACTGAGGATATATGTATCAACTAATCGATGAATTCGAGCTCG
Puf4 F1 (LT)	GAGAACTAAGCGCTGTAACATTTTTAAGTGGACCTACGTTCGGATCCCCGGGTTAATTAA
Puf4 R1 (LT)	GCTAACGTAAAAAAAGCTAAACTGAGGATATATGTATCAAGAATTCGAGCTCGTTTAAAC
Puf4 UpStr. F	CAGCAAACAGTACCTCACGT
Puf4 Internal F	TGTTGAAACCAAGAGCCATCG
Puf6 S1 (Janke)	TAGAGTACTGAAATAAAGCACAATCAGGAATAACAAATTAACTGACAATGCGTACGCTGCAGGTCGAC
Puf6 S2 (Janke)	TGTACAGATGCTTATATACCAAATATTGTGACTTTATCGTAGAAAATTTAATCGATGAATTCGAGCTCG

Primer Name	Sequence (5`-3`)
Puf6 F1 (LT)	CTGAAATAAAGCACAATCAGGAATAACAAATTAACTGACACGGATCCCCGGGTTAATTAA
Puf6 R1(LT)	ATGCTTATATACCAAATATTGTGACTTTATCGTAGAAAATGAATTCGAGCTCGTTTAAAC
Puf6 UpStr. F	AGGTAAAAGGAAGGAGACGCA
Puf6 Internal F	ACCGAAGAAGAGCACCCAAT
Rps2 F	TCTGGTATCGTCGCTTCTCC
Rps2 R	AACTGGCAATGGTTGTTCGG
Rps24b F	CGTCTTGCACCCAAACAGAG
Rps24b R	TCAGCCAAACCGTATCTGACT
Spt15 F	CAACTGTGACTTTGGGGTGC
Spt15 R	CAACCATTTTCCCTGAGGCA
Rps20 RunOn F	GGTCAAGAAGGGTCCAGTCA
Rps20 RunOn R	TTCGACATCCACACCAGGTT
Rpl21b RunOn F	CAACAAGATGGTCGGTAACAGA
Rpl21b RunOn R	TGGTTGAGCTGGTTGTCTCT
Act1 RunOn F	TGAAGTGTGATGTCGATGTCC
Act1 RunOn R	AGAACCACCAATCCAGACGG
Ubc6 RunOn F	GAATGGACGTTTCAAGCCCA
Ubc6 RunOn R	TGTAATTGATCCTGTCGTGGC
Mpt5 TAA-del F	CACTTTGCCACCCGGGTACT
Mpt5 TAA-del R	AGTACCCGGGTGGCAAAGTG
Mpt5 NLS TAA-del F	AAAACGCAAAGTGCCCGGGTACTTTT
Mpt5 NLS TAA-del R	AAAAGTACCCGGGCACTTTGCGTTTT
Mpt5 NES TAA-del F	GGCATTGGCTTGCCCGGGTACTTT
Mpt5 NES TAA-del R	AAAGTACCCGGGCAAGCCAATGCC
Xrn1 F1 (LT)	ACTTGTAACAACAGCAGCAACAAATATATATCAGTACGGTCGGATCCCCGGGTTAATTAA

Primer Name	Sequence (5`-3`)
Xrn1 R1 (LT)	TAAAGTAACCTCGAATATACTTCGTTTTTAGTCGTATGTTGAATTCGAGCTCGTTTAAAC
Xrn1 UpStr. F	TCCTTTGCTCGTCTTTTCGC
Xrn1 Internal	ACCCATTACACCCTCACCAG
Mx4 R	CTGCAGCGAGGAGCCGTAAT
E3V6NEXT	ACACTCTTTCCCTACACGACGCTCTTCCGAT CT[BC8][UMI10][T30]VN
E5V6NEXT	ACACTCTTTCCCTACACGACGCrGrGrG
SINGV6	ACACTCTTTCCCTACACGACGC
P5NEXTPT5	AATGATACGGCGACCACCGAGATCTACACTCTTT CCCTACACGACGCTCTTCCG*A*T*C*T
i7 Index Primer	CAAGCAGAAGACGGCATACGAGAT[i7]GTCTCGTGGGCTCGG

5.4.2 Plasmids

Table 2: Plasmids used in this study. Plasmid name, source, and description is given.

Plasmid	Source	Description or Integrated Cassette
pRS413	(Sikorski & Hieter, 1989)	pBluescript II; Amp^R; HIS3
pRS414	(Sikorski & Hieter, 1989)	pBluescript II; Amp^R; TRP
pFA6a-13myc	(Longtine *et al.*, 1998)	Amp^R; 13myc-HIS3
pFA6a-GFP	(Longtine *et al.*, 1998)	Amp^R; GFP(S65T)-HIS3
pFA6a-His	(Longtine *et al.*, 1998)	Amp^R; HIS3
pFA6a-HphNT1	(Janke *et al.*, 2004)	Amp^R; HphNT1 (Hygromycin B)
Phyg-AID*-9Myc	(Morawska and Ulrich, 2013)	Amp^R; C-terminal AID*9Myc-HphNT1 (Hygromycin B)
pNHK53	(Morawska and Ulrich, 2013)	Amp^R; OsTIR1-LEU2
pST1760	(Tanaka *et al.*, 2015)	Amp^R; OsTIR1/TetR-HIS3
pST1868	(Tanaka *et al.*, 2015)	Amp^R; OsTIR1/TetR-LEU2
pST1872	(Tanaka *et al.*, 2015)	Amp^R; Tet Prom/N-terminal 3x mini-AID-HphNT1 (Hygromycin B)

Plasmid	Source	Description or Integrated Cassette
pH3K56A	Lab Collection	Amp^R; Alanine substitution at H3K56; TRP (shuffle)
pH3K56R	This Study	Amp^R; Arginine substitution at H3K56; TRP (shuffle)
pH3K56Q	This Study	Amp^R; Glutamine substitution at H3K56; TRP (shuffle)
pH4K16A	This Study	Amp^R; Alanine substitution at H4K16; TRP (shuffle)
pH4K16Q	This Study	Amp^R; Glutamine substitution at H4K16; TRP (shuffle)
pH3K4R	This Study	Amp^R; Arginine substitution at H3K4; TRP (shuffle)
pH3K56A-Leu	This Study	Amp^R; Alanine substitution at H3K56; LEU2 (shuffle)
pH3K56Q-Leu	This Study	Amp^R; Glutamine substitution at H3K56; LEU2 (shuffle)
pH3/H4-Trp	Lab Collection	Amp^R; HHT2/HHF2; TRP (shuffle)
pH3/H4-Leu	This Study	Amp^R; HHT2/HHF2; LEU2 (shuffle)
pH3K36R	This Study	Amp^R; Arginine substitution at H3K36R; TRP (shuffle)
Mpt5-Myc (pRS413)	This Study	pRS413; Mpt5-13Myc; HIS (shuffle)
Mpt5-RBD (pRS413)	This Study	pRS413; Mpt5-RNA Binding Mutant; HIS (shuffle)
Mpt5-NLS (pRS413)	This Study	pRS413; C-terminal Mpt5-NLS tag; HIS (shuffle)
Mpt5-NES (pRS413)	This Study	pRS413; C-terminal Mpt5-NES tag; HIS (shuffle)
Mpt5-Real-(pRS413)	This Study	pRS413; Mpt5-truncated promoter; HIS (shuffle)
Mpt5-Full-(pRS413)	This Study	pRS413; Mpt5; HIS (shuffle)
Mpt5-GFP (pRS413)	This Study	pRS413; C-terminal Mpt5-GFP tag; HIS (shuffle)
Mpt5-NLS-GFP (pRS413)	This Study	pRS413; C-terminal Mpt5-NLS/GFP tag; HIS (shuffle)
Mpt5-NES-GFP (pRS413)	This Study	pRS413; C-terminal Mpt5-NES/GFP tag; HIS (shuffle)

5.4.3 Bacterial strains

Table 3: Bacterial strains used in this study. Strain nomenclature, source, and genotype are provided.

Strain	Source	Genotype
NEB Turbo	New England Biolabs	F′ proA+B+ lacIqΔ lacZ M15/ fhuA2 Δ(lac-proAB) glnV gal R(zgb-210::Tn10)TetSendA1 thi-1 Δ(hsdS-mcrB)5
DH5α	Lab	F⁻ *endA1 glnV44 thi-1 recA1 relA1 gyrA96 deoR nupG purB20* φ80d*lacZ*ΔM15 Δ(*lacZYA-argF*)U169, hsdR17($r_K^-m_K^+$), λ⁻

5.4.4 *S. cerevisiae* strains

Table 4: Yeast strains used in this study. Strain nomenclature is indicated by PTY-numbering. If source refers to the PTY number, then the strain was constructed in this study. Genotype details are also provided.

PTY	Source	Genotype
1021	W303/Lab Collection	Mata; ade2-1; ura3-1; his3-11,15; trp1-1; leu2-3,112; can1-100; hht1-hhf1::kanMX4; hht2-hhf2::natMX4; p(URA3)-HHT2/HHF2
1229	1021	Mata; ade2-1; ura3-1; his3-11,15; trp1-1; leu2-3,112; can1-100; hht1-hhf1::kanMX4; hht2-hhf2::natMX4; p(URA3)-HHT2/HHF2; p(TRP1)-HHT2/HHF2
1230	1021	Mata; ade2-1; ura3-1; his3-11,15; trp1-1; leu2-3,112; can1-100; hht1-hhf1::kanMX4; hht2-hhf2::natMX4; p(URA3)-HHT2/HHF2; p(TRP1)-hht2-K56A/HHF2
1231	1021	Mata; ade2-1; ura3-1; his3-11,15; trp1-1; leu2-3,112; can1-100; hht1-hhf1::kanMX4; hht2-hhf2::natMX4; p(URA3)-HHT2/HHF2; p(TRP1)-hht2-K56Q/HHF2
1232	1021	Mata; ade2-1; ura3-1; his3-11,15; trp1-1; leu2-3,112; can1-100; hht1-hhf1::kanMX4; hht2-hhf2::natMX4; p(URA3)-HHT2/HHF2; p(TRP1)-hht2-K56R/HHF2
1233	1021	Mata; ade2-1; ura3-1; his3-11,15; trp1-1; leu2-3,112; can1-100; hht1-hhf1::kanMX4; hht2-hhf2::natMX4; p(URA3)-HHT2/HHF2; mpt5Δ::hphNT1
1234	1233	Mata; ade2-1; ura3-1; his3-11,15; trp1-1; leu2-3,112; can1-100; hht1-hhf1::kanMX4; hht2-hhf2::natMX4; p(URA3)-HHT2/HHF2; mpt5Δ::hphNT1; p(TRP1)-HHT2/HHF2
1235	1233	Mata; ade2-1; ura3-1; his3-11,15; trp1-1; leu2-3,112; can1-100; hht1-hhf1::kanMX4; hht2-hhf2::natMX4; p(URA3)-HHT2/HHF2; mpt5Δ::hphNT1; p(TRP1)-hht2-K56A/HHF2
1236	1233	Mata; ade2-1; ura3-1; his3-11,15; trp1-1; leu2-3,112; can1-100; hht1-hhf1::kanMX4; hht2-hhf2::natMX4; p(URA3)-HHT2/HHF2; mpt5Δ::hphNT1; p(TRP1)-hht2-K56R/HHF2
1237	1233	Mata; ade2-1; ura3-1; his3-11,15; trp1-1; leu2-3,112; can1-100; hht1-hhf1::kanMX4; hht2-hhf2::natMX4; p(URA3)-HHT2/HHF2; mpt5Δ::hphNT1; p(TRP1)-hht2-K56Q/HHF2
1238	1021	Mata; ade2-1; ura3-1; his3-11,15; trp1-1; leu2-3,112; can1-100; hht1-hhf1::kanMX4; hht2-hhf2::natMX4; p(URA3)-HHT2/HHF2; pop2Δ::hphNT1

PTY	Source	Genotype
1239	1238	Mata; ade2-1; ura3-1; his3-11,15; trp1-1; leu2-3,112; can1-100; hht1-hhf1::kanMX4; hht2-hhf2::natMX4; p(URA3)-HHT2/HHF2; pop2Δ::hphNT1; p(TRP1)-HHT2/HHF2
1240	1238	Mata; ade2-1; ura3-1; his3-11,15; trp1-1; leu2-3,112; can1-100; hht1-hhf1::kanMX4; hht2-hhf2::natMX4; p(URA3)-HHT2/HHF2; pop2Δ::hphNT1; p(TRP1)-hht2-K56A/HHF2
1241	1238	Mata; ade2-1; ura3-1; his3-11,15; trp1-1; leu2-3,112; can1-100; hht1-hhf1::kanMX4; hht2-hhf2::natMX4; p(URA3)-HHT2/HHF2; pop2Δ::hphNT1; p(TRP1)-hht2-K56R/HHF2
1242	1238	Mata; ade2-1; ura3-1; his3-11,15; trp1-1; leu2-3,112; can1-100; hht1-hhf1::kanMX4; hht2-hhf2::natMX4; p(URA3)-HHT2/HHF2; pop2Δ::hphNT1; p(TRP1)-hht2-K56Q/HHF2
1243	1021	Mata; ade2-1; ura3-1; his3-11,15; trp1-1; leu2-3,112; can1-100; hht1-hhf1::kanMX4; hht2-hhf2::natMX4; p(URA3)-HHT2/HHF2; ccr4Δ::HIS3
1244	1243	Mata; ade2-1; ura3-1; his3-11,15; trp1-1; leu2-3,112; can1-100; hht1-hhf1::kanMX4; hht2-hhf2::natMX4; p(URA3)-HHT2/HHF2; ccr4Δ::HIS3; p(TRP1)-HHT2/HHF2
1245	1243	Mata; ade2-1; ura3-1; his3-11,15; trp1-1; leu2-3,112; can1-100; hht1-hhf1::kanMX4; hht2-hhf2::natMX4; p(URA3)-HHT2/HHF2; ccr4Δ::HIS3; p(TRP1)-hht2-K56A/HHF2
1246	1243	Mata; ade2-1; ura3-1; his3-11,15; trp1-1; leu2-3,112; can1-100; hht1-hhf1::kanMX4; hht2-hhf2::natMX4; p(URA3)-HHT2/HHF2; ccr4Δ::HIS3; p(TRP1)-hht2-K56R/HHF2
1247	1243	Mata; ade2-1; ura3-1; his3-11,15; trp1-1; leu2-3,112; can1-100; hht1-hhf1::kanMX4; hht2-hhf2::natMX4; p(URA3)-HHT2/HHF2; ccr4Δ::HIS3; p(TRP1)-hht2-K56Q/HHF2
1248	1021	Mata; ade2-1; ura3-1; his3-11,15; trp1-1; leu2-3,112; can1-100; hht1-hhf1::kanMX4; hht2-hhf2::natMX4; p(URA3)-HHT2/HHF2; mpt5::MYC-HIS3
1249	1248	Mata; ade2-1; ura3-1; his3-11,15; trp1-1; leu2-3,112; can1-100; hht1-hhf1::kanMX4; hht2-hhf2::natMX4; p(URA3)-HHT2/HHF2; mpt5::MYC-HIS3; p(TRP1)-HHT2/HHF2
1250	1248	Mata; ade2-1; ura3-1; his3-11,15; trp1-1; leu2-3,112; can1-100; hht1-hhf1::kanMX4; hht2-hhf2::natMX4; p(URA3)-HHT2/HHF2; mpt5::MYC-HIS3; p(TRP1)-hht2-56A/HHF2
1251	1233	Mata; ade2-1; ura3-1; his3-11,15; trp1-1; leu2-3,112; can1-100; hht1-hhf1::kanMX4; hht2-hhf2::natMX4; p(URA3)-HHT2/HHF2; mpt5Δ::hphNT1; p(LEU2)-HHT2/HHF2
1252	1233	Mata; ade2-1; ura3-1; his3-11,15; trp1-1; leu2-3,112; can1-100; hht1-hhf1::kanMX4; hht2-hhf2::natMX4; p(URA3)-HHT2/HHF2; mpt5Δ::hphNT1; p(LEU2)-hht2-K56A/HHF2
1253	1233	Mata; ade2-1; ura3-1; his3-11,15; trp1-1; leu2-3,112; can1-100; hht1-hhf1::kanMX4; hht2-hhf2::natMX4; p(URA3)-HHT2/HHF2; mpt5Δ::hphNT1; p(LEU2)-hht2-K56Q/HHF2
1254	1021	Mata; ade2-1; ura3-1; his3-11,15; trp1-1; leu2-3,112; can1-100; hht1-hhf1::kanMX4; hht2-hhf2::natMX4; p(URA3)-HHT2/HHF2; puf3Δ::hphNT1

PTY	Source	Genotype
1255	1254	Mata; ade2-1; ura3-1; his3-11,15; trp1-1; leu2-3,112; can1-100; hht1-hhf1::kanMX4; hht2-hhf2::natMX4; p(URA3)-HHT2/HHF2; puf3Δ::hphNT1; p(TRP1)-HHT2/HHF2
1256	1254	Mata; ade2-1; ura3-1; his3-11,15; trp1-1; leu2-3,112; can1-100; hht1-hhf1::kanMX4; hht2-hhf2::natMX4; p(URA3)-HHT2/HHF2; puf3Δ::hphNT1; p(TRP1)-hht2-K56A/HHF2
1257	1254	Mata; ade2-1; ura3-1; his3-11,15; trp1-1; leu2-3,112; can1-100; hht1-hhf1::kanMX4; hht2-hhf2::natMX4; p(URA3)-HHT2/HHF2; puf3Δ::hphNT1; p(TRP1)-hht2-K56Q/HHF2
1258	1021	Mata; ade2-1; ura3-1; his3-11,15; trp1-1; leu2-3,112; can1-100; hht1-hhf1::kanMX4; hht2-hhf2::natMX4; p(URA3)-HHT2/HHF2; puf4Δ::hphNT1
1259	1258	Mata; ade2-1; ura3-1; his3-11,15; trp1-1; leu2-3,112; can1-100; hht1-hhf1::kanMX4; hht2-hhf2::natMX4; p(URA3)-HHT2/HHF2; puf4Δ::hphNT1; p(TRP1)-HHT2/HHF2
1260	1258	Mata; ade2-1; ura3-1; his3-11,15; trp1-1; leu2-3,112; can1-100; hht1-hhf1::kanMX4; hht2-hhf2::natMX4; p(URA3)-HHT2/HHF2; puf4Δ::hphNT1; p(TRP1)-hht2-K56A/HHF2
1261	1258	Mata; ade2-1; ura3-1; his3-11,15; trp1-1; leu2-3,112; can1-100; hht1-hhf1::kanMX4; hht2-hhf2::natMX4; p(URA3)-HHT2/HHF2; puf4Δ::hphNT1; p(TRP1)-hht2-K56Q/HHF2
1262	1021	Mata; ade2-1; ura3-1; his3-11,15; trp1-1; leu2-3,112; can1-100; hht1-hhf1::kanMX4; hht2-hhf2::natMX4; p(URA3)-HHT2/HHF2; puf1Δ::HIS3
1263	1262	Mata; ade2-1; ura3-1; his3-11,15; trp1-1; leu2-3,112; can1-100; hht1-hhf1::kanMX4; hht2-hhf2::natMX4; p(URA3)-HHT2/HHF2; puf1Δ::HIS3; p(TRP1)-HHT2/HHF2
1264	1262	Mata; ade2-1; ura3-1; his3-11,15; trp1-1; leu2-3,112; can1-100; hht1-hhf1::kanMX4; hht2-hhf2::natMX4; p(URA3)-HHT2/HHF2; puf1Δ::HIS3; p(TRP1)-hht2-K56A/HHF2
1265	1262	Mata; ade2-1; ura3-1; his3-11,15; trp1-1; leu2-3,112; can1-100; hht1-hhf1::kanMX4; hht2-hhf2::natMX4; p(URA3)-HHT2/HHF2; puf1Δ::HIS3; p(TRP1)-hht2-K56Q/HHF2
1266	1021	Mata; ade2-1; ura3-1; his3-11,15; trp1-1; leu2-3,112; can1-100; hht1-hhf1::kanMX4; hht2-hhf2::natMX4; p(URA3)-HHT2/HHF2; puf2Δ::HIS3
1267	1266	Mata; ade2-1; ura3-1; his3-11,15; trp1-1; leu2-3,112; can1-100; hht1-hhf1::kanMX4; hht2-hhf2::natMX4; p(URA3)-HHT2/HHF2; puf2Δ::HIS3; p(TRP1)-HHT2/HHF2
1268	1266	Mata; ade2-1; ura3-1; his3-11,15; trp1-1; leu2-3,112; can1-100; hht1-hhf1::kanMX4; hht2-hhf2::natMX4; p(URA3)-HHT2/HHF2; puf2Δ::HIS3; p(TRP1)-hht2-K56A/HHF2
1269	1266	Mata; ade2-1; ura3-1; his3-11,15; trp1-1; leu2-3,112; can1-100; hht1-hhf1::kanMX4; hht2-hhf2::natMX4; p(URA3)-HHT2/HHF2; puf2Δ::HIS3; p(TRP1)-hht2-K56Q/HHF2
1270	1021	Mata; ade2-1; ura3-1; his3-11,15; trp1-1; leu2-3,112; can1-100; hht1-hhf1::kanMX4; hht2-hhf2::natMX4; p(URA3)-HHT2/HHF2; puf6Δ::HIS3

PTY	Source	Genotype
1271	1270	Mata; ade2-1; ura3-1; his3-11,15; trp1-1; leu2-3,112; can1-100; hht1-hhf1::kanMX4; hht2-hhf2::natMX4; p(URA3)-HHT2/HHF2; puf6Δ::HIS3; p(TRP1)-HHT2/HHF2
1272	1270	Mata; ade2-1; ura3-1; his3-11,15; trp1-1; leu2-3,112; can1-100; hht1-hhf1::kanMX4; hht2-hhf2::natMX4; p(URA3)-HHT2/HHF2; puf6Δ::HIS3; p(TRP1)-hht2-K56A/HHF2
1273	1270	Mata; ade2-1; ura3-1; his3-11,15; trp1-1; leu2-3,112; can1-100; hht1-hhf1::kanMX4; hht2-hhf2::natMX4; p(URA3)-HHT2/HHF2; puf6Δ::HIS3; p(TRP1)-hht2-K56Q/HHF2
1274	1021	Mata; ade2-1; ura3-1; his3-11,15; trp1-1; leu2-3,112; can1-100; hht1-hhf1::kanMX4; hht2-hhf2::natMX4; p(URA3)-HHT2/HHF2; p(TRP1)-hht2-K4R/HHF2
1275	1021	Mata; ade2-1; ura3-1; his3-11,15; trp1-1; leu2-3,112; can1-100; hht1-hhf1::kanMX4; hht2-hhf2::natMX4; p(URA3)-HHT2/HHF2; p(TRP1)-hht2-K36R/HHF2
1276	1021	Mata; ade2-1; ura3-1; his3-11,15; trp1-1; leu2-3,112; can1-100; hht1-hhf1::kanMX4; hht2-hhf2::natMX4; p(URA3)-HHT2/HHF2; p(TRP1)-HHT2/hhf2-K16A
1277	1021	Mata; ade2-1; ura3-1; his3-11,15; trp1-1; leu2-3,112; can1-100; hht1-hhf1::kanMX4; hht2-hhf2::natMX4; p(URA3)-HHT2/HHF2; p(TRP1)-HHT2/hhf2-K16Q
1278	1021	Mata; ade2-1; ura3-1; his3-11,15; trp1-1; leu2-3,112; can1-100; hht1-hhf1::kanMX4; hht2-hhf2::natMX4; p(URA3)-HHT2/HHF2; p(TRP1)-HHT2/hhf2-K5A
1279	1021	Mata; ade2-1; ura3-1; his3-11,15; trp1-1; leu2-3,112; can1-100; hht1-hhf1::kanMX4; hht2-hhf2::natMX4; p(URA3)-HHT2/HHF2; p(TRP1)-hht2-K79A/HHF2
1280	1021	Mata; ade2-1; ura3-1; his3-11,15; trp1-1; leu2-3,112; can1-100; hht1-hhf1::kanMX4; hht2-hhf2::natMX4; p(URA3)-HHT2/HHF2; p(TRP1)-HHT2/hhf2-K12A
1281	1021	Mata; ade2-1; ura3-1; his3-11,15; trp1-1; leu2-3,112; can1-100; hht1-hhf1::kanMX4; hht2-hhf2::natMX4; p(URA3)-HHT2/HHF2; p(TRP1)-HHT2/hhf2-K5-12AA
1282	1233	Mata; ade2-1; ura3-1; his3-11,15; trp1-1; leu2-3,112; can1-100; hht1-hhf1::kanMX4; hht2-hhf2::natMX4; p(URA3)-HHT2/HHF2; mpt5Δ::hphNT1; p(TRP1)-hht2-K4R/HHF2
1283	1233	Mata; ade2-1; ura3-1; his3-11,15; trp1-1; leu2-3,112; can1-100; hht1-hhf1::kanMX4; hht2-hhf2::natMX4; p(URA3)-HHT2/HHF2; mpt5Δ::hphNT1; p(TRP1)-hht2-K36R/HHF2
1284	1233	Mata; ade2-1; ura3-1; his3-11,15; trp1-1; leu2-3,112; can1-100; hht1-hhf1::kanMX4; hht2-hhf2::natMX4; p(URA3)-HHT2/HHF2; mpt5Δ::hphNT1; p(TRP1)-HHT2/hhf2-K16A
1285	1233	Mata; ade2-1; ura3-1; his3-11,15; trp1-1; leu2-3,112; can1-100; hht1-hhf1::kanMX4; hht2-hhf2::natMX4; p(URA3)-HHT2/HHF2; mpt5Δ::hphNT1; p(TRP1)-HHT2/hhf2-K16Q
1286	1233	Mata; ade2-1; ura3-1; his3-11,15; trp1-1; leu2-3,112; can1-100; hht1-hhf1::kanMX4; hht2-hhf2::natMX4; p(URA3)-HHT2/HHF2; mpt5Δ::hphNT1; p(TRP1)-hht2-K79A/HHF2

PTY	Source	Genotype
1287	1233	Mata; ade2-1; ura3-1; his3-11,15; trp1-1; leu2-3,112; can1-100; hht1-hhf1::kanMX4; hht2-hhf2::natMX4; p(URA3)-HHT2/HHF2; mpt5Δ::hphNT1; p(TRP1)-HHT2/hhf2-K5A
1288	1233	Mata; ade2-1; ura3-1; his3-11,15; trp1-1; leu2-3,112; can1-100; hht1-hhf1::kanMX4; hht2-hhf2::natMX4; p(URA3)-HHT2/HHF2; mpt5Δ::hphNT1; p(TRP1)-HHT2/hhf2-K12A
1289	1233	Mata; ade2-1; ura3-1; his3-11,15; trp1-1; leu2-3,112; can1-100; hht1-hhf1::kanMX4; hht2-hhf2::natMX4; p(URA3)-HHT2/HHF2; mpt5Δ::hphNT1; p(TRP1)-HHT2/hhf2-K5-12AA
1290	1243	Mata; ade2-1; ura3-1; his3-11,15; trp1-1; leu2-3,112; can1-100; hht1-hhf1::kanMX4; hht2-hhf2::natMX4; p(URA3)-HHT2/HHF2; ccr4Δ::HIS3; p(TRP1)-hht2-K4R/HHF2
1291	1243	Mata; ade2-1; ura3-1; his3-11,15; trp1-1; leu2-3,112; can1-100; hht1-hhf1::kanMX4; hht2-hhf2::natMX4; p(URA3)-HHT2/HHF2; ccr4Δ::HIS3; p(TRP1)-hht2-K36R/HHF2
1292	1243	Mata; ade2-1; ura3-1; his3-11,15; trp1-1; leu2-3,112; can1-100; hht1-hhf1::kanMX4; hht2-hhf2::natMX4; p(URA3)-HHT2/HHF2; ccr4Δ::HIS3; p(TRP1)-HHT2/hhf2-K16A
1293	1243	Mata; ade2-1; ura3-1; his3-11,15; trp1-1; leu2-3,112; can1-100; hht1-hhf1::kanMX4; hht2-hhf2::natMX4; p(URA3)-HHT2/HHF2; ccr4Δ::HIS3; p(TRP1)-HHT2/hhf2-K16Q
1294	1238	Mata; ade2-1; ura3-1; his3-11,15; trp1-1; leu2-3,112; can1-100; hht1-hhf1::kanMX4; hht2-hhf2::natMX4; p(URA3)-HHT2/HHF2; pop2Δ::HIS3; p(TRP1)-hht2-K4R/HHF2
1295	1238	Mata; ade2-1; ura3-1; his3-11,15; trp1-1; leu2-3,112; can1-100; hht1-hhf1::kanMX4; hht2-hhf2::natMX4; p(URA3)-HHT2/HHF2; pop2Δ::HIS3; p(TRP1)-hht2-K36R/HHF2
1296	1238	Mata; ade2-1; ura3-1; his3-11,15; trp1-1; leu2-3,112; can1-100; hht1-hhf1::kanMX4; hht2-hhf2::natMX4; p(URA3)-HHT2/HHF2; pop2Δ::HIS3; p(TRP1)-HHT2/hhf2-K16A
1297	1238	Mata; ade2-1; ura3-1; his3-11,15; trp1-1; leu2-3,112; can1-100; hht1-hhf1::kanMX4; hht2-hhf2::natMX4; p(URA3)-HHT2/HHF2; pop2Δ::HIS3; p(TRP1)-HHT2/hhf2-K16Q
1298	1233	Mata; ade2-1; ura3-1; his3-11,15; trp1-1; leu2-3,112; can1-100; hht1-hhf1::kanMX4; hht2-hhf2::natMX4; p(URA3)-HHT2/HHF2; mpt5Δ::hphNT1; p(HIS3)-empty; p(TRP1)-hht2-K56A/HHF2
1299	1233	Mata; ade2-1; ura3-1; his3-11,15; trp1-1; leu2-3,112; can1-100; hht1-hhf1::kanMX4; hht2-hhf2::natMX4; p(URA3)-HHT2/HHF2; mpt5Δ::hphNT1; mpt5::HIS3; p(TRP1)-hht2-K56A/HHF2
1300	1233	Mata; ade2-1; ura3-1; his3-11,15; trp1-1; leu2-3,112; can1-100; hht1-hhf1::kanMX4; hht2-hhf2::natMX4; p(URA3)-HHT2/HHF2; mpt5Δ::hphNT1; p(HIS3)-mpt5::NLS
1301	1300	Mata; ade2-1; ura3-1; his3-11,15; trp1-1; leu2-3,112; can1-100; hht1-hhf1::kanMX4; hht2-hhf2::natMX4; p(URA3)-HHT2/HHF2; mpt5Δ::hphNT1; p(HIS3)-mpt5::NLS; p(TRP1)-HHT2/HHF2
1302	1233	Mata; ade2-1; ura3-1; his3-11,15; trp1-1; leu2-3,112; can1-100; hht1-hhf1::kanMX4; hht2-hhf2::natMX4; p(URA3)-HHT2/HHF2; mpt5Δ::hphNT1; p(HIS3)-mpt5::NES

PTY	Source	Genotype
1303	1302	Mata; ade2-1; ura3-1; his3-11,15; trp1-1; leu2-3,112; can1-100; hht1-hhf1::kanMX4; hht2-hhf2::natMX4; p(URA3)-HHT2/HHF2; mpt5Δ::hphNT1; p(HIS3)-mpt5::NES; p(TRP1)-HHT2/HHF2
1304	1300	Mata; ade2-1; ura3-1; his3-11,15; trp1-1; leu2-3,112; can1-100; hht1-hhf1::kanMX4; hht2-hhf2::natMX4; p(URA3)-HHT2/HHF2; mpt5Δ::hphNT1; p(HIS3)-mpt5::NLS; p(TRP1)-hht2-K56A/HHF2
1305	1302	Mata; ade2-1; ura3-1; his3-11,15; trp1-1; leu2-3,112; can1-100; hht1-hhf1::kanMX4; hht2-hhf2::natMX4; p(URA3)-HHT2/HHF2; mpt5Δ::hphNT1; p(HIS3)-mpt5::NES; p(TRP1)-hht2-K56A/HHF2
1306	1300	Mata; ade2-1; ura3-1; his3-11,15; trp1-1; leu2-3,112; can1-100; hht1-hhf1::kanMX4; hht2-hhf2::natMX4; p(URA3)-HHT2/HHF2; mpt5Δ::hphNT1; p(HIS3)-mpt5::NLS; p(TRP1)-hht2-K4R/HHF2
1307	1302	Mata; ade2-1; ura3-1; his3-11,15; trp1-1; leu2-3,112; can1-100; hht1-hhf1::kanMX4; hht2-hhf2::natMX4; p(URA3)-HHT2/HHF2; mpt5Δ::hphNT1; p(HIS3)-mpt5::NES; p(TRP1)-hht2-K4R/HHF2
1308	1021	Mata; ade2-1; ura3-1; his3-11,15; trp1-1; leu2-3,112; can1-100; hht1-hhf1::kanMX4; hht2-hhf2::natMX4; p(URA3)-HHT2/HHF2; p(LEU2)-HHT2/HHF2
1309	1021	Mata; ade2-1; ura3-1; his3-11,15; trp1-1; leu2-3,112; can1-100; hht1-hhf1::kanMX4; hht2-hhf2::natMX4; p(URA3)-HHT2/HHF2; p(LEU2)-hht2-K56A/HHF2
1310	1021	Mata; ade2-1; ura3-1; his3-11,15; trp1-1; leu2-3,112; can1-100; hht1-hhf1::kanMX4; hht2-hhf2::natMX4; p(URA3)-HHT2/HHF2; p(LEU2)-hht2-K56Q/HHF2
1311	1233	Mata; ade2-1; ura3-1; his3-11,15; trp1-1; leu2-3,112; can1-100; hht1-hhf1::kanMX4; hht2-hhf2::natMX4; p(URA3)-HHT2/HHF2; mpt5Δ::hphNT1; mpt5::GFP-HIS3; p(TRP1)-hht2-K56A/HHF2
1312	1300	Mata; ade2-1; ura3-1; his3-11,15; trp1-1; leu2-3,112; can1-100; hht1-hhf1::kanMX4; hht2-hhf2::natMX4; p(URA3)-HHT2/HHF2; mpt5Δ::hphNT1; p(HIS3)-mpt5::GFP-NLS; p(TRP1)-hht2-K56A/HHF2
1313	1238	Mata; ade2-1; ura3-1; his3-11,15; trp1-1; leu2-3,112; can1-100; hht1-hhf1::kanMX4; hht2-hhf2::natMX4; p(URA3)-HHT2/HHF2; mpt5::MYC-HIS3; pop2Δ::hphNT1
1314	1238	Mata; ade2-1; ura3-1; his3-11,15; trp1-1; leu2-3,112; can1-100; hht1-hhf1::kanMX4; hht2-hhf2::natMX4; p(URA3)-HHT2/HHF2; mpt5::MYC-HIS3; pop2Δ::hphNT1; p(TRP1)-HHT2/HHF2
1315	1302	Mata; ade2-1; ura3-1; his3-11,15; trp1-1; leu2-3,112; can1-100; hht1-hhf1::kanMX4; hht2-hhf2::natMX4; p(URA3)-HHT2/HHF2; mpt5Δ::hphNT1; p(HIS3)-mpt5::GFP-NES; p(TRP1)-hht2-K56A/HHF2
1316	1233	Mata; ade2-1; ura3-1; his3-11,15; trp1-1; leu2-3,112; can1-100; hht1-hhf1::kanMX4; hht2-hhf2::natMX4; p(URA3)-HHT2/HHF2; mpt5Δ::hphNT1; p(HIS3)-mpt5::RBDmut; p(TRP1)-hht2-K56A/HHF2
1317	1233	Mata; ade2-1; ura3-1; his3-11,15; trp1-1; leu2-3,112; can1-100; hht1-hhf1::kanMX4; hht2-hhf2::natMX4; p(URA3)-HHT2/HHF2; mpt5Δ::hphNT1; p(HIS3)-mpt5::truncprom; p(TRP1)-hht2-K56A/HHF2
1318	1233	Mata; ade2-1; ura3-1; his3-11,15; trp1-1; leu2-3,112; can1-100; hht1-hhf1::kanMX4; hht2-hhf2::natMX4; p(URA3)-HHT2/HHF2; mpt5Δ::hphNT1; mpt5::RBDmut-HIS3

PTY	Source	Genotype
1319	1021	Mata; ade2-1; ura3-1; his3-11,15; trp1-1; leu2-3,112; can1-100; hht1-hhf1::kanMX4; hht2-hhf2::natMX4; p(LEU2)-OsTir1; p(TRP1)-HHT2/HHF2
1320	1021	Mata; ade2-1; ura3-1; his3-11,15; trp1-1; leu2-3,112; can1-100; hht1-hhf1::kanMX4; hht2-hhf2::natMX4; p(LEU2)-OsTir1; p(TRP1)-hht2-K56A/HHF2
1321	1021	Mata; ade2-1; ura3-1; his3-11,15; trp1-1; leu2-3,112; can1-100; hht1-hhf1::kanMX4; hht2-hhf2::natMX4; mpt5::c-terminal AID*9Myc-HphNT1; p(TRP1)-hht2-K56A/HHF2
1322	1021	Mata; ade2-1; ura3-1; his3-11,15; trp1-1; leu2-3,112; can1-100; hht1-hhf1::kanMX4; hht2-hhf2::natMX4; mpt5::c-terminal AID*9Myc-HphNT1; p(LEU2)-OsTir1; p(TRP1)-HHT2/HHF2
1323	1021	Mata; ade2-1; ura3-1; his3-11,15; trp1-1; leu2-3,112; can1-100; hht1-hhf1::kanMX4; hht2-hhf2::natMX4; mpt5::c-terminal AID*9Myc-HphNT1; p(LEU2)-OsTir1; p(TRP1)-hht2-K56A/HHF2
1324	1248	Mata; ade2-1; ura3-1; his3-11,15; trp1-1; leu2-3,112; can1-100; hht1-hhf1::kanMX4; hht2-hhf2::natMX4; p(URA3)-HHT2/HHF2; mpt5::MYC-HIS3; mpt5::tetprom/N-terminal3xmini-AID-hphNT1; p(LEU2)OsTIR1/TetR
1325	1248	Mata; ade2-1; ura3-1; his3-11,15; trp1-1; leu2-3,112; can1-100; hht1-hhf1::kanMX4; hht2-hhf2::natMX4; p(URA3)-HHT2/HHF2; mpt5::MYC-HIS3; p(LEU2)OsTIR1/TetR; p(TRP1)-HHT2/HHF2
1326	1248	Mata; ade2-1; ura3-1; his3-11,15; trp1-1; leu2-3,112; can1-100; hht1-hhf1::kanMX4; hht2-hhf2::natMX4; p(URA3)-HHT2/HHF2; mpt5::MYC-HIS3; p(LEU2)OsTIR1/TetR; p(TRP1)-hht2-K56A/HHF2
1327	1233	Mata; ade2-1; ura3-1; his3-11,15; trp1-1; leu2-3,112; can1-100; hht1-hhf1::kanMX4; hht2-hhf2::natMX4; p(URA3)-HHT2/HHF2; mpt5Δ::hphNT1; p(LEU2)OsTIR1/TetR; p(TRP1)-HHT2/HHF2
1328	1248	Mata; ade2-1; ura3-1; his3-11,15; trp1-1; leu2-3,112; can1-100; hht1-hhf1::kanMX4; hht2-hhf2::natMX4; p(URA3)-HHT2/HHF2; mpt5::MYC-HIS3; mpt5::tetprom/N-terminal3xmini-AID-hphNT1; p(LEU2)OsTIR1/TetR; p(TRP1)-hht2-K56A/HHF2
1329	1021	Mata; ade2-1; ura3-1; his3-11,15; trp1-1; leu2-3,112; can1-100; hht1-hhf1::kanMX4; hht2-hhf2::natMX4; p(URA3)-HHT2/HHF2; xrn1Δ::HIS3
1330	1248	Mata; ade2-1; ura3-1; his3-11,15; trp1-1; leu2-3,112; can1-100; hht1-hhf1::kanMX4; hht2-hhf2::natMX4; p(URA3)-HHT2/HHF2; mpt5::MYC-HIS3; mpt5::tetprom/N-terminal3xmini-AID-hphNT1
1331	1248	Mata; ade2-1; ura3-1; his3-11,15; trp1-1; leu2-3,112; can1-100; hht1-hhf1::kanMX4; hht2-hhf2::natMX4; p(URA3)-HHT2/HHF2; mpt5::MYC-HIS3; p(LEU2)OsTIR1/TetR; p(TRP1)-hht2-K4R/HHF2
1332	1248	Mata; ade2-1; ura3-1; his3-11,15; trp1-1; leu2-3,112; can1-100; hht1-hhf1::kanMX4; hht2-hhf2::natMX4; p(URA3)-HHT2/HHF2; mpt5::MYC-HIS3; mpt5::tetprom/N-terminal3xmini-AID-hphNT1; p(LEU2)OsTIR1/TetR; p(TRP1)-hht2-K4R/HHF2

5.5 Chemicals

All chemicals used in the study were analytical grade and purchased from Roth or Sigma.

5.6 Growth media

5.6.1 Growth media components

Amino Acids (for Drop Out Medium)	Roth
Yeast Nitrogen Base without Amino Acids	Roth
Yeast Extract	Serva/Roth
Glucose, monohydrate	Roth
Peptone ex meat	Roth
Drop Out Mix (Minus)	US Biological Life Sciences
Drop Out Mix (Complete)	US Biological Life Sciences
Agar	Roth
5-FOA (Hydrate)	Cayman Chemical/TRC Canada

5.6.2 Growth media formulas

Name	Formula
LB-Media (Bacteria)	1% Peptone
	0.5% Yeast Extract
	1% NaCl
	(2% Agar)
YPD-Media (Yeast)	2% Peptone
	1% Yeast Extract
	2% Glucose
	(2% Agar)

5.7 Antibodies

Mouse α -actin	GeneTex
Rabbit α -Gapdh	Sigma Aldrich
Mouse α -Puromyocin	EMD Milipore Corp

Mouse α -C-Myc	Sigma Aldrich
Rabbit α -H3K56ac	Active Motif
Mouse α -Anti-AID-tag	MBL International
Rabbit α -H3ac	Active Motif
Rabbit α -H3	ABcam
Goat α -rabbit IgG (horseradish peroxidase)	Cell Signaling
Horse α -mouse IgG (horseradish peroxidase)	Cell Signaling

5.8 Antibiotics

Ampicillin (100 μg/mL)	Roth
Doxycycline (0.2-40 μg/mL)	Sigma-Aldrich
Hygromycin B (150 μg/mL)	Applichem
CloNAT (100 μg/mL)	Sigma
Kanamycin (20 μg/mL)	Roth

5.9 Enzymes and miscellaneous proteins

Phusion High-Fidelity Polymerase	New England Biolabs
RNase A	Sigma
Restriction Enzymes	New England Biolabs
T4 DNA Polymerase	New England Biolabs
DNA Pol. Lg. Fragm. exo-	New England Biolabs
T4 Polynucleotide Kinase (PNK)	New England Biolabs
Dream Taq Polymerase	Thermo Fisher Scientific

5.10 Kits

NucleoSpin Plasmid EasyPure	Macherey-Nagel
NucleoSpin Gel and PCR Clean-up	Macherey-Nagel
QIAprep Spin Miniprep Kit	Qiagen
High Pure Plasmid Isolation Kit	Roche
Zyppy Plasmid Miniprep Kit	Zymoresearch

YeaStar Genomic DNA Kit	Zymoresearch
Western Turbo Blot Kit	Bio-Rad

6 Methods

6.1 Molecular biology methods

6.1.1 Molecular cloning

All molecular cloning performed in this study was based on the guidelines and recommendations in previous literature (Malke, 1990). Plasmid preparation and DNA extraction in the molecular cloning process was performed using the previously mentioned kits (5.10).

6.1.2 Agarose gel electrophoresis

Agarose flat-bed gels with concentrations between 0.8 – 1% in 1x TBE buffer were poured and run to separate DNA-fragments in an electrical field (10 – 20 V/cm) for analytical or preparative use. The desired amount of agarose was boiled in 1x TBE buffer until completely molten. After cooling to ~60°C, ethidium bromide solution (5 µL per 100 mL agarose) was mixed into the liquid agar, and then the solution was poured into a flat-bed tray with combs. After solidification of the agar, the DNA in DNA-loading buffer was pipetted into the lanes and separated through electrophoresis. The DNA was then detected using a Gel Viewer-BL Star 16 (Biometra).

6.1.3 Site-directed mutagenesis

Site-directed mutagenesis (SDM) is a method to create specific, targeted changes in double stranded plasmid DNA such as nucleotide insertions, deletions, and substitutions, in order to investigate how these changes influence protein activity and cell phenotype.

In this study, the SDM protocol was performed based on the QuikChange II Site-Directed Mutagenesis Kit (Agilent Technologies). Primers were designed based on the guidelines provided in the QuikChange II kit. PCR reactions were performed using the Phusion HF Polymerase and Phusion HF Reaction Buffer (New England Biolabs) with 50 ng of dsDNA template, 125 ng of each primer, and ensuring that the PCR program extension time was adequate enough to cover the entire plasmid length based on the Phusion HF Polymerase parameters. Following PCR amplification, 1 µL of Dpn restriction enzyme (New England

Biolabs) was added directly to each PCR amplification, the tubes were gently vortexed, and incubated for 60 min at 37°C. Following incubation, the amplified/digested plasmid was transformed using DH5α E. coli, and the DH5α cells were plated on the corresponding selection LB plates and incubated overnight at 37°C to select for positive colonies. The following day, the QIAprep Spin Miniprep Kit (Qiagen) was used to extract and purify the plasmids.

6.2 *S. cerevisiae* techniques

6.2.1 Transformation of *S. cerevisiae* cells

S. cerevisae cells have a very efficient recombination system; about 50 base pairs of homologous sequence, flanking large non-homologous sequence stretches, are sufficient for a targeted insertion into the yeast genome. This approach can be utilized to generate gene deletions by replacing the coding sequences with selection markers, or to insert fusions into the genome, such as specific C-terminal or N-terminal tags. The knock-out and insertion cassettes were amplified from vectors by PCR (Table 1), using specific primer designs based on previous literature (Janke et al., 2004; Longtine et al., 1998). The resulting PCR product ("transformation product") was transformed into yeast cells with the following protocol, and potentially positive clones were tested for correct gene deletion or gene fusion by PCR.

Single yeast colonies were picked and inoculated overnight in 4 mL of YPD media at 30°C. The following day, the cultures were diluted to an OD595 of ~0.15 in YPD media (with 10 mL of yeast cells per each individual transformation), and grown in canonical flasks at 30°C to an OD595 of 0.5-0.8. The cultures were transferred to 50 mL Falcon tubes, centrifuged at 3,000 rpm for 3 min at 20°C, and the supernatant was removed. Transformation wash was then added to each pellet based on ½ of the total volume of yeast culture in the previous step, the cells were vortexed briefly, and centrifuged at 3,000 rpm for 3 min at 20°C. The supernatant was discarded by pouring; the pellet was resuspended with the remaining supernatant using a 1000 μL pipette and transferred to a clean 1.5 mL Eppendorf tube. The tubes were centrifuged at max speed for 5 sec at 20°C, the supernatant was removed, the pellet was resuspended in 1 mL of transformation wash, and the tubes were centrifuged at 5,000 rpm for 2 min at 20°C. The supernatant was removed, 100 μL of transformation wash, per each individual transformation, was added and the tubes were vortexed. 100 μL of cells were then added to each corresponding 1.5 mL Eppendorf tube (each individual transformation), followed by 20 μL of Salmon Sperm DNA solution (10mg/ml) and the tubes were vortexed (Salmon Sperm DNA solution was boiled for 10 min in a heat block and then snap frozen on ice before use to ensure the DNA was single

stranded). The "transformation product" was then added to each tube (up to 15 µL if PCR product or 0.5 µL if shuffle plasmid), 600 µL of PEG mix was added, the tubes were vortexed vigorously, incubated in a heat block for 40 min at 30°C, and then directly incubated again in a water bath for 18 min at 42°C. The tubes were then centrifuged at 3,000 rpm for 2 min at 20°C, the supernatant was removed, and the pellet was resuspended in 100 µL of YPD media. Finally, each transformation was plated onto selective plates and incubated at 30°C for two days if selection was done through auxotrophic markers. Alternatively, if selection was done through antibiotic resistance, cells were plated for one night on YPD plates, followed by replica-plating onto selection plates.

Transformation wash:

0.1M LiAc

PEG mix:

40% PEG

0.1M LiAc

Salmon Sperm DNA:

Resuspend 200mg of DNA in 20 mL of ddH_2O in a 50 mL Falcon tube, boil in a glass beaker, snap cool on ice, and filter.

6.2.2 Serial dilution spot tests

In order to visualize *S. cerevisiae* growth phenotypes at a higher resolution and to test growth behavior of different strains under various conditions, serial dilution spot tests were performed.

Single yeast colonies were picked and inoculated overnight in 5 mL of YPD media at 30°C. The next day, the cell cultures were diluted to an OD_{595} of 1.0 in 200 µL of water, and 5-fold serial dilutions were performed in a 96-well plate. Spotting of the yeast cells was performed in parallel and in triplicate, on both selection media plates (to induce the mutation) and SD media plates (to verify equal quantity of yeast cells). Plates were incubated at 30°C for two to three days, and images were taken using the ChemiDoc MP system (Bio-Rad).

6.3 Hot phenol RNA extraction

Single yeast colonies were picked and inoculated overnight in 5 mL of YPD media at 30°C. The next day, the cultures were diluted in 10 mL of YPD media to an OD_{595} of ~0.15

and grown in canonical flasks at 30°C until an OD_{595} of 0.5-1.0 (with care being take to not exceed an OD_{595} greater than 1.0). The cultures were then transferred to 15 mL tubes and centrifuged at 3000 rpm for 3 min at 20°C. The supernatant was discarded, the pellet was resuspended in 1 mL of room temperature DNAse/RNAse free water (Invitrogen), transferred to a DNAse/RNAse free 1.5 mL Eppendorf tube, and then centrifuged at max speed for 10 sec at 20°C and the supernatant was removed. At this point, the pellet was snap frozen in liquid nitrogen and stored at -80°C until the protocol was continued.

The pellet was resuspend in 400 μL of TES solution, 400 μL of RNA extraction phenol was added, and the tubes were vortexed vigorously for 10 sec. The tubes were then incubated for 60 min in a heat block at 65°C, with brief vortexing every 15 min. Following incubation, the tubes were placed on ice for 5 min and then centrifuged at max speed for 5 min at 4°C. The aqueous phase was then transferred to a clean DNAse/RNAse free Eppendorf tube (with care being taken to not disturb the phases), 400 μL of RNA extraction phenol was added to the extracted aqueous phase, the tubes were vortexed vigorously, placed on ice for 5 min, and then centrifuged at max speed for 5 min at 4°C. The aqueous phase was transferred again to a clean DNAse/RNAse free Eppendorf tube (with care being taken to not disturb the phases), 400 μL of chloroform was added, the tubes were vortexed vigorously, and then centrifuged at max speed, for 5 min at 4°C. The aqueous phase was transferred a final time to a clean DNAse/RNAse free Eppendorf tube (with care being taken to not disturb the phases), 40 μL of 3 M sodium acetate with a pH of 5.3 and 1 mL of ice-cold 100% ethanol was added, the tubes were mixed by gentle inversion and precipitated overnight at -20°C. The following day, the tubes were centrifuged at 11,000 rpm for 5 min at 4°C, and the supernatant was removed with a vacuum pump (with care being taken to remove as much of the supernatant as possible without disturbing the pellet). The RNA pellet was then resuspended and vortexed briefly in 1 mL of ice-cold 70% ethanol, and the tubes were centrifuge at 11,000 rpm for 5 min at 4°C. The supernatant was removed; the pellet was resuspended in 50 μL of DNAse/RNAse free water (Invitrogen), and the tubes were incubated in a heat block for 7 min at 65°C. Finally, the quality and concentration of the RNA was determined using a Nano-photometer (Implen), and the RNA was stored at -80°C until further use.

TES Solution (in Invitrogen H$_2$O):

10 mM Tris, pH 7.5

10 mM EDTA

0.5% SDS

6.4   Protein analysis

6.4.1   Protein extraction

Single yeast colonies were picked and inoculated overnight in 5 mL of YPD media at 30°C. The next day, the cultures were diluted in 10 mL of YPD media to an OD_{595} of ~0.2 and grown in canonical flasks at 30°C until an OD_{595} of 0.5-0.8. A volume equivalent to one OD_{595} was pipetted into a 2 mL Eppendorf tube, and the tubes were centrifuged at 5,000 rpm for 3 min at 20°C and the supernatant was removed. At this point, the cells were either stored at -20°C or the protocol was continued.

The pellet was resuspended in 240 µL of 1.85 M NaOH and 1.06 M 2-mercaptoethanol solution and incubated on ice for 10 min. An equal volume of 50% Trichloroacetic acid was then added, the tubes were incubated on ice for 10 min, and centrifuged at 13,000 rpm for 10 min at 4°C. Next, the supernatant was removed, the pellet was washed in 1 mL of 1 M Tris base, and the tubes were centrifuged at 13,000 rpm for 10 min at 4°C. The supernatant was removed, 50 µL of 2x Laemmli protein loading buffer was added (Laemmli, 1970), and the tubes were boiled in a heat block for 5 min and then stored at -20°C.

6.4.2   Gel-electrophoresis with SDS-PAGE

Proteins of different sizes can be denatured and separated by SDS-Polyacrylamide gel electrophoresis (SDS-PAGE). The gels used in this technique are composed of two distinct sections: A lower resolving gel, with polyacrylamide concentrations ranging from 8 to 15% depending on the size of the proteins of interest; and an upper stacking gel with 4% polyacrylamide, used to arrange the proteins before they move into the resolving gel. SDS-polyacrylamide gels of varying concentrations were made using the formula provided below (quantities provided are for two mini gels):

	8%	10%	12%	15%	Stacking
Water (mL)	4.6	4.0	3.3	2.3	4.1
30% Acrylamide (mL)	2.7	3.3	4.0	5.0	1.0
1.5M Tris (pH 8.0) (mL)	2.5	2.5	2.5	2.5	0.75 (pH 6.8)
10% SDS (µL)	100	100	100	100	60
10% APS (µL)	100	100	100	100	60
TEMED (µL)	6	4	4	4	6

Once the gels solidified, 10 µL of prepared protein sample (6.4.1) and 5 µL of PageRuler prestained protein ladder (Thermo Fisher Scientific) were loaded into the SDS-polyacrylamide gel slots using a micropipette and long-tailed tips. All gels were run at 120 V using a Power Pac – Basic (Bio-Rad) in 1x SDS gel running buffer until the gel front reached the bottom of the gel plates, thus ensuring optimal separation of the proteins.

6.4.3   Western blot of SDS-PAGE gels

The western blot technique allows for transfer of proteins separated through SDS-PAGE (reference section) from the SDS-polyacrylamide gel to a nitrocellulose membrane through the application of an electric field; thus allowing for subsequent immunodetection of the proteins of interest. In this study, transfer of proteins from SDS-polyacrylamide gels to nitrocellulose membranes was performed using the Western blot transfer system (Bio-Rad), by following the instructions and using the reagents/components in the Bio-Rad Western Turbo Blot Kit (5.10). Once proteins were transferred to a nitrocellulose membrane using the Bio-Rad transfer system, the proteins of interest were detected using immunological methods. First, the nitrocellulose membrane was stained with Ponceau S solution for two min to ensure equal and proper transfer of proteins to the membrane and for reference as a loading control. The dye was then washed away with water, the membrane was blocked by incubation in 5% milk solution (5% milk powder in 1x TBST) for one hour at room temperature, and then the membrane was incubated in the primary antibody at 4°C overnight (antibodies were diluted in 5% milk solution based on the manufacturer's instructions). The following day, the membrane was washed three times with 1x TBST for 10 min each time, and then the membrane was incubated in the secondary antibody for one hour at room temperature (secondary antibody was diluted 1:10,000 in 5% milk solution). All secondary antibodies used in this study were conjugated with horseradish peroxidase, which produces an optically active hydroxyl peroxide through Enhanced chemiluminescence (ECL). After incubation in the secondary antibody, the membrane was washed three times with 1x TBST for 10 min each time, and then exposed to ECL Western Blotting Substrate (Promega) for 3 min, with care being taken to expose the membrane evenly to the ECL substrate. Next, the membrane was placed in a clear foil sheet, placed within a film developing cassette (Roth), exposed to Amersham hyperfilm ECL (GE Healthcare) for 1 to 40 min depending on the protein of interest and antibody used, and then the hyperfilm was developed using the Curix 60 (AGFA).

Ponceau S Solution:

0.1% (w/v) Ponceau S

1% (v/v) Acetic Acid

1x TBST Buffer:

10 mM Tris/HCl (pH 7.5)

150 mM NaCl

0.1% (v/v) Tween 20

6.5 Chromatin immunoprecipitation (ChIP)

The chromatin immunoprecipitation (ChIP) assay is a technique used for probing protein-DNA interactions and to identify the scope of specific histone modifications within the chromatin landscape of the cell. In this study, the ChIP assay was performed and ChIP-seq libraries were constructed in order to investigate genome wide changes for specific histone modifications.

6.5.1 ChIP pulldown

Day One

Single yeast colonies were picked and inoculated overnight in 5 mL of YPD media at 30°C. The next day, the cultures were diluted in 60 mL of YPD media to an OD_{595} of ~0.15 and grown in canonical flasks at 30°C until an OD_{595} of 0.6-0.8. 50 mL of yeast culture was then transferred to 50 mL Falcon tubes, 1.35 mL of 37% Formaldehyde (1% final Formaldehyde concentration) was added, and the tubes were incubated on a shaker for 60 min at 20°C. Next, the tubes were centrifuged at 3,000 rpm for 2 min at 4°C, the supernatant was discarded, the pellet was resuspended in 10 mL of ice-cold PBS, centrifuged again at 3,000 rpm for 2 min at 4ºC, and the supernatant was discarded. The wash step was then repeated with 10 mL of ice-cold PBS and centrifugation at the same settings, but then 8 mL of PBS supernatant was removed, and the pellet was resuspended in the remaining supernatant and transferred to a 2 mL Eppendorf tube. The tubes were centrifuged at max speed for 10 sec at 4°C, the supernatant was removed, and the pellet was stored on ice (pellets can also be snap frozen in liquid nitrogen and stored at -80°C until further use). The pellet was then resuspended in 500 μL of ice-cold SDS buffer and 200 μL of glass beads were added to the tubes. Next, the tubes were vortexed on the highest setting for 1 min using a Vortex Genie 2 (Scientific Industries) followed by incubation on ice for 3 min (this vortex/incubation cycle was repeated four times). The bottom

of the tubes were then needle pierced, the tubes were placed in 15 mL Falcon tubes, and the tubes were centrifuged at 2,000 rpm for 30 sec at 4°C to get rid of the cell debris. The cells were then sonicated using the M220 sonicator (Covaris) with the program: peak power 75, cycles/burst 200, duty factor 25, duration 5 min. The sonicated cells were then transferred to a 15 mL Falcon tube, centrifuged at 14,000 rpm for 20 min at 4°C, the supernatant was removed, and the pellets were resuspended in up to 10 mL of ice-cold IP buffer. At this point, a 30 µL aliquot was taken as an input control and stored at -20ºC. With the remaining cells, 1 mL aliquots were pipetted into siliconized Eppendorf tubes, and 2-5 µL of antibody was added to each tube. The tubes were then incubated on a rotating wheel overnight at 4ºC.

Day Two

After incubation, 30 µL of Protein G Dynabeads (Invitrogen), washed in IP buffer, were added to the tubes and incubated on a rotating wheel for 60 min at 20°C. The beads were then washed with the listed buffers using a magnet system and incubation on the rotating wheel with the listed timeframes:

1ml TSE-150 (3 min)

1ml TSE-500 (3 min)

1ml LiCl wash (3 min)

Add 1ml TE pH8 (3min)

After the washes, 200 µL of Elution buffer was added and the tubes were incubated on the rotating wheel for 30 min at 20°C. Next, 20 µL of 5M NaCl and 10 µL of DNase-free RNase was added, and the tubes were incubated in a heat block overnight at 65ºC.

Day Three

All samples were purified using the Macherey-Nagel NucleoSpin Gel and PCR Clean-up kit (1.10), and then eluted in 40-50 µL of DNAse/RNAse free water. Finally, either the samples were used for ChIP Library prep (6.5.2), or 1-2 µL were used for qPCR analysis.

IP Buffer

0.01% SDS

1.1%Triton-X-100

1.2mM EDTA

16.7mM Tris HCl (pH 8.0)

167mM NaCl

0.5mM PMSF

0.8 µg/ml Pepstatin A

0.6 µg/ml leupeptin.

TSE-150/500

1% Triton-X-100

0.1%SDS

2mM EDTA

20mM Tris HCl (pH 8.0)

150mM/500mM NaCl

SDS Buffer

1% SDS

10mM EDTA

50mM Tris HCl (pH 8.0)

0.5mM PMSF-EtOH

0.8 µg/ml pepstatin A

0.6 µg/ml leupeptin

Elution Buffer

1% SDS

0.1M NaHCO3

LiCl Wash

0.25M LiCl

1% NP-40

1% dioxycholate

1mM EDTA

10mM Tris HCl (pH 8.0

6.5.2 ChIP library prep

Twenty microliters of prepared ChIP DNA (6.5.1) was used in the following steps for the ChIP library prep.

<u>Blunt DNA Ends (End Repair)</u>

The following formula was followed and the tubes were incubated in a heat block for 30 min at 20˚C:

20 µL ChIP DNA (≈10ng)

5 µL NEB T4 DNA ligase buffer (without ATP)

5 µL ATP (10 mM)

2 µL dNTP`s (10 mM)

0,5 µL End-Repair-Enzyme-Mix*

17,5 µL H_2O

*End-Repair Mix:

5 µL T4 DNA Polymerase

1 µL Klenow fragment

5 µL T4 PNK

After the incubation step, 90 µL of Ampure XP beads (Beckman Coulter), per 50 µL of reaction volume, were added to each tube, mixed by pipetting, and then incubated for 5 min at 20ºC. Next, the samples were placed on a magnet system until a clear solution formed (~3 min), and the supernatant was removed. The beads were then washed twice with 70% EtOH, air dried for 5 min, and then the samples were eluted in 22 µL of water for 5 min, but only 18 µL of the elute was transferred to a new Eppendorf tube.

<u>Addition of "A" bases to the 3' ends of the DNA fragments</u>

After the Ampure XP bead clean up, the following formula was followed and the tubes were incubated in a heat block for 30 min at 37˚C, directly followed by incubation for 5 min at 70˚C.

16.5 µL End-repaired DNA

2 µL NEB buffer 2 (10X)

1 µL dATP (4mM)

0,5 µL Klenow 3' to 5' exo minus (5 U/µl)

<u>Ligation of adapters to DNA fragments</u>

After addition of "A" bases, the following formula was followed and the tubes were incubated in a heat block for 15 min at 20˚C, directly followed by incubation for 15 min at 30 ˚C.

20 µL A-tailed DNA

27.25 µL 2X Quick ligase buffer

2.5 µL Annealed adapters

375 µL H$_2$O

1 µL Quick Ligase (2000 U/µl NEB)

*Following the incubation step, 5.5 µl of 0.5 M EDTA with a pH of 8.0 was added.

After addition of 0.5 M EDTA, 108 µL of Ampure XP beads (per 60 µL of reaction volume) were added to each tube, mixed by pipetting, and then incubated for 5 min at 20ºC. Next, the samples were placed on a magnet system until a clear solution formed (~3 min) and the supernatant was removed. The beads were then washed twice with 70% EtOH, air dried for 5 min, and then the samples were eluted in 24 µL of water for 5 min, but only 20 µL of the elute was transferred to a new Eppendorf tube.

Amplification of Library by PCR

After the Ampure XP bead clean up, the following PCR reaction was set up and performed using the T100 Thermal Cycler (Bio-Rad) with a specified program (45 sec at 98˚C; 17 cycles of 15 sec at 98˚C, 30 sec at 63˚C, 30 sec at 72˚C; 60 sec at 72˚C):

19 µL of DNA ligated

1 µL PCR primer Mix

20 µL HiFi HotStart 2X Kapa Mix

Double Sided Size Selection (≈200-650bp)

After the PCR reaction, 20 µl of Ampure XP beads were added to 40 µl of the PCR product (0.5 ratio) and the samples were mixed by pipetting. Next, the samples were placed on a magnet system until a clear solution formed (~3 min) and the supernatant was transferred to a new Eppendorf tube. 12 µl of Ampure XP beads were then added to the transferred supernatant (0.3 ratio), the samples were mixed by pipetting, and incubated for 5 min at 20˚C. The samples were then placed on a magnet system until a clear solution formed (~3 min) and the supernatant was removed. The beads were then washed twice with 85% EtOH, air dried for 5 min, and then the samples were eluted in 24 µL of water for 5 min, but only 20 µL of the elute was transferred to a new Eppendorf tube.

Library quality was checked using the tape station 2200 (Agilent Technologies) and samples were sent for sequencing to the Max Planck Institute for Plant Breeding Research in Cologne. Bioinformatics analysis of the data was performed by Dr. Swati Parkesh.

6.6 Improved Auxin-Inducible Degron (iAID) system and time course sample extractions

An improved Auxin-Inducible Degron (iAID) system, which incorporates a Tet_{OFF} promoter in parallel to target-specific AID mediated protein degradation, was also applied in this study (Tanaka et al., 2015). The iAID system was generated by amplification of specific vectors through PCR (5.4.2) and by following the previously described *S. cerevisiae* cell transformation protocol (6.2.1). To induce and analyze growth phenotypes and collect cell samples for further analysis, the following growth and cell preparation protocol was applied.

Single yeast colonies were picked and inoculated overnight in 5 mL of YPD media at 30°C. The next day, the cultures were diluted in 20 mL of YPD media to an OD_{595} of ~0.15 and grown in canonical flasks at 30°C until an OD_{595} of 0.6-0.8. From each cell culture, 10 mL were collected for RNA extraction (6.3), one OD_{595} for protein extraction (6.4.1), and 1 mL of cell culture was diluted in 4 mL of YPD media containing 0.25 µg/mL of Doxycycline (Sigma) and incubated overnight at 30°C. The following day, the overnight cultures were diluted in 40 mL of YPD media containing 0.25 µg/mL of Doxycycline to an OD_{595} of 0.2 and incubated at 30°C to an OD_{595} of 0.6-0.8. From each cell culture, 10 mL were then collected for RNA extraction (6.3), 1 OD_{595} for protein extraction (6.4.1), and the remaining cell culture was diluted in 40 mL of YPD media containing 40 µg/mL of Doxycycline and 1mM Auxin to an OD_{595} of ~0.2. The cell cultures were then incubated at 30°C for 90 min. After 90 min, OD_{595} measurements were taken, 10 mL of cell culture was collected for RNA extraction (6.3), one OD_{595} for protein extraction (6.4.1), and the remaining cell culture was incubated again at 30°C. After an additional 150 min of incubation, OD_{595} measurements were taken, 10 mL of cell cuture was collected for RNA extraction (6.3), one OD_{595} for protein extraction (6.4.1), and the remaining cell culture was incubated at 30°C. Finally, after 120 more min of incubation, OD_{595} measurements were taken.

Growth curves were generated based on the OD_{595} measurements, and RNA and protein extraction was done on the collected cells as previously described (6.3 and 6.4.1).

6.7 Bulk-RNA-Unique Molecular Identifier (UMI) sequencing library prep

Common high-throughput RNA sequencing techniques rely on a PCR amplification step that may result in different amplification rates between molecules, thus resulting in an overrepresentation of some transcripts due to PCR duplicates. Unique molecular identifiers (UMI) are molecular tags that can be incorporated into the RNA sequencing process to detect and quantify polyadenylated transcripts without PCR duplicate bias. In this study, the UMI approach was applied to bulk RNA-seq libraries.

RNA extraction was performed on the cells as previously described (6.3), and the following protocol was used to generate bulk-RNA-UMI-seq libraries. All primers used in the generation of the libraries can be found in Table 1.

Reverse Transcription

The following Reverse Transcription Mix was prepared and combined with 50 ng of total RNA per sample, and reverse transcription was performed in the T100 Thermal Cycler (Bio-Rad) for 90 min at 42°C:

Maxima H Minus RT	0.125 μL
Maxima RT Buffer (5x)	2 μL
dNTPs (25mM)	0.4 μL
Uni. E5V6NEXT (100uM)	0.1 μL
E3V6NEXT-UMI (2uM)	1 μL
H20*	6.375 μ*
RNA	(50 ng)

*adjust H_2O volume based on volume of RNA added

cDNA Pooling and Purification

All reverse transcribed samples were pooled into a single 2 mL Eppendorf tube, Ampure XP (Invitrogen) beads were added at a volume to volume ratio of 1:1, mixed by pipetting, and then incubated for 5 min at 20 ºC. Next, the samples were placed on a magnet system until a clear solution formed (~3 min), and the supernatant was removed. The beads were then washed twice with 80% EtOH, air dried for 4 min, and then the samples was eluted in 20 μL of water for 5 min, but only 17 μL of the elute was transferred to a new PCR tube.

Exonuclease Treatment

1 µL of Exonuclease (New England Biolabs) and 2 µL of Exonuclease buffer (New England Biolabs) was added to the 17 µL of pooled and purified samples, and the samples were incubated in the T100 Thermal Cycler (Bio-Rad) for 20 min at 37°C, followed by heat inactivation for 10 min at 80°C.

Full Length cDNA Amplification

25 µL of NXT 2x reaction mix (New England Biolabs), 1 µL of SINGV6 Primer (10µM), and 4 µL of DNAse/RNAse free water was added to the Exonuclease treated samples, and the following PCR program was run:

Step	Temp.	Time	
Initial Denaturation	98°C	3min	
Denaturation	98°C	15sec	
Annealing	65°C	30sec	10 cycles
Elongation	68°C	4min	
Final Elongation	72°C	10min	
Store	4°C	store	

Full Length cDNA Purification

The PCR product was transferred to a 1.5 mL Eppendorf tube, Ampure XP beads were added at a volume to volume ratio of 0:8, mixed by pipetting, and then incubated for 5 min at 20 ℃. Next, the samples were placed on a magnet system until a clear solution formed (~3 min), and the supernatant was removed. The beads were then washed twice with 80% EtOH, air dried for 4 min, and then the samples were eluted in 12 µL of water for 5 min, but only 10 µL of the elute was transferred to a new PCR tube.

Tagmentation

The purified cDNA samples were quantified using the Qubit 3 Fluoromoeter (Thermo Fisher Scientific), and the following tagmentation mix was prepared and added to five separate technical repeats:

	1x
cDNA (0.8 ng in total per replicate)	0.8ng total
Tagment DNA Buffer	10μL
Amplicon Tagment Mix	5 μL
H_2O^*	4 μL *
Total	20 μL

*adjust H_2O volume based on volume of cDNA added

Each technical repeat was then incubated for 10 min at 55°C, followed by addition of 5 μL of NT buffer (Illumina) and incubation for 5 min at 20°C.

Library Completion

25 μL of Index PCR mix (Illumina) was prepared and added to each tagmentation replicate based on the following formula:

	1x
P7NXX (i7 Index) Primer (5 uM)	0.5μL
P5NextPT5 Primer (5 uM)	0.5μL
NPM PCR Mix	15μL
H_2O	9μL
Total	25μL

Each tagmentation replicate was then amplified with the following PCR program:

Step	Temp.	Time	
Elongation	72°C	3min	
Initial Denaturation	95°C	30sec	
Denaturation	95°C	10sec	
Annealing	55°C	30sec	13 cycles
Elongation	72°C	1min	
Final Elongation	72°C	5min	
Store	4°C	store	

Following PCR amplification, all technical repeats were pooled into a single 1.5 mL Eppendorf tube, Ampure XP beads were added at a volume to volume ratio of 0:6, mixed by pipetting, and then incubated for 5 min at 20 ℃. Next, the samples were placed on a magnet

system until a clear solution formed (~3 min), and the supernatant was removed. The beads were then washed twice with 80% EtOH, air dried for 4 min, and then the sample was eluted in 22 μL of water for 5 min, but only 20 μL of the elute was transferred to a new PCR tube.

Finally, the quantity and quality of the UMI-seq library was checked using the Tape station 2200 (Agilent Technologies) and DNA High-Sensitivity tape (Agilent Technologies), and the UMI-seq libraries were sent off for sequencing to the Max Planck Institute for Molecular Genetics in Berlin. Bioinformatics analysis of the data was performed by Dr. Swati Parkesh based on previous literature (Parekh et al., 2018).

6.8   Staining and imaging of *S. cerevisiae* cells

6.8.1   DAPI staining *S. cerevisiae* cells

Single yeast colonies were picked and inoculated overnight in 5 mL of minimal media at 30°C. The following day, 900 μL of cell culture was transferred to a 1.5 mL Eppendorf tube containing 100 μL of 37% formaldehyde (3.7% formaldehyde final concentration) and the tubes were mixed by inversion. The tubes were incubated for 25 min at 20°C with gentle rotation, centrifuged at 3,000 rpm for 3 min at 20°C, the supernatant was removed, and the pellet was washed with 1x PBS. The tubes were centrifuged again at 3,000 rpm for 3 min at 20°C, the supernatant was removed, and the pellet was resuspended in 1x PBS/0.1% Triton x-100 and incubated for 10 min at 20°C. The tubes were then centrifuged at 3,000 rpm for 3 min at 20°C, the supernatant was removed and the pellet was resuspended in 1x PBS, and the centrifugation step was repeated. The supernatant was then removed, the pellet was resuspended in 1 mL of 1x PBS, 1 μL of 0.5 mg/mL DAPI (Thermo Fisher Scientific) was added, and the tubes were incubated in the dark for 10 min at 20°C with gentle rotation. Following incubation, the cells were washed two times with PBS as described previously, and the pellet was resuspended in KPO_4/Sorbitol buffer. At this point, cells could be stored in the dark for 1-2 weeks at 4°C).

KPO_4/Sorbitol buffer:
41.7 mL 1 M K_2HPO_4 (pH 7.5)
8.3 mL 1 M KH_2PO_4 (pH 7.5)
109.23 g Sorbitol
dH_2O to 500 mL

6.8.2 Microscopy imaging of DAPI stained cells

Cover slips (VWR) were coated with 5 µL of 0.5 mg/mL con A, allowed to air dry for 20 min, 3 µL of DAPI-stained cells (2.8.1) were pipetted onto the con A coated cover slip, and the cover slip was placed on a clean glass slide (VWR). Imaging was performed using a gSTED Superresolution and Confocal Microscope (CLSM, TCT SP8 gSTED, Leica) equipped with a tunable white laser (470-670 nm) and 20x (PL Apo 20x/0.75 multi-immersion) objective at the CECAD imaging facility in Cologne. Images were processed using FIJI (version 1.5f, Wayne Rasband National Institute for Health).

6.9 Thiouracil (4TU) pulse-chase labelling

Pulse-chase labelling is a technique that allows for the examination of cellular processes, such as protein or transcript degradation, by exposing the cells to a labelled compound (pulse) and then to the same compound in an unlabeled form (chase) over a specific timeframe (Zeiner et al., 2008). In this study, 4-thiouracil (4TU) labelling was utilized to measure the degradation rate of specific transcripts.

Single yeast colonies were picked and inoculated overnight in 5 mL of YPD media at 30°C. The following day, the cultures were diluted to an OD_{595} of ~1.5 in drop-out media supplemented with 0.1 mM uracil and 0.2 mM 4TU (Sigma-Aldrich) and incubated at 30°C for 300 min (pulse). The cells were then centrifuged at 3,000 g for 2 min at 20°C, and resuspended in drop-out media supplemented with 20 mM uracil (chase). Next, cell samples were collected every 30 min (0, 30, and 60 min following the chase) and RNA extraction was performed (2.3). The extracted RNA was then biotinylated and purified according to Zeiner et al., 2008, and qRT-PCR analysis was performed on the purified RNA.

6.10 Surface Sensing of Translation (SUnSET) assay

The Surface Sensing Translation (SUnSET) assay is a technique used to monitor and quantify global protein synthesis without the use of radioactive fluorescence (Schmidt et al., 2009). Instead, protein synthesis is measured by immunodetection of puromycin, an aminonucleoside antibiotic, which is incorporated into the nascent polypeptide chain.

S. cerevisiae cultures were grown and prepared as previously described (2.6), and for each experimental sample, three, 1 OD_{595} aliquots were collected into individual 2 mL Eppendorf tubes. Cycloheximide (Sigma Aldrich) was then added to two of the aliquots to a final concentration of 100 µg/ml. To only one of these aliquots, a 1:1000 dilution of 10 mg/mL

puromycin (Millipore Sigma) was also added, while to the third aliquot, neither cycloheximide nor puromycin was added. All the samples were then incubated at 30°C for 15 min. Protein extraction and Gel-Electrophoresis with SDS-PAGE was then performed as previously described (2.4), and western blot analysis was then performed using a Puromycin antibody (Millipore Sigma) as previously described (2.4.3

6.11 Cell cycle arrest with α-factor and sytox-stained flow cytometry analysis

Flow Cytometry is a technique used to detect and measure physical and chemical characteristics of a population of cells. In this study, flow cytometry was used to perform cell cycle analysis in *S. cerevisiae* by measuring DNA content through Sytox Green labelled cells

Single yeast colonies were picked and inoculated overnight in 5 mL of YPD media at 30°C. The next day, the cultures were diluted in 10 mL of YPD media to an OD_{595} of ~0.2 and grown in canonical flasks at 30°C until an OD_{595} of 0.5 (with care being taken not to exceed an OD_{595} of 0.8). The cells were then centrifuged at 3,000 rpm for 3 min at 20°C, the supernatant was removed, the pellet was washed with 50 mL of water, the cells were centrifuged again at 3,000 rpm for 3 min at 20°C, and the supernatant was removed. The cells were then resuspended in YPD media containing 100 µM α-factor (Zymoresearch) and incubated at 30°C for 120 min. Following incubation, the cells were centrifuged at 3,000 rpm for 3 min at 20°C, the supernatant was removed, the pellet was resuspended in water, and this wash step was repeated. After the second wash step, the cell culture pellet was resuspended in YPD media to an OD_{595} of 0.4 and incubated at 30°C. 312 µL aliquots of the cell culture were then pipetted into individual 1.5 mL Eppendorf tubes every 10 min for 90 min, with 624 µL of 95% EtOH being added immediately to each aliquot. The tubes were then vortexed and stored at -20°C overnight.

After overnight incubation, the cells were centrifuged at 6700 rpm for 20 min at 4°C, the supernatant was removed (with care being taken to not disrupt the cell pellet), the pellet was resuspended in 800 µL of 50 mM Sodium Citrate (pH 7.2), vortexed, and incubated at room temperature for 10 min. Next, the cells were centrifuged at 6700 rpm for 20 min at 20°C, the supernatant was removed, and the Sodium Citrate wash/incubation step was repeated. After the second wash, the supernatant was removed, the pellet was resuspended in 500 µL of 50 mM Sodium Citrate (pH 7.2) containing 20 µg/mL of RNase A (Thermo Fisher Scientific) and 2.5 µM Helix NP Green (Biozol). The tubes were then incubated in the dark for 60 min at 37°C. Following digestion, 10 µL of 20 mg/mL proteinase K (Thermo Fisher Scientific) was added,

the tubes were vortexed, and incubated in the dark for 60 min at 55°C. Finally, after incubation, the tubes were stored in the dark for at least one night before Flow-Cytometric Analysis (Sytox Green stained cells are stable in the dark at 4°C for weeks).

Flow-cytometric analysis was performed at the Max Planck Institute for Biology of Ageing by the FACS core facility following guidelines from previously published literature (Rosebrock, 2017).

7 References

Alves, L.R., and Goldenberg, S. (2016). RNA-binding proteins related to stress response and differentiation in protozoa. World journal of biological chemistry *7*, 78-87.

Ashburner, M., Ball, C.A., Blake, J.A., Botstein, D., Butler, H., Cherry, J.M., Davis, A.P., Dolinski, K., Dwight, S.S., Eppig, J.T.*, et al.* (2000). Gene ontology: tool for the unification of biology. The Gene Ontology Consortium. Nature genetics *25*, 25-29.

Bannister, A.J., and Kouzarides, T. (2011). Regulation of chromatin by histone modifications. Cell Res *21*, 381-395.

Barnes, C.E., English, D.M., and Cowley, S.M. (2019). Acetylation & Co: an expanding repertoire of histone acylations regulates chromatin and transcription. Essays Biochem *63*, 97-107.

Boehm, V., Gerbracht, J.V., Marx, M.C., and Gehring, N.H. (2016). Interrogating the degradation pathways of unstable mRNAs with XRN1-resistant sequences. Nature communications *7*, 13691.

Champagne, K.S., and Kutateladze, T.G. (2009). Structural insight into histone recognition by the ING PHD fingers. Current drug targets *10*, 432-441.

Chen, H., Fan, M., Pfeffer, L.M., and Laribee, R.N. (2012). The histone H3 lysine 56 acetylation pathway is regulated by target of rapamycin (TOR) signaling and functions directly in ribosomal RNA biogenesis. Nucleic Acids Res *40*, 6534-6546.

Collart, M.A. (2016). The Ccr4-Not complex is a key regulator of eukaryotic gene expression. Wiley Interdiscip Rev RNA *7*, 438-454.

Collart, M.A., and Panasenko, O.O. (2012). The Ccr4--not complex. Gene *492*, 42-53.

Costanzo, M., Baryshnikova, A., VanderSluis, B., Andrews, B., Myers, C.L., and Boone, C. (2013). Chapter 6 - Genetic Networks. In Handbook of Systems Biology, A.J.M. Walhout, M. Vidal, and J. Dekker, eds. (San Diego: Academic Press), pp. 115-135.

Costelloe, T., and Lowndes, N.F. (2010). Chromatin assembly and signalling the end of DNA repair requires acetylation of histone H3 on lysine 56. Subcell Biochem *50*, 43-54.

Cruz, C., Della Rosa, M., Krueger, C., Gao, Q., Horkai, D., King, M., Field, L., and Houseley, J. (2018). Tri-methylation of histone H3 lysine 4 facilitates gene expression in ageing cells. Elife *7*.

Dang, W., Steffen, K.K., Perry, R., Dorsey, J.A., Johnson, F.B., Shilatifard, A., Kaeberlein, M., Kennedy, B.K., and Berger, S.L. (2009). Histone H4 lysine 16 acetylation regulates cellular lifespan. Nature *459*, 802-807.

Decker, C.J., and Parker, R. (2002). mRNA decay enzymes: decappers conserved between yeast and mammals. Proc Natl Acad Sci U S A *99*, 12512-12514.

Decker, C.J., and Parker, R. (2012). P-bodies and stress granules: possible roles in the control of translation and mRNA degradation. Cold Spring Harb Perspect Biol *4*, a012286.

Di Lorenzo, A., and Bedford, M.T. (2011). Histone arginine methylation. FEBS Lett *585*, 2024-2031.

Fierz, B., and Poirier, M.G. (2019). Biophysics of Chromatin Dynamics. Annual review of biophysics *48*, 321-345.

Finn, R.D., Mistry, J., Tate, J., Coggill, P., Heger, A., Pollington, J.E., Gavin, O.L., Gunasekaran, P., Ceric, G., Forslund, K.*, et al.* (2010). The Pfam protein families database. Nucleic Acids Res *38*, D211-222.

Garcia, R., Pulido, V., Orellana-Munoz, S., Nombela, C., Vazquez de Aldana, C.R., Rodriguez-Pena, J.M., and Arroyo, J. (2019). Signalling through the yeast MAPK Cell Wall Integrity pathway controls P-body assembly upon cell wall stress. Scientific reports *9*, 3186.

Gerber, A.P., Herschlag, D., and Brown, P.O. (2004). Extensive association of functionally and cytotopically related mRNAs with Puf family RNA-binding proteins in yeast. PLoS biology *2*, E79.

Goldstrohm, A.C., Hook, B.A., Seay, D.J., and Wickens, M. (2006). PUF proteins bind Pop2p to regulate messenger RNAs. Nat Struct Mol Biol *13*, 533-539.

Goldstrohm, A.C., Seay, D.J., Hook, B.A., and Wickens, M. (2007). PUF protein-mediated deadenylation is catalyzed by Ccr4p. The Journal of biological chemistry *282*, 109-114.

Ho, B., Baryshnikova, A., and Brown, G.W. (2018). Unification of Protein Abundance Datasets Yields a Quantitative Saccharomyces cerevisiae Proteome. Cell Syst *6*, 192-205 e193.

Howe, F.S., Fischl, H., Murray, S.C., and Mellor, J. (2017). Is H3K4me3 instructive for transcription activation? Bioessays *39*, 1-12.

Huang, Z.L., Dai, J., Luo, W.H., Wang, X.G., Tan, J.H., Chen, S.B., and Huang, Z.S. (2018). Identification of G-Quadruplex-Binding Protein from the Exploration of RGG Motif/G-Quadruplex Interactions. Journal of the American Chemical Society *140*, 17945-17955.

Hyun, K., Jeon, J., Park, K., and Kim, J. (2017). Writing, erasing and reading histone lysine methylations. Experimental & molecular medicine *49*, e324.

Iberg, A.N., Espejo, A., Cheng, D., Kim, D., Michaud-Levesque, J., Richard, S., and Bedford, M.T. (2008). Arginine methylation of the histone H3 tail impedes effector binding. The Journal of biological chemistry *283*, 3006-3010.

Jambhekar, A., Dhall, A., and Shi, Y. (2019). Roles and regulation of histone methylation in animal development. Nat Rev Mol Cell Biol *20*, 625-641.

Janke, C., Magiera, M.M., Rathfelder, N., Taxis, C., Reber, S., Maekawa, H., Moreno-Borchart, A., Doenges, G., Schwob, E., Schiebel, E.*, et al.* (2004). A versatile toolbox for PCR-based tagging of yeast genes: new fluorescent proteins, more markers and promoter substitution cassettes. Yeast *21*, 947-962.

Kaeberlein, M., Andalis, A.A., Liszt, G.B., Fink, G.R., and Guarente, L. (2004). Saccharomyces cerevisiae SSD1-V confers longevity by a Sir2p-independent mechanism. Genetics *166*, 1661-1672.

Kaeberlein, M., and Guarente, L. (2002). Saccharomyces cerevisiae MPT5 and SSD1 function in parallel pathways to promote cell wall integrity. Genetics *160*, 83-95.

Kaeberlein, M., and Kennedy, B.K. (2005). Large-scale identification in yeast of conserved ageing genes. Mechanisms of ageing and development *126*, 17-21.

Kamina, A.D., and Williams, N. (2017). Non-canonical binding interactions of the RNA recognition motif (RRM) domains of P34 protein modulate binding within the 5S ribonucleoprotein particle (5S RNP). PLoS One *12*, e0177890.

Kaplan, T., Liu, C.L., Erkmann, J.A., Holik, J., Grunstein, M., Kaufman, P.D., Friedman, N., and Rando, O.J. (2008). Cell cycle- and chaperone-mediated regulation of H3K56ac incorporation in yeast. PLoS Genet *4*, e1000270.

Kennedy, B.K., Austriaco, N.R., Jr., Zhang, J., and Guarente, L. (1995). Mutation in the silencing gene SIR4 can delay aging in S. cerevisiae. Cell *80*, 485-496.

Kennedy, B.K., Gotta, M., Sinclair, D.A., Mills, K., McNabb, D.S., Murthy, M., Pak, S.M., Laroche, T., Gasser, S.M., and Guarente, L. (1997). Redistribution of silencing proteins from telomeres to the nucleolus is associated with extension of life span in S. cerevisiae. Cell *89*, 381-391.

Kilchert, C., Wittmann, S., and Vasiljeva, L. (2016). The regulation and functions of the nuclear RNA exosome complex. Nat Rev Mol Cell Biol *17*, 227-239.

Kim, T., and Buratowski, S. (2009). Dimethylation of H3K4 by Set1 recruits the Set3 histone deacetylase complex to 5' transcribed regions. Cell *137*, 259-272.

Kirkconnell, K.S., Paulsen, M.T., Magnuson, B., Bedi, K., and Ljungman, M. (2016). Capturing the dynamic nascent transcriptome during acute cellular responses: The serum response. Biology open *5*, 837-847.

Kosugi, S., Hasebe, M., Tomita, M., and Yanagawa, H. (2008). Nuclear export signal consensus sequences defined using a localization-based yeast selection system. Traffic *9*, 2053-2062.

Kurat, C.F., Recht, J., Radovani, E., Durbic, T., Andrews, B., and Fillingham, J. (2014). Regulation of histone gene transcription in yeast. Cellular and molecular life sciences : CMLS *71*, 599-613.

Kurdistani, S.K., and Grunstein, M. (2003). Histone acetylation and deacetylation in yeast. Nat Rev Mol Cell Biol *4*, 276-284.

Laemmli, U.K. (1970). Cleavage of structural proteins during the assembly of the head of bacteriophage T4. Nature *227*, 680-685.

Lapointe, C.P., Preston, M.A., Wilinski, D., Saunders, H.A.J., Campbell, Z.T., and Wickens, M. (2017). Architecture and dynamics of overlapped RNA regulatory networks. Rna *23*, 1636-1647.

Lawrence, M., Daujat, S., and Schneider, R. (2016). Lateral Thinking: How Histone Modifications Regulate Gene Expression. Trends Genet *32*, 42-56.

Lee, C.D., and Tu, B.P. (2015). Glucose-Regulated Phosphorylation of the PUF Protein Puf3 Regulates the Translational Fate of Its Bound mRNAs and Association with RNA Granules. Cell reports *11*, 1638-1650.

Li, Q., Zhou, H., Wurtele, H., Davies, B., Horazdovsky, B., Verreault, A., and Zhang, Z. (2008). Acetylation of histone H3 lysine 56 regulates replication-coupled nucleosome assembly. Cell *134*, 244-255.

Liu, B., and Qian, S.B. (2014). Translational reprogramming in cellular stress response. Wiley Interdiscip Rev RNA *5*, 301-315.

Liu, Y., Beyer, A., and Aebersold, R. (2016). On the Dependency of Cellular Protein Levels on mRNA Abundance. Cell *165*, 535-550.

Liu, Y., Chen, S., Wang, S., Soares, F., Fischer, M., Meng, F., Du, Z., Lin, C., Meyer, C., DeCaprio, J.A.*, et al.* (2017). Transcriptional landscape of the human cell cycle. Proc Natl Acad Sci U S A *114*, 3473-3478.

Longtine, M.S., McKenzie, A., 3rd, Demarini, D.J., Shah, N.G., Wach, A., Brachat, A., Philippsen, P., and Pringle, J.R. (1998). Additional modules for versatile and economical PCR-based gene deletion and modification in Saccharomyces cerevisiae. Yeast *14*, 953-961.

Luo, Y., Na, Z., and Slavoff, S.A. (2018). P-Bodies: Composition, Properties, and Functions. Biochemistry *57*, 2424-2431.

Malke, H. (1990). J. SAMBROCK, E. F. FRITSCH and T. MANIATIS, Molecular Cloning, A Laboratory Manual (Second Edition), Volumes 1, 2 and 3. 1625 S., zahlreiche Abb. und Tab. Cold Spring Harbor 1989. Cold Spring Harbor Laboratory Press. $ 115.00. ISBN: 0-87969-309-6. Journal of Basic Microbiology *30*, 623-623.

Masumoto, H., Hawke, D., Kobayashi, R., and Verreault, A. (2005). A role for cell-cycle-regulated histone H3 lysine 56 acetylation in the DNA damage response. Nature *436*, 294-298.

Miller, J.E., and Reese, J.C. (2012). Ccr4-Not complex: the control freak of eukaryotic cells. Crit Rev Biochem Mol Biol *47*, 315-333.

Moon, S.L., Morisaki, T., Khong, A., Lyon, K., Parker, R., and Stasevich, T.J. (2019). Multicolour single-molecule tracking of mRNA interactions with RNP granules. Nat Cell Biol.

Mugridge, J.S., Coller, J., and Gross, J.D. (2018). Structural and molecular mechanisms for the control of eukaryotic 5'-3' mRNA decay. Nat Struct Mol Biol *25*, 1077-1085.

Neumann, H., Hancock, S.M., Buning, R., Routh, A., Chapman, L., Somers, J., Owen-Hughes, T., van Noort, J., Rhodes, D., and Chin, J.W. (2009). A method for genetically installing site-specific acetylation in recombinant histones defines the effects of H3 K56 acetylation. Mol Cell *36*, 153-163.

Neymotin, B., Ettorre, V., and Gresham, D. (2016). Multiple Transcript Properties Related to Translation Affect mRNA Degradation Rates in Saccharomyces cerevisiae. G3 (Bethesda) *6*, 3475-3483.

Nielsen, P.R., Nietlispach, D., Mott, H.R., Callaghan, J., Bannister, A., Kouzarides, T., Murzin, A.G., Murzina, N.V., and Laue, E.D. (2002). Structure of the HP1 chromodomain bound to histone H3 methylated at lysine 9. Nature *416*, 103-107.

Oliveira, C., Faoro, H., Alves, L.R., and Goldenberg, S. (2017). RNA-binding proteins and their role in the regulation of gene expression in Trypanosoma cruzi and Saccharomyces cerevisiae. Genetics and molecular biology *40*, 22-30.

Parekh, S., Ziegenhain, C., Vieth, B., Enard, W., and Hellmann, I. (2018). zUMIs - A fast and flexible pipeline to process RNA sequencing data with UMIs. GigaScience *7*.

Parker, R. (2012). RNA degradation in Saccharomyces cerevisae. Genetics *191*, 671-702.

Perez-Ortin, J.E., Medina, D.A., Chavez, S., and Moreno, J. (2013). What do you mean by transcription rate?: the conceptual difference between nascent transcription rate and mRNA synthesis rate is essential for the proper understanding of transcriptomic analyses. Bioessays *35*, 1056-1062.

Pérez-Ortín, J.E., Mena, A., Barba-Aliaga, M., Alonso-Monge, R., Singh, A., Chávez, S., and García-Martínez, J. (2019).

Poss, Z.C., Ebmeier, C.C., and Taatjes, D.J. (2013). The Mediator complex and transcription regulation. Crit Rev Biochem Mol Biol *48*, 575-608.

Rea, S., Eisenhaber, F., O'Carroll, D., Strahl, B.D., Sun, Z.W., Schmid, M., Opravil, S., Mechtler, K., Ponting, C.P., Allis, C.D.*, et al.* (2000). Regulation of chromatin structure by site-specific histone H3 methyltransferases. Nature *406*, 593-599.

Recht, J., Tsubota, T., Tanny, J.C., Diaz, R.L., Berger, J.M., Zhang, X., Garcia, B.A., Shabanowitz, J., Burlingame, A.L., Hunt, D.F.*, et al.* (2006). Histone chaperone Asf1 is required for histone H3 lysine 56 acetylation, a modification associated with S phase in mitosis and meiosis. Proc Natl Acad Sci U S A *103*, 6988-6993.

Rege, M., Subramanian, V., Zhu, C., Hsieh, T.H., Weiner, A., Friedman, N., Clauder-Munster, S., Steinmetz, L.M., Rando, O.J., Boyer, L.A.*, et al.* (2015). Chromatin Dynamics and the RNA Exosome Function in Concert to Regulate Transcriptional Homeostasis. Cell reports *13*, 1610-1622.

Rosebrock, A.P. (2017). Analysis of the Budding Yeast Cell Cycle by Flow Cytometry. Cold Spring Harb Protoc *2017*.

Ruan, K., Yamamoto, T.G., Asakawa, H., Chikashige, Y., Kimura, H., Masukata, H., Haraguchi, T., and Hiraoka, Y. (2015). Histone H4 acetylation required for chromatin decompaction during DNA replication. Scientific reports *5*, 12720.

Schmidt, E.K., Clavarino, G., Ceppi, M., and Pierre, P. (2009). SUnSET, a nonradioactive method to monitor protein synthesis. Nat Methods *6*, 275-277.

Schneider-Poetsch, T., Ju, J., Eyler, D.E., Dang, Y., Bhat, S., Merrick, W.C., Green, R., Shen, B., and Liu, J.O. (2010). Inhibition of eukaryotic translation elongation by cycloheximide and lactimidomycin. Nat Chem Biol *6*, 209-217.

Shang, W.H., Hori, T., Westhorpe, F.G., Godek, K.M., Toyoda, A., Misu, S., Monma, N., Ikeo, K., Carroll, C.W., Takami, Y.*, et al.* (2016). Acetylation of histone H4 lysine 5 and 12 is required for CENP-A deposition into centromeres. Nature communications *7*, 13465.

Skalska, L., Beltran-Nebot, M., Ule, J., and Jenner, R.G. (2017). Regulatory feedback from nascent RNA to chromatin and transcription. Nat Rev Mol Cell Biol *18*, 331-337.

Sternburg, E.L., Estep, J.A., Nguyen, D.K., Li, Y., and Karginov, F.V. (2018). Antagonistic and cooperative AGO2-PUM interactions in regulating mRNAs. Scientific reports *8*, 15316.

Stewart, M.S., Krause, S.A., McGhie, J., and Gray, J.V. (2007). Mpt5p, a stress tolerance- and lifespan-promoting PUF protein in Saccharomyces cerevisiae, acts upstream of the cell wall integrity pathway. Eukaryotic cell *6*, 262-270.

Szklarczyk, D., Gable, A.L., Lyon, D., Junge, A., Wyder, S., Huerta-Cepas, J., Simonovic, M., Doncheva, N.T., Morris, J.H., Bork, P.*, et al.* (2019). STRING v11: protein-protein association networks with increased coverage, supporting functional discovery in genome-wide experimental datasets. Nucleic Acids Res *47*, D607-d613.

Tan, Y., Xue, Y., Song, C., and Grunstein, M. (2013). Acetylated histone H3K56 interacts with Oct4 to promote mouse embryonic stem cell pluripotency. Proc Natl Acad Sci U S A *110*, 11493-11498.

Tanaka, S., Miyazawa-Onami, M., Iida, T., and Araki, H. (2015). iAID: an improved auxin-inducible degron system for the construction of a 'tight' conditional mutant in the budding yeast Saccharomyces cerevisiae. Yeast *32*, 567-581.

Tessarz, P., and Kouzarides, T. (2014). Histone core modifications regulating nucleosome structure and dynamics. Nat Rev Mol Cell Biol *15*, 703-708.

Teste, M.A., Duquenne, M., Francois, J.M., and Parrou, J.L. (2009). Validation of reference genes for quantitative expression analysis by real-time RT-PCR in Saccharomyces cerevisiae. BMC Mol Biol *10*, 99.

Thapa, M., Bommakanti, A., Shamsuzzaman, M., Gregory, B., Samsel, L., Zengel, J.M., and Lindahl, L. (2013). Repressed synthesis of ribosomal proteins generates protein-specific cell cycle and morphological phenotypes. Mol Biol Cell *24*, 3620-3633.

Tie, F., Banerjee, R., Stratton, C.A., Prasad-Sinha, J., Stepanik, V., Zlobin, A., Diaz, M.O., Scacheri, P.C., and Harte, P.J. (2009). CBP-mediated acetylation of histone H3 lysine 27 antagonizes Drosophila Polycomb silencing. Development (Cambridge, England) *136*, 3131-3141.

Topal, S., Vasseur, P., Radman-Livaja, M., and Peterson, C.L. (2019). Distinct transcriptional roles for Histone H3-K56 acetylation during the cell cycle in Yeast. Nature communications *10*, 4372.

Tye, B.W., Commins, N., Ryazanova, L.V., Wuhr, M., Springer, M., Pincus, D., and Churchman, L.S. (2019). Proteotoxicity from aberrant ribosome biogenesis compromises cell fitness. Elife *8*.

Villanyi, Z., and Collart, M.A. (2015). Ccr4-Not is at the core of the eukaryotic gene expression circuitry. Biochem Soc Trans *43*, 1253-1258.

Voichek, Y., Bar-Ziv, R., and Barkai, N. (2016). Expression homeostasis during DNA replication. Science (New York, NY) *351*, 1087-1090.

Voichek, Y., Mittelman, K., Gordon, Y., Bar-Ziv, R., Lifshitz Smit, D., Shenhav, R., and Barkai, N. (2018). Epigenetic Control of Expression Homeostasis during Replication Is Stabilized by the Replication Checkpoint. Mol Cell *70*, 1121-1133 e1129.

Wang, C., Schmich, F., Srivatsa, S., Weidner, J., Beerenwinkel, N., and Spang, A. (2018a). Context-dependent deposition and regulation of mRNAs in P-bodies. Elife *7*.

Wang, J., Zhao, Y., Zhou, X., Hiebert, S.W., Liu, Q., and Shyr, Y. (2018b). Nascent RNA sequencing analysis provides insights into enhancer-mediated gene regulation. BMC genomics *19*, 633.

Wang, Y., Yuan, Q., and Xie, L. (2018c). Histone Modifications in Aging: The Underlying Mechanisms and Implications. Current stem cell research & therapy *13*, 125-135.

Warmerdam, D.O., and Wolthuis, R.M.F. (2019). Keeping ribosomal DNA intact: a repeating challenge. Chromosome Res *27*, 57-72.

Watanabe, S., Resch, M., Lilyestrom, W., Clark, N., Hansen, J.C., Peterson, C., and Luger, K. (2010). Structural characterization of H3K56Q nucleosomes and nucleosomal arrays. Biochim Biophys Acta *1799*, 480-486.

Webster, M.W., Chen, Y.H., Stowell, J.A.W., Alhusaini, N., Sweet, T., Graveley, B.R., Coller, J., and Passmore, L.A. (2018). mRNA Deadenylation Is Coupled to Translation Rates by the Differential Activities of Ccr4-Not Nucleases. Mol Cell *70*, 1089-1100 e1088.

Wilinski, D., Qiu, C., Lapointe, C.P., Nevil, M., Campbell, Z.T., Tanaka Hall, T.M., and Wickens, M. (2015). RNA regulatory networks diversified through curvature of the PUF protein scaffold. Nature communications *6*, 8213.

Williams, S.K., Truong, D., and Tyler, J.K. (2008). Acetylation in the globular core of histone H3 on lysine-56 promotes chromatin disassembly during transcriptional activation. Proc Natl Acad Sci U S A *105*, 9000-9005.

Wullschleger, S., Loewith, R., and Hall, M.N. (2006). TOR signaling in growth and metabolism. Cell *124*, 471-484.

Xiang, S., Cooper-Morgan, A., Jiao, X., Kiledjian, M., Manley, J.L., and Tong, L. (2009). Structure and function of the 5'-->3' exoribonuclease Rat1 and its activating partner Rai1. Nature *458*, 784-788.

Xie, W., Song, C., Young, N.L., Sperling, A.S., Xu, F., Sridharan, R., Conway, A.E., Garcia, B.A., Plath, K., Clark, A.T.*, et al.* (2009). Histone h3 lysine 56 acetylation is linked to the core transcriptional network in human embryonic stem cells. Mol Cell *33*, 417-427.

Xu, F., Zhang, K., and Grunstein, M. (2005). Acetylation in histone H3 globular domain regulates gene expression in yeast. Cell *121*, 375-385.

Yi, H., Park, J., Ha, M., Lim, J., Chang, H., and Kim, V.N. (2018). PABP Cooperates with the CCR4-NOT Complex to Promote mRNA Deadenylation and Block Precocious Decay. Mol Cell *70*, 1081-1088 e1085.

Zeiner, G.M., Cleary, M.D., Fouts, A.E., Meiring, C.D., Mocarski, E.S., and Boothroyd, J.C. (2008). RNA analysis by biosynthetic tagging using 4-thiouracil and uracil phosphoribosyltransferase. Methods in molecular biology (Clifton, NJ) *419*, 135-146.

Zhang, J., Jing, L., Li, M., He, L., and Guo, Z. (2019). Regulation of histone arginine methylation/demethylation by methylase and demethylase (Review). Molecular medicine reports *19*, 3963-3971.

Zhao, R., Nakamura, T., Fu, Y., Lazar, Z., and Spector, D.L. (2011). Gene bookmarking accelerates the kinetics of post-mitotic transcriptional re-activation. Nat Cell Biol *13*, 1295-1304.

Zhou, Y., Zhou, B., Pache, L., Chang, M., Khodabakhshi, A.H., Tanaseichuk, O., Benner, C., and Chanda, S.K. (2019). Metascape provides a biologist-oriented resource for the analysis of systems-level datasets. Nature communications *10*, 1523.

Zhu, X., Zhang, Y., Bjornsdottir, G., Liu, Z., Quan, A., Costanzo, M., Davila Lopez, M., Westholm, J.O., Ronne, H., Boone, C.*, et al.* (2011). Histone modifications influence mediator interactions with chromatin. Nucleic Acids Res *39*, 8342-8354.

8 Acknowledgements

I would like to thank Dr. Peter Tessarz for giving me the opportunity to complete a PhD in his lab and for the years of advice and guidance during the process. I would also like to thank the Tessarz lab, especially Dr. Julia Mawer and Dr. Chrysa Nikopoulou for being awesome and for their guidance throughout the years.

I would like to thank the Cologne Graduate School of Ageing Research for the opportunity, training, and funding. Special thanks to Dr. Daniela Morick for answering my many questions and for the support.

I would like to thank my parents Ewa and Andrzej Kochan for everything, I would not be in the position I am in if it wasn't for you. Last but not least, I would like to thank my amazing wife, Dr. Sandra Kochan; thank you for the love, support, and always being there.

9 Eidesstattliche Erklärung

„Hiermit versichere ich an Eides statt, dass ich die vorliegende Dissertation selbstständig und ohne die Benutzung anderer als der angegebenen Hilfsmittel und Literatur angefertigt habe. Alle Stellen, die wörtlich oder sinngemäß aus veröffentlichten und nicht veröffentlichten Werken dem Wortlaut oder dem Sinn nach entnommen wurden, sind als solche kenntlich gemacht. Ich versichere an Eides statt, dass diese Dissertation noch keiner anderen Fakultät oder Universität zur Prüfung vorgelegen hat; dass sie - abgesehen von unten angegebenen Teilpublikationen und eingebundenen Artikeln und Manuskripten - noch nicht veröffentlicht worden ist sowie, dass ich eine Veröffentlichung der Dissertation vor Abschluss der Promotion nicht ohne Genehmigung des Promotionsausschusses vornehmen werde. Die Bestimmungen dieser Ordnung sind mir bekannt. Darüber hinaus erkläre ich hiermit, dass ich die Ordnung zur Sicherung guter wissenschaftlicher Praxis und zum Umgang mit wissenschaftlichem Fehlverhalten der Universität zu Köln gelesen und sie bei der Durchführung der Dissertation zugrundeliegenden Arbeiten und der schriftlich verfassten Dissertation beachtet habe und verpflichte mich hiermit, die dort genannten Vorgaben bei allen wissenschaftlichen Tätigkeiten zu beachten und umzusetzen. Ich versichere, dass die eingereichte elektronische Fassung der eingereichten Druckfassung vollständig entspricht."

Teilpublikationen:

28.05.2020, David Kochan, D.
Datum, Name und Unterschrift

10 Declaration for the doctoral thesis (dissertation)

"I hereby declare that I have completed the present dissertation independently and without the use of any aids or literature other than those referred to. All passages that have been taken, either literally or in sense, from published and unpublished works, are marked as such. I declare that this dissertation has not been submitted to any other faculty or university; that - apart from the partial publications and included articles and manuscripts listed below - it has not yet been published, and that I will not publish the dissertation before completing my doctorate without the permission of the PhD Committee. I am aware of the terms of the doctoral regulations. In addition, I hereby declare that I am aware of the "Regulations for Safeguarding Good Scientific Practice and Dealing with Scientific Misconduct" of the University of Cologne, and that I have observed them during the work on the thesis project and the written doctoral thesis. I hereby commit myself to observe and implement the guidelines mentioned there in all scientific activities. I assure that the submitted electronic version is identical to the submitted printed version".

Partial publications of the thesis:

28.05.2020, David Kochan,

Date, name, and signature

11 Curriculum Vitae

Personal Details

Name	David Zygmunt Kochan
Date and location of birth	11 April 1985, Lublin, Poland
Present work address	Max Planck Institute for Biology of Ageing
	Joseph-Stelzmann-Str. 9B, 50931 Cologne,
	Germany
E-mail	davidzkochan@gmail.com

Scientific Education

06/2016 – present	PhD student
01/2013 – 04/2015	Master of Science (Biology)
	University of Lethbridge, AB, Canada
	Thesis: "Breast cancer and circadian disruption: An epigenetic link"
09/2009 – 12/2012	Bachelor of Science (Cellular and Molecular Biology)
	University of Lethbridge, AB, Canada
	Independent study: "Genetic diversity in the *Warbling Vireo*"